NUMERICAL INVESTIGATION OF AIR MIXER PERFORMANCE FOR HVAC TESTING APPLICATIONS

By

MANSOOR AHMED

Bachelor of Science in Mechanical Engineering
University of Engineering and Technology
Lahore, Pakistan
2007

Master of Science in Engineering Mechanics
KTH-Royal Institute of Technology,
Stockholm, Sweden
2011

Submitted to the Faculty of the
Graduate College of
Oklahoma State University
in partial fulfillment of
the requirements for
the Degree of
MASTER OF SCIENCE
May, 2019

NUMERICAL INVESTIGATION OF AIR MIXER PERFORMANCE FOR HVAC TESTING APPLICATIONS

Thesis Approved:

Omer San

Thesis Advisor

Christian K. Bach

Craig R. Bradshaw

ACKNOWLEDGMENTS

First I want to say thanks to almighty ALLAH who gave me the strength to perform this research. After that I owe gratitude to my thesis advisor, Dr. Omer San, not only for giving me the opportunity to work on this topic but also for his support during learning journey. He helped me a lot for improving my knowledge and technical writing skills. I would like to thank to Dr. Christian K. Bach, for guiding me throughout this research and being my thesis committee member. His continuous feedback on my investigations gave me a better idea to come up with improved results. Beside this, I am also grateful to my committee member Dr. Craig R. Bradshaw for his time and valuable suggestions. Thanks is also due to Dr. Aaron Alexander for helping me to learn Star-CCM+. I am also grateful to ASHRAE committee members, and our guides for testing and manufacturing laboratories (UL, Intertek, Lennox, Trane). I want to thank to my friend, Nadeem Amjad, who shared his knowledge and SolidWorks skills with me and other friends for their moral support. I also want to say thanks to my lab mates especially Prashant Tarey, Hyunjin Park and Suraj Pawar. Last but not least, many thanks to my family. Certainly this task was impossible to complete without their support.

Dedicated to my mother and daughter who left me during this journey.

Acknowledgments reflect the views of the author and are not endorsed by committee members or Oklahoma State University.

Dedicated to my mother and daughter who left me during this journey.

Dedication reflect the views of the author and are not endorsed by committee members or Oklahoma State University.

Name: MANSOOR AHMED

Date of Degree: May, 2019

Title of Study: NUMERICAL INVESTIGATION OF AIR MIXER PERFORMANCE FOR HVAC TESTING APPLICATIONS

Major Field: MECHANICAL ENGINEERING

Abstract:

The ever-increasing energy demand is one of the biggest challenges of the design processes in heating, ventilation, and air-conditioning (HVAC) systems. Accurate performance measurements of equipment in the laboratory requires air mixing to reduce measurement error. The National Bureau of Standards conducted in depth experimental research on the required air mixing devices in the late 1960s. At this point, very limited guidelines are available for air mixers, with ASHRAE RP-1733 addressing this gap.

In this thesis, CFD analyses have been conducted to predict the mixing effectiveness and pressure losses of candidate air-mixers of RP-1733. Both existing and new air mixer models have been investigated for their mixing effectiveness and pressure drop characteristics. It was found that the proposed static air mixing models, consisting of louvers-baffles, louvers, and orifice-target parts, add turbulence to the airstream to enhance the mixing process. I have also investigated the pressure drop characteristics with respect to the flowrate. I found that the louver-baffle mixer has significantly more pressure drop as compared to the louver mixer with a negligible small increase in mixing efficiency. Therefore, I conclude that the louver mixer (without baffle) is a better option when we consider the trade-off between mixing efficiency and pressure drop characteristics, which might provide further insights to our co-designed experimental studies.

TABLE OF CONTENTS

LIST OF TABLES

LIST OF FIGURES

ABBREVIATIONS

Acronym	**W**hat (it) **S**tands **F**or
HVAC	**H**eating **V**entilating **A**ir **C**onditioning
ASHVE	**A**merican **S**ociety **H**eating **V**entilating **E**ngineers
CFM	**C**ubic **F**eet per **M**inute
ANSI	**A**merican **N**ational **S**tandards **I**nstitute
AHU	**A**ir **H**andling **U**nit
AHRI	**A**ir conditioning **H**eating **R**efrigeration **I**nstitute
US	**U**nited **S**tates
CFR	**C**ode of **F**ederal **R**egulations
DOE	**D**epartment **O**F **E**nergy
TRP	**T**he **R**esearch **P**roject
CAE	**C**omputer **A**ided **E**ngineering
CFD	**C**omputational **F**luid **D**ynamics
FEA	**F**inite **E**lement **A**nalysis
MBD	**M**ulti- **B**ody **D**ynamics
PDEs	**P**artial **P**ifferential **E**quation
FDM	**F**inite **D**ifference **M**ethod
FVM	**F**inite **V**olume **M**ethod
N-S	**N**avier-**S**tokes
EIA	**E**nergy **I**nformation **A**dministration
NIST	**N**ational **I**nstitute of **S**tandards and **T**echnology
CIBSE	**C**hartered **I**nstitute of **B**uilding **S**ervices **E**ngineers

CAD	**C**omputer **A**ided **D**esign
D	**D**imension
STEP	**St**andard for the **E**xchange of **P**roduct model data
IGES	**I**nitial **G**raphics **E**xchange and **S**pecification
RANS	**R**eynolds-**A**veraged **N**avier-**S**tokes equation
LES	**L**arge **E**ddy **S**imulation
DES	**D**etached **E**ddy **S**imulation
TKE	**T**urbulent **K**inetic **E**nergy
SMACNA	**S**heet **M**etal and **A**ir conditioning **C**ontractor **N**ational and **A**ssociation

CHAPTER I

INTRODUCTION

1.1 Introduction to HVAC

The term HVAC stands for heating, ventilating and air-conditioning. It describes the field that is concerned with air processing for the indoor environment in order to meet the health, safety and comfort needs of the occupant either they are living in the buildings or mobile vehicles. In the eighteenth and nineteenth centuries, scientist and engineers began to study the sources of indoor air contaminants and the effects of these contaminants on human health. In 1895, the American Society of Heating and Ventilating Engineers (ASHVE) approved 30 cubic feet per minute (CFM) of outdoor air per occupant as a minimum ventilation rate for public buildings. American Society of Heating, Refrigerating and Air-Conditioning Engineers (ASHRAE), the successor of ASHVE, is currently studying the out-door air ventilation rates that are required to produce acceptable indoor air quality for various occupancies. ANSI/ASHRAE Standard 62.1-2007- Ventilation for Acceptable Indoor Air Quality is devoted to the subject of indoor air quality (Angel, 2011).

To meet acceptable indoor air quality, the characterization of HVAC ductwork systems in buildings is crucial to maintain these standards. Proper design of indoor environment requires detailed information of indoor air distribution, such as airflow pattern, velocity, temperature, and contaminant concentrations. The information can be obtained by experimental measurements and computational simulations. The efficiency of the duct system can have an effect on the overall efficiency of a heating and cooling system, and thus must be evaluated and improved. Static pressure

losses through residential ductwork systems effect residential HVAC equipment energy efficiency and performance. The well-known design guidelines are provided by the ASHRAE Fundamentals Handbook (HandbookFundamentals and Edition, 2009). The handbook by Idelchik (1994) also provides an extensive data of pressure losses across air delivery ductworks of HVAC systems.

Not only in the buildings, the properties of air in the air handling units (AHU) are important to be known to see the efficiency and effectiveness of equipment. AHUs are designed to carry new air to the ventilated zone and to extract the contaminated air from this zone. In real flows, the properties of air may be not uniform across the AHU, ducts or in the room. Measurements of air properties in unitary equipment are important to check if air follows the anticipated paths and thus identify potential problems and correct those at early stages to optimize the performance of the equipment. Any change in the inlet conditions of air will change the output of the equipment so the equipment performance is highly dependent on the surrounding in which measurements are taken or is being tested. To reduce the effect of surrounding, the equipment rating performance test chambers are developed. These test chambers are called psychrometric chambers.

The psychrometric chambers, which are of different sizes for different types of equipment with different controllers, are designed in such away that different flow parameters can be controlled. These allow scientist and engineers to perform tests at controlled conditions. Accurate measurements of the air flowrate, including the inlet and outlet air conditions are required for psychrometric performance testing of HVAC&R equipment. Both heating and cooling tolerances, for Air-Conditioning, Heating, and Refrigeration Institute (AHRI) standards (210/240, 340/360, and 365), ASHRAE 33, and in the US federal regulations, (10 CFR; DOE, 2017) for capacity and efficiency measurements, are limited to 5%. Although equipment testing is performed in a very controlled environment, even then there is some difference in the performance

rating when tests are being performed at different testing facilities. This variability in the performance rating could be for many reasons including the improper mixing of fluid or difference in the design of air sampler and air-mixer apparatus.

One method to obtain uniform properties of air across the duct cross-section is to use mixing devices. In general, there are two types of mixing devices; active and passive. Active (dynamic) like moving blades include fans whereas passive (static) include perforated plates. These mixing devices not only enhance the mixing but also causes pressure drop, which depends on the design of air-mixers. To compensate this pressure drop we need to add extra fan power to drive the air with the exact, required flowrate. This brings another parameter into the consideration for cooling load calculations which is the pressure drop due to the mixer apparatus. There are limited guidelines available for the combination sampling and mixing devices to obtain accurate measurements of air side conditions.

Due to limited guidelines, differences in the quality of mixing and sampling can lead to remarkable variability between the psychrometric capacity and measured experimental conditions, not only in comparison to the outside facilities but also within the same facility. To minimize this disparity, there is a need to design and test different air-mixer and air-sampler apparatuses for different flow conditions. It is not only impractical by means of money and time, but also cumbersome to manufacture number of air-mixers and air-samplers with different designs and then perform testing under different flow conditions. Due to these reasons, engineers and scientists are using computer aided engineering (CAE), which includes computational fluid dynamics (CFD), finite element analysis (FEA), multi-body dynamics (MBD) and optimization. In this research, we are using computational fluid dynamics (CFD) to analyze air-mixing effectiveness with different air-mixer designs and flow parameters. In the next section, there is a brief introduction about CFD for the readers.

1.2 Introduction to CFD

The physical aspects of any fluid flow are governed by the fundamental principles of conservation of mass, momentum, and energy. These fundamental principles can be expressed in terms of mathematical equations; usually these equations are partial differential equations (PDEs). CFD is the art of replacing these PDEs of fluid flow with numbers and advancing these numbers in space and time to obtain a final numerical description of the complete flow field of interest. To solve these equations initial conditions and boundary conditions are specified around the boundary of the system. These PDEs are highly nonlinear and are not solvable by explicit, closed form analytical methods. Due of this, spatial approximation methods such as Finite Difference Method (FDM), Finite Element Method (FEM), and Finite Volume Methods (FVM) can be used to solve these PDEs. Due to the use of these approximations methods, CFD results are always approximate. This is one of the reasons for differences between computed results and reality.

The advantages of CFD are conditional on being able to solve the Navier-Stokes (N-S) equations accurately, which is extremely difficult for most flows of engineering interest. The results of CFD are as valid as the physical models incorporating the governing equations and boundary conditions, and therefore are subjected to error, especially for turbulent flows. In order to validate the models, we have to rely on experimental data. If we are unable to obtain accurate solutions for flows, we have to determine what we can produce and learn to analyze and judge the results.

CFD results are usually presented in various graphical formats to show the anticipated performance. These visualization techniques are useful for both qualitative and quantitative analyses. Usually, qualitative results are used to determine the feasibility of the concept. On the other hand, the functionality between different features of the designs is proved with the use of quantitative simulations. CFD studies are used for building designs to find the optimized practical solution for problems related to

ventilation, thermal comfort, and wind movement around building.

However, both experimental and numerical methods have their own advantages and disadvantages due to different limitations. For example, it is very easy to control the air-side conditions to investigate the effects of different inlet conditions on the equipment process in numerical studies as compared to the experimental methods. On other hand, to model and numerically investigate the exact geometry, the task becomes impractical. For example, in case of fin and tube heat exchanger, to mesh same number of fins as we have in our coil it is computationally not feasible. CAE engineers most of the time simplify the geometry without losing the important information required for the analysis. The geometric approximation which are made during this investigation will be discussed in Chapter 4 of this thesis.

1.3 ASHRAE RP-1733

This study is the part of ASHRAE research project (RP-1733) project entitled "Develop Design Criteria for Psychrometric Air Sampler and Mixer Apparatus for Use in ASHRAE Test Standards" sponsored by ASHRAE technical committee (TC) 8.11 (Unitary and Room Air Conditioners and Heat Pumps). The complete project is focused on providing guidelines for air-mixer design in regard to their mixing effectiveness and the pressure drop in the duct due to these mixing devices. In addition to this, to provide a suitable location to measure the properties of bulk air with air-sampler and sampler-less arrangement.

1.4 Motivation

There are limited guidelines available for the design of the air-mixer. The motivation behind this study is to investigate the existing air-mixers models for their mixing effectiveness and validate the CFD results with existing experimental data wherever it is applicable. Based on the outcomes of these results some new models designs will be

proposed and investigated. This study is done numerically because there are number of parameters involved in this study, which makes it experimentally cumbersome, expensive and time consuming.

The ultimate goal of our study is to devise a new co-designed experimental and computational framework for better understanding of HVAC mixing systems that will advance the state-of-the-art technologies providing improved air-mixers for increased measurement accuracy.

CHAPTER II

LITERATURE REVIEW

2.1 Background

According to the survey conducted by Energy Information Administration (EIA) in 2015, space heating and cooling comprise 15% and 17%, respectively of the total U.S. energy consumption by resdential buildings(Woodward and Berry, 5 22). The number and size of the commercial buildings are increasing in the U.S. and worldwide. So the energy consumption is also increasing for heating and cooling of the space. To minimize the energy consumption there is a need to use this energy efficiently. Scientist and engineers are performing experimental and computational studies on HVAC system to predict flow characteristics temperature, pressure loses and sources of noise and dissipation in ductflow systems. Air-side capacity is one of the certified value audited by AHRI and Department of Energy (DOE) on yearly basis because it is main output of the system. The differences in air-mixers design may lead to inconsistency in measured efficiency, so may exceed the allowable tolerance.

In computational fluid dynamics (CFD) studies, several modeling approaches to determine the indoor airflow pattern and temperature distribution may be found in the literature: zonal models (Inard et al., 1996; Wurtz et al., 1999; Riederer et al., 2002; Megri and Haghighat, 2007), state-space models (Peng and Van Paassen, 1998; Yao et al., 2013), neural network models (Ruano et al., 2006; Mustafaraj et al., 2011), multi-zone models (Axley, 2007; Maatouk, 2007), and computational fluid dynamics models (Whittle, 1986; Maatouk, 2007; Whittle, 1986; Awbi, 1989; Jones and Whittle, 1992; Jiang et al., 1992; Gan, 1995; Chow and Fung, 1996; Baker et al.,

1997; Emmerich and McGrattan, 1998; Lam and Chan, 2001; Srebric and Chen, 2002; Zhao et al., 2003; Stamou and Katsiris, 2006; Tripathi and Moulic, 2007; Chen, 2009; Kim et al., 2013; Teodosiu et al., 2014). CFD models are widely employed and can provide detailed and accurate information for indoor environment designs.

Other than HVAC, CFD techniques are also used in process industry, and their usage is growing exponentially over the years (Norton and Sun, 2006). For example, in food industry, CFD is used to measure governing physical phenomena including sterilization (Siriwattanayotin et al., 2006; Varma and Kannan, 2006), drying processes (Huang et al., 2003), production facilities (Burfoot et al., 1999; Harral and Burfoot, 2005), and mixing (Song and Han, 2005). On macroscale, common mixing methods are choatic advection (Ottino and Ottino, 1989) and generation of turbulence (Brodkey, 1975). To get a general understanding of mixing on transport phenomena, interested readers are directed to Bird et al. (1960); Ottino (1990). Reviews of mixing applications in microfluidics can also be found elsewhere (Nguyen and Wu, 2004; Hessel et al., 2005).

2.2 Experimental Studies

In experimental studies, to improve the measuring techniques of air streams for capacity of air-conditioning, heating, and refrigeration equipment the National Bureau of Standards (NIST) has conducted a study of mixing devices (Faison et al., 1966). They designed an apparatus for experimental study of mixing process and evaluation of mixing devices. Readers that are more concerned with experimental setup are referred to (Faison et al., 1966). They studied several parameters, e.g, non-uniformity of temperature and humidity at the inlet to the mixer, average air velocity etc. In the beginning, they performed tests without any mixing device to see the inherent mixing in the flow. In this study, it was observed that inherent mixing between the two stations was very small. A pair of metal louvered mixer was used to see the mix-

ing effectiveness using the same flow parameters and apparatus. Both mixers were at a distance of $0.92D_h$. Results from this study showed that mixing was almost completed at the plane where maximum static-pressure regain was first observed. The static pressure profile for this study with louvered type mixer shown in figure 2.1.

Unfortunately, there is no agreed method to calculate the mixing effectiveness. Robinson (2001) used a modified range mixing effectiveness method,

$$\text{Mixing Effectiveness} = (1 - \frac{T_{hot,downstream} - T_{cold,downstream}}{T_{hot,upstream} - T_{cold,downstream}}) \tag{2.1}$$

Important point to note is that he used averaged air temperature of the inlet airstream rather than the temperature measured prior to the mixing apparatus. Faison et al. (1966), defined the mixing effectiveness in their study in different way,

$$\text{Percent Effectiveness} = \frac{Max\Delta T_{upstream} - Max\Delta T_{downstream}}{Max\Delta T_{upstream}} \times 100, \tag{2.2}$$

where $Max\Delta T_{upstream}$ and $Max\Delta T_{downstream}$ refer to maximum temperature difference at upstream and downstream locations, respectively.

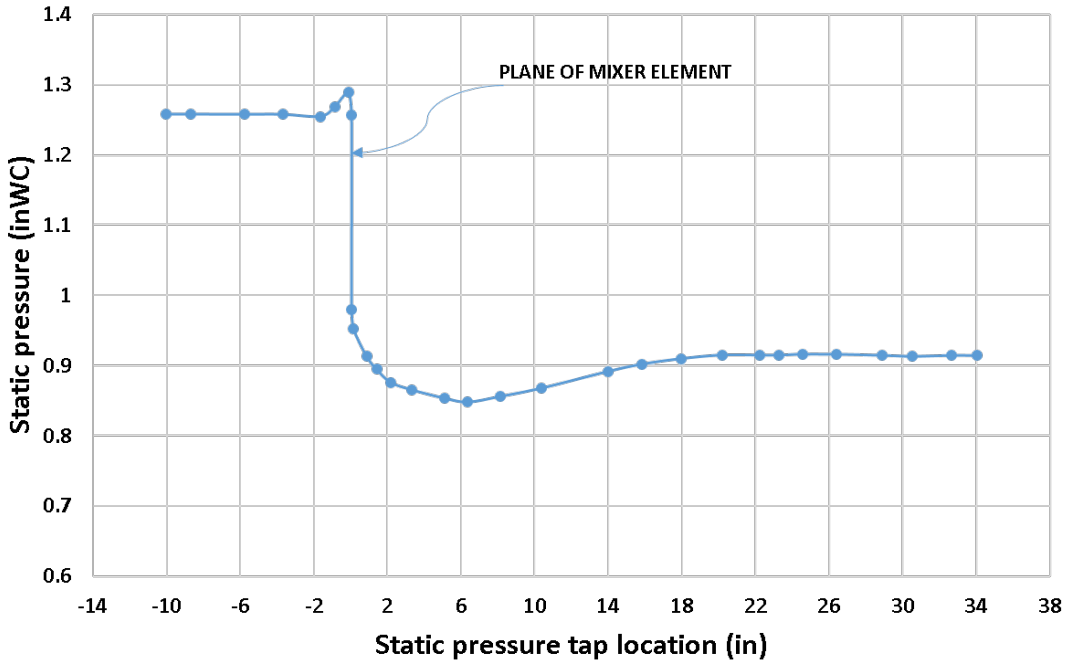

Figure 2.1: Static pressure profile for louvered mixer. Data for image: Faison et al. (1966)

Faison et al. (1967) performed another study at NIST using a similar apparatus but different type of mixer. In this study they used square edged orifice in combination with target which was a circular baffle to see the effect of mixing on temperature of air-stream which was initially non-uniform. Three different throat diameters were used (i.e., 8 inches, 12 inches, and 16 inches orifices). This mixing arrangement is shown in figure 2.2. Initial study was done without target. The result of this investigation showed that the orifice with 8 inches case (i.e., 0.33 duct hydraulic diameter) is more effective as compared to the other two cases as shown in figure 2.3. Static pressure profile for 12 inches throttle diameter orifice is shown in figure 2.4. Three different target sizes 8, 12 and 16 inches were used in combination with the same orifice of 12 inches to see the effect of target on the mixing effectiveness. From this study, it was also concluded that with the use of target there is no gain in mixing effectiveness. Faison et al. (1967) calculated the mixing effectiveness by using standard deviation approach instead of averaging which was used in their previous studies,

$$\text{Mixing Effectiveness} = \left(1 - \frac{S.D._{downstream}}{S.D._{upstream}}\right) \times 100 \tag{2.3}$$

.

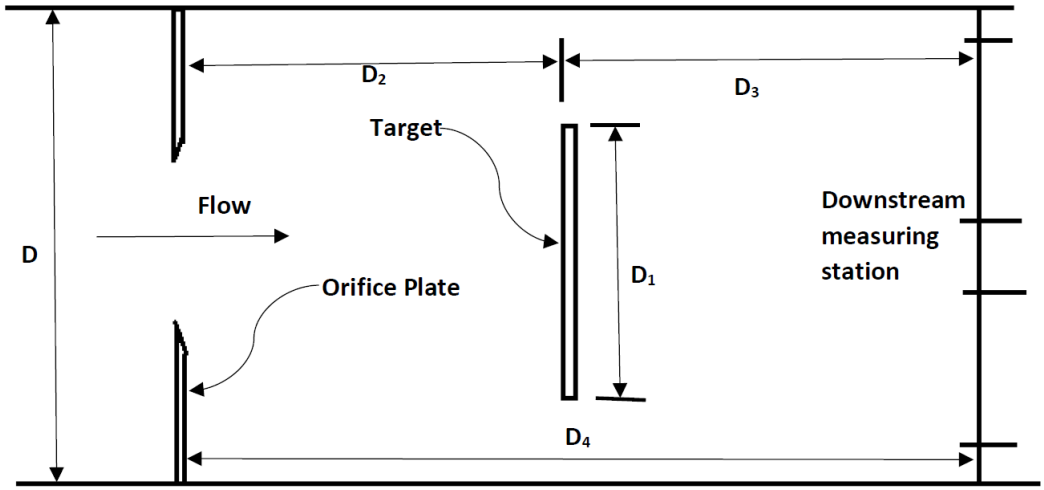

Figure 2.2: Orifice-target combination. Data points are extracted from the study Faison et al. (1967)

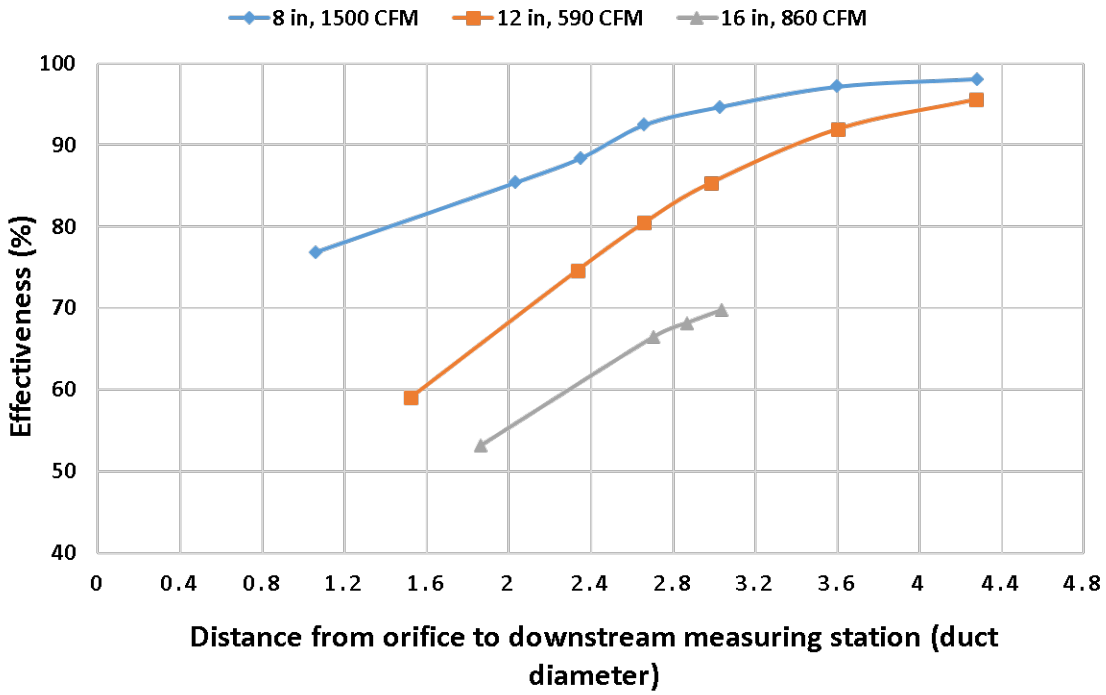

Figure 2.3: Mixing effectiveness for orifice-target combination. Data points are extracted from the study Faison et al. (1967)

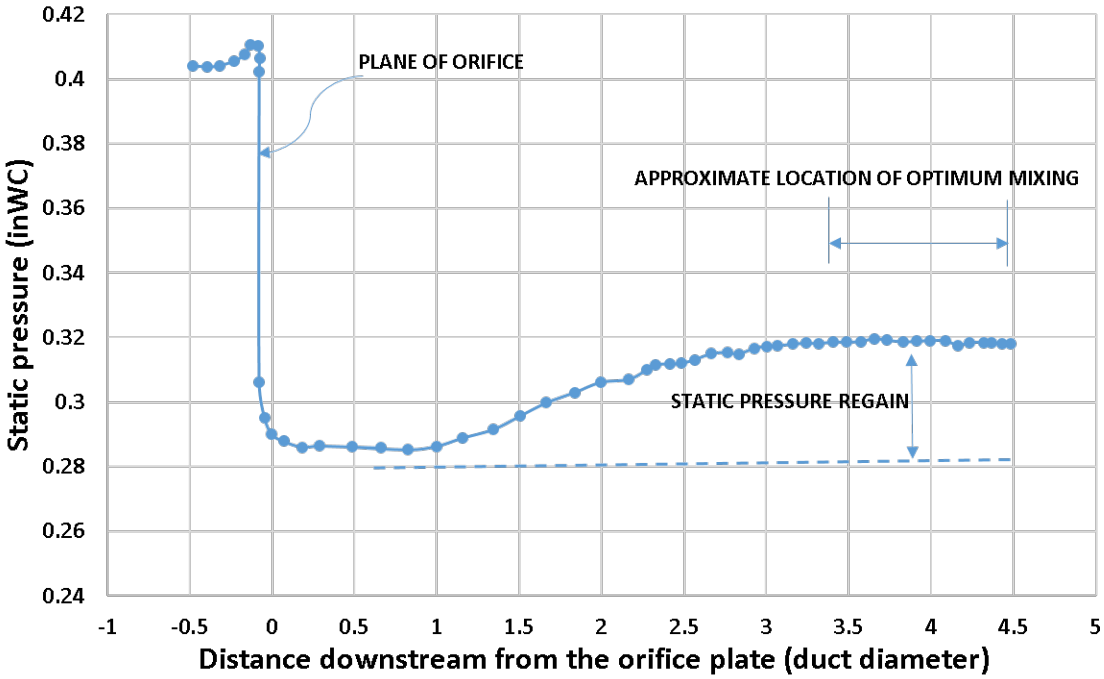

Figure 2.4: Static pressure profile for 12 inch orifice. Data points are extracted from the study Faison et al. (1967)

As a squeal of the same study at NIST in 1970, Faison et al. (1970) conducted few more experiments involving three louvered mixing devices with objective to reduce the thermal gradients within air stream. The three mixer were louvered, concentric louvers and louvered-baffles as shown in the figures 2.5, 2.6 and 2.7. They found that in case of louvered mixer the mixing effectiveness increased with increasing distance between mixers until the distance reached twice the hydraulic diameter of the duct then becoming constant thereafter. This is shown in the figure 2.8. For louvered-baffle the mixing effectiveness increased with increasing distance until the distance became equal to one hydraulic diameter, whereas for concentric mixers, the mixing effectiveness increased till two hydraulic diameter. Thereafter, mixing effectiveness started to decrease with increasing distance. All of this trend is presented in figure 2.9 and 2.10.

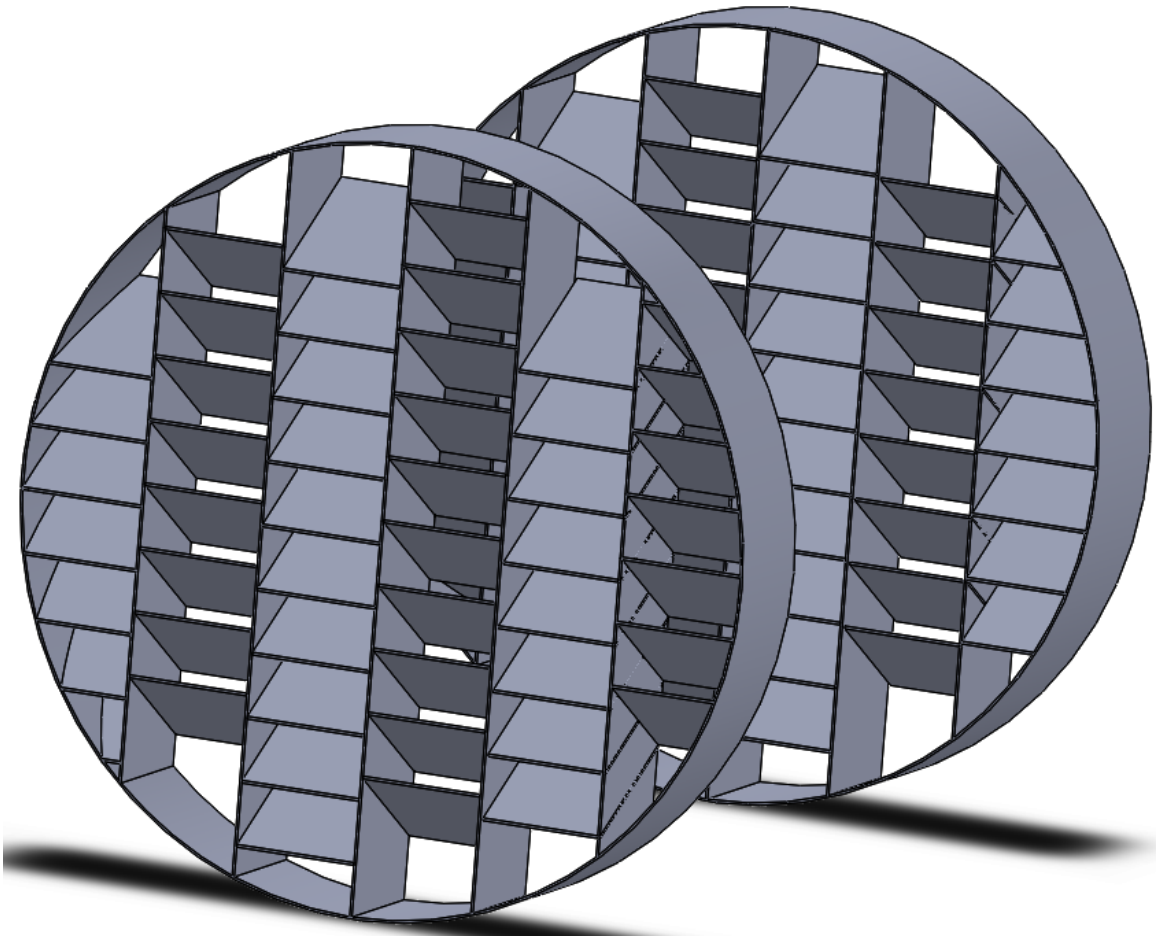

Figure 2.5: Louvered mixer similar to the mixer used by Faison et al. (1970)

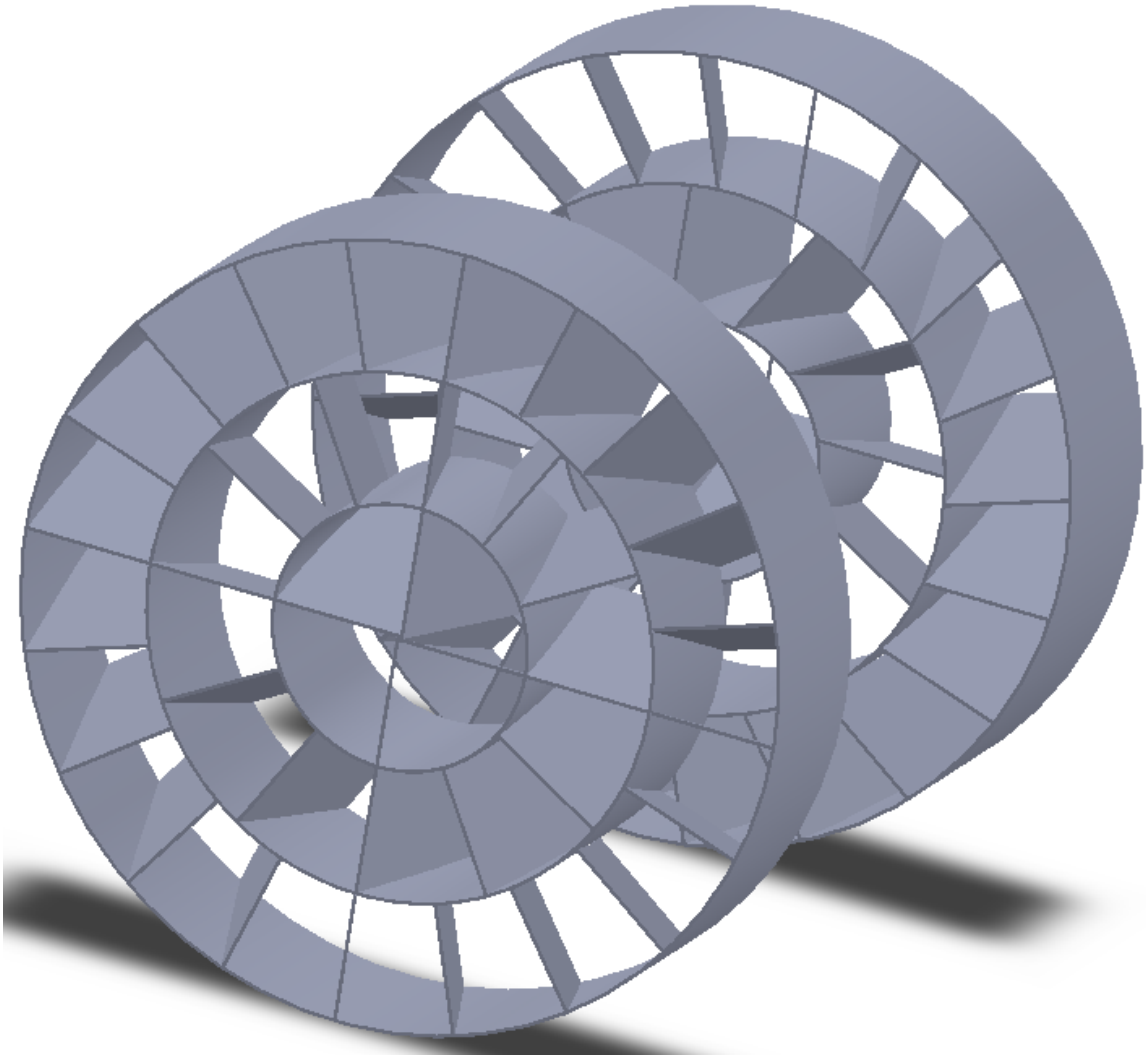

Figure 2.6: Concentric louvers similar to the mixer used by Faison et al. (1970)

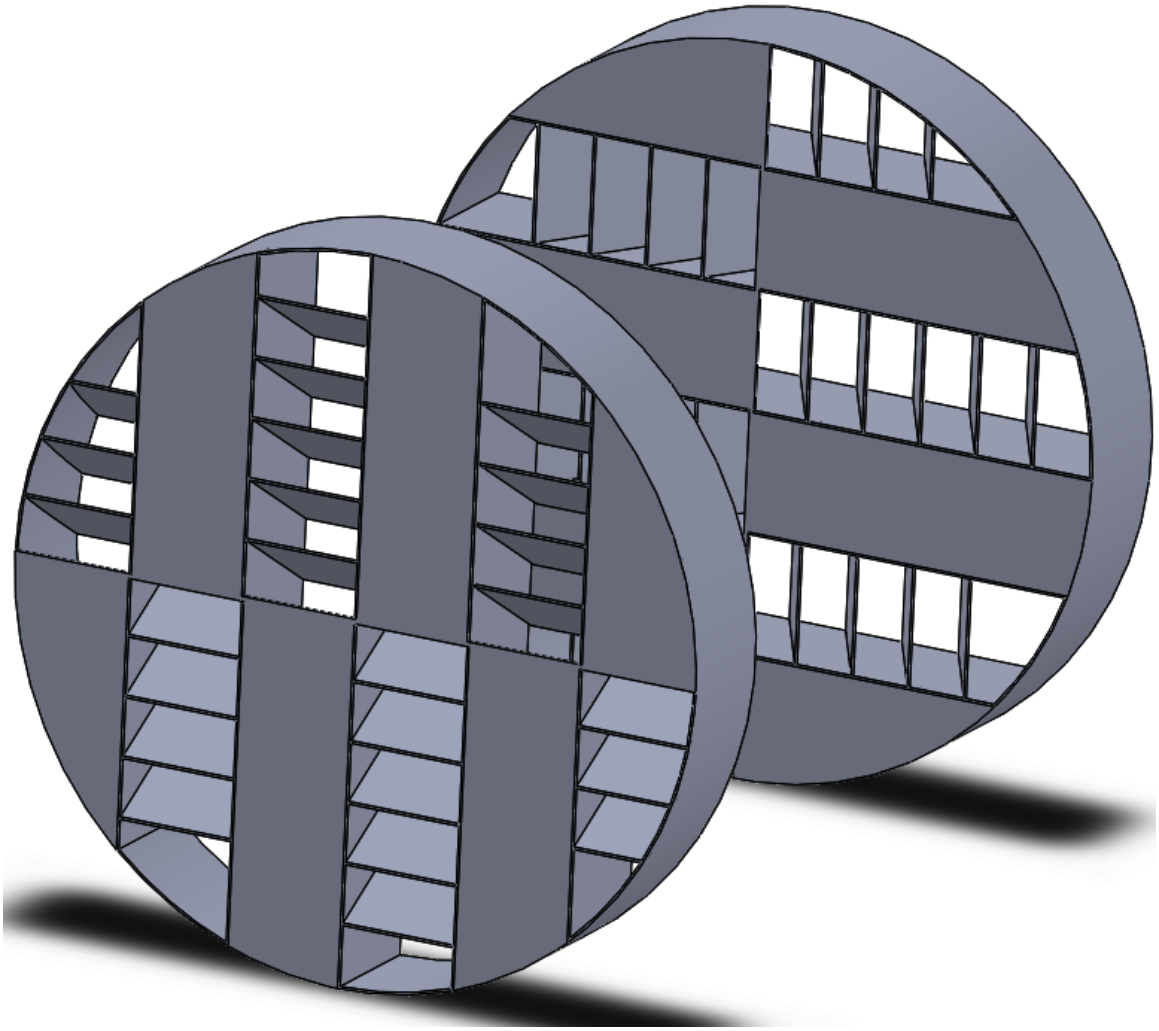

Figure 2.7: Louvered-baffles similar to the mixer used by Faison et al. (1970)

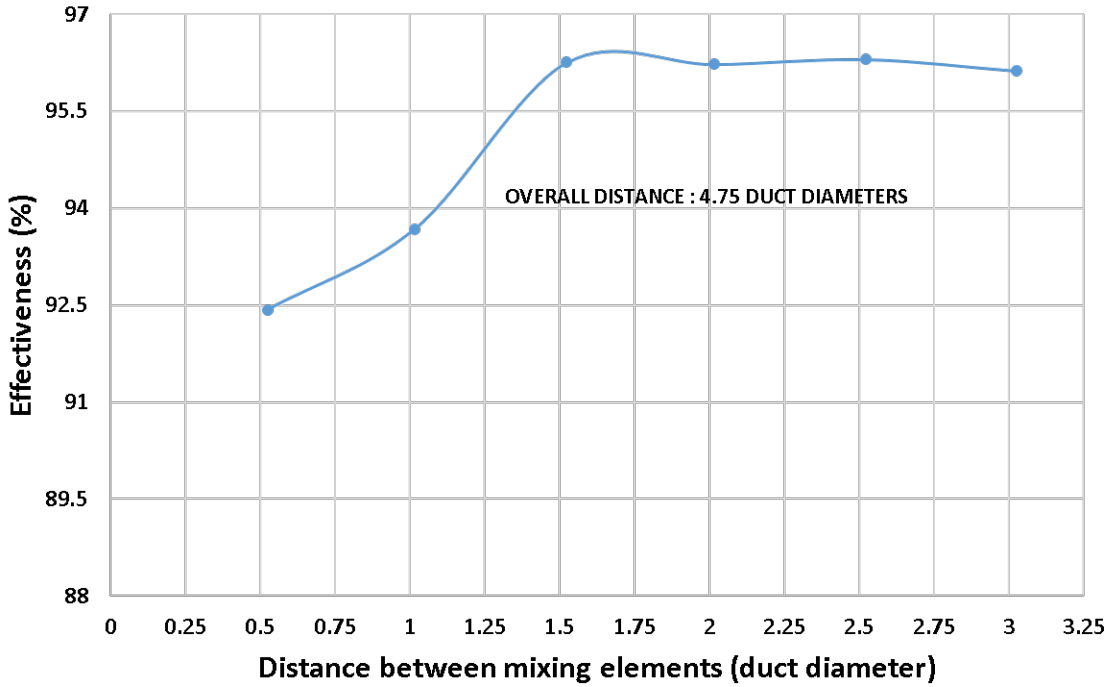

Figure 2.8: Mixing effectiveness louvered mixer relative to the distance between two mixers. Data points are extracted from the study Faison et al. (1970)

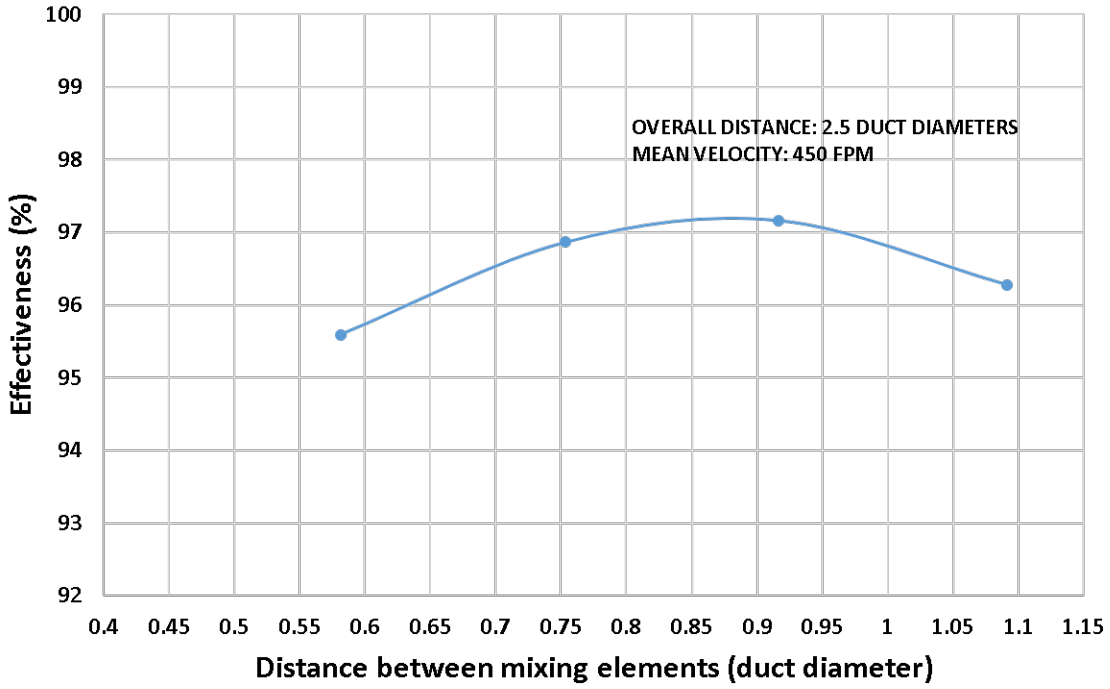

Figure 2.9: Mixing effectiveness louvered-baffle mixer relative to the distance between two mixers. Data points are extracted from the study Faison et al. (1970)

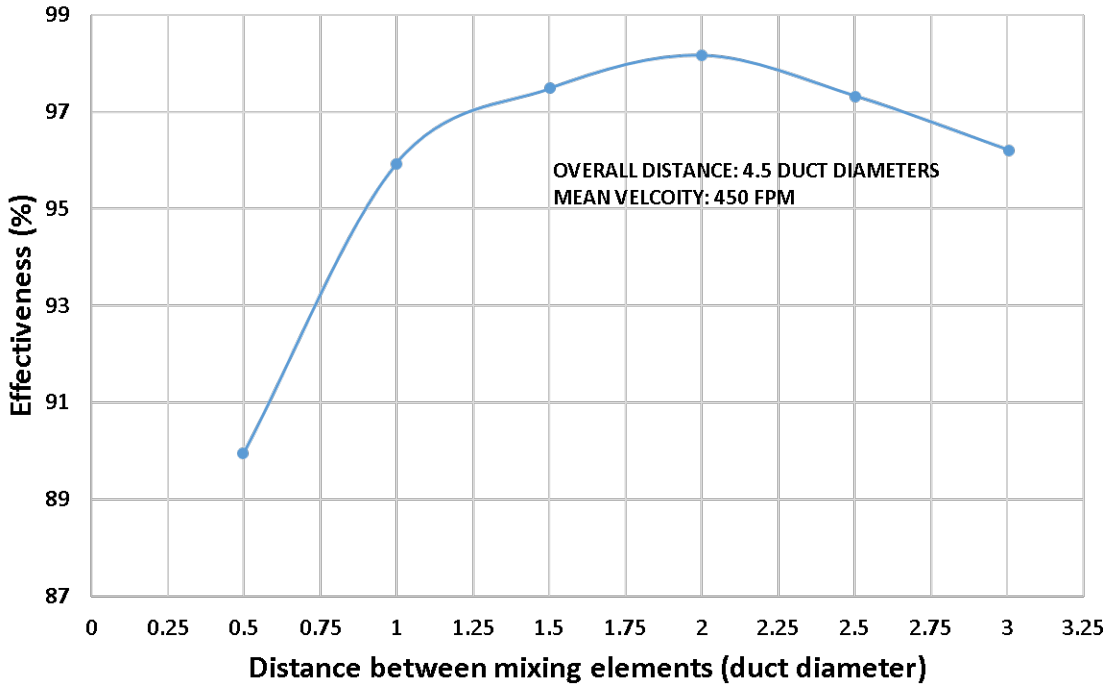

Figure 2.10: Mixing effectiveness concentric-louvered mixer relative to the distance between two mixers. Data points are extracted from the study Faison et al. (1970)

In the same study, the effect of louvered angle on mixing effectiveness was also investigated. It was seen that mixing effectiveness increased with the increasing angle until 60° with respect to the mean flow path. This corresponds to an increase of 30% with respect to the mixing at zero louvered angle. Further increase in angle decreased the mixing effectiveness. Results of this investigation is presented in the figure 2.11.

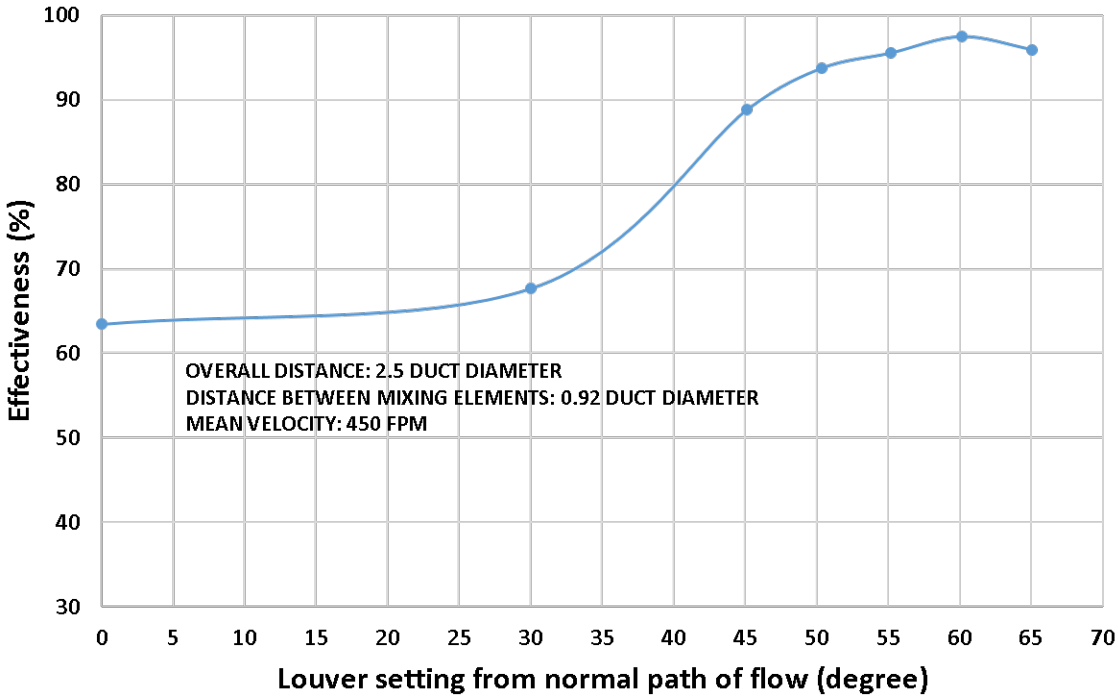

Figure 2.11: Relation of mixing effectiveness to the louvered angle for louvered-baffle mixer. Data points are extracted from the study Faison et al. (1970)

In an experimental study performed by Launder and Ying (1972), the emphasis was on the measurement of the turbulence-induced secondary flows in square ducts with equally roughened surfaces. Here the secondary flow is a substantially larger proportion of the axial flow than is the case in smooth-walled ducts. With the secondary velocities normalized by the friction velocity, however, the resultant profiles for smooth and rough surfaces are the same, within the precision of the measurements.

2.3 Computational Modeling

Advances in CFD and available computational resources have promised a renaissance in the analysis and understanding of complex flow patterns and heat transfer characteristics in indoor environments for optimizing thermal comfort and maximizing energy saving. In addition to the numerical methods of solving discrete mass, momentum, and energy equations, as well as prescribed boundary conditions, turbu-

lence modeling is a critical factor influencing the accuracy of the simulation results Xu (1998). Computational studies in an indoor space can be done at a variety of levels, depending on accuracy requirements and available computational resources: direct numerical simulation (DNS) considering all temporal and spatial fluctuations down to the Kolmogorov scale, Reynolds averaged Navier Stokes (RANS) equation modeling with a consideration of the average flow properties on coarser grids, and large eddy simulation (LES) modeling where the large scales are directly computed and small scales are modeled.

Most of the previous studies utilized the Reynolds averaged Navier Stokes (RANS) based turbulence models for indoor airflow simulations (Chen, 1995; Srebric et al., 1999; Wan and Chao, 2005; Zhai et al., 2007; Chen et al., 2012; Chiang et al., 2012; Pulat and Ersan, 2015). The computational cost of the RANS simulations is much lower that the equivalent DNS. However, the accuracy of RANS models can be questioned because RANS models cannot provide instantaneous information concerning high Rayleigh numbers turbulent flows, which is important for indoor airflow modeling and thermal comfort design. Although there is a vast literature on comparing several RANS models commonly offered in commercially available CFD software, including ANSYS Fluent, ANSYS CFX, STAR-CD and COMSOL, there is no consensus on the best Reynolds stress model among researchers (e.g., see Pulat and Ersan (2015) for a recent discussion).

On the other hand, LES is becoming an important and powerful tool in studying turbulence for indoor environment design. Previous comparative studies revealed that the LES approach provides a better agreement with experimental results than RANS models (Chen, 2000; Su et al., 2001; Abdilghanie et al., 2009; Liu and Novoselac, 2014). In addition to capturing the temporal and spatial turbulent fluctuations, the subgrid scale models in LES generally contain fewer empirical coefficient and artificial factors than those used in the Reynolds stress models of the RANS equa-

tions. However, RANS modeling approach is considered the state-of-the-art computational model in many HVAC systems, and therefore we utilize RANS computational paradigm in our study.

A CFD study has been performed by Zhai (2006) in building design, demonstrates its typical application in designing a thermally conformable, healthy and energy-efficient building. It is challenging to accurately calculate the mean and turbulence flow parameters of airflow in indoor environment, because both of these have errors, when calculated using CFD. These challenges were also discussed is the study done by Zhai (2006). In the study conducted by Shao and Riffat (1995), accuracy of the CFD approach was investigated. They found that the combination of the k-ϵ model and the higher order QUICK scheme produced the highest accuracy. Grid dependency tests showed that a relatively low grid density in the straight sections upstream/downstream of the duct fitting is sufficient but a higher density in the duct axis direction is required in the section containing the duct fitting.

In the study conducted by Ai and Mak (2013), experimental and numerical investigation is done for pressure losses across multiple fitting used in ventilation ducts. They found that pressure loss across multiple similar individual fittings is higher than that of single fitting, while the percentage increase is dependent on the configuration and combination of the fittings. This implies that the pressure loss across multiple similar individual fittings is higher than that across multiple interactive fittings, however configuration and combinations of the fittings influenced the percentage decrease of pressure loss. This shows that the pressure loss, provided in the ASHRAE handbook and the CIBSE guide, across multiple closely installed fittings is over predicted as it is calculated by summing the pressure loss across individual fittings.

A free and forced convection in both laminar and turbulent flows in a three dimensional duct is studied by Mokhtari et al. (2017). Different fins arrangement is made to see their influence on the heat transfer. In their model constant heat flux

condition is provided on the lower duct wall while keeping the others walls insulated. They found that heat transfer is highly improved by replacing simple fin arrangement with inclined fins. In turbulent flow the heat transfer increased 15-20% as compared to their base model while in laminar flow 40-50% increase was seen.

CHAPTER III

METHODOLOGY

3.1 Introduction

Computational fluid dynamics (CFD) studies can be divided into five steps when using commercial CFD packages. First step, is to define the geometry completely which is usually done in computer aided design (CAD) software. Second step is to divide the continuous geometric model with discrete domain which is called mesh and the process is called meshing. Third step, defining the physics which includes boundary conditions and solver settings. Fourth step is initialize the simulation. After getting the solution from solver package, fifth and the final step, is the post-processing which includes the analysis of results.

3.2 Geometry

For CFD analysis, fully defined geometry is very important, software those are used in these analysis cannot make any calculations unless the geometry is defined completely. Geometry can be classified as 1D, 2D, and 3D. In most of the industrial applications, we have 3D models to study flow behaviour because all of the three parameters are comparable to each other. Before using the 2D geometry for industrial purpose, it is important to validate that 2D simplification is applicable and will not disguise the 3D flow phenomena. The simplification is done to reduce the use of computational resources.

Most of the available CFD solvers do not have powerful modelling packages because this complex CAD modelling is mostly done in other software like SolidWorks.

These models are then imported to the solver package. There are few more problems those are associated with the importing the file. Different solver support different file format of the CAD model. For example, 3D-CAD model of Star-CCM+ support the following models *.sldprt*/*.sldasm* - SolidWorks files, $.x_t/.x_b$ - Parasolid Transmit files, *.step*/*.stp* - STEP files, and *.iges*/*.igs* - IGES files etc. These solvers have their own geometric tolerance. It is very important to have the same geometric tolerance for CAD software and solver package to avoid geometric error.

On the other hand, some meshing software provide option to check the validity and repair invalid bodies before importing the CAD model. For example, In star-CCM+ it is recommended to enable the *check the part's validity* option. But about *repair invalid bodies* the box should be unchecked. If it is enabled software will try to repair the model itself and can destroy the shape of the CAD model which is not required for analysis.

Geometry clean-up is another important step in pre-processing of CFD simulations. Due to availability of advanced computational tool detailed CAD models are designed to get the complete idea of product model. Due to this detail designs, these models may contain unwanted or irrelevant features those are not important for CFD analysis. It is important to remove unnecessary detail from CAD model, those are either not important or feasible for CFD simulations. Defeaturing or removal of these unwanted details require ample user interaction (Quadros and Owen, 2009). Few meshing packages provides specialized tools to remove these details to reduce the effort and time of users, in case of Star-CCM+ surface repair tool option for surface wrapper. It is preferable to clean the CAD model in the same software in which it is created. In case of ANSYS-Fluent meshing, it is relatively easy to extract the required parts from the whole geometry. Once geometry clean-up is done, meshing process becomes very easy and smooth.

3.3 Meshing

Mesh is the discrete representation of the geometric model. It has a considerable impact on the convergence rate, accuracy of the solution, and computational time. Meshing process can be classified into three categories based on the topology of the cells/elements that fill the domain. These three categories are structured or block as shown in figure 3.1, unstructured as shown in figure 3.2 and hybrid/multi-block. Elements have the topology of a regular grid in structured mesh as shown in figure 3.1. It require more effort and expertise to generate but easier to compute. Selection of mesh topology is based on the shape of the geometry and underlying physics of the problem.

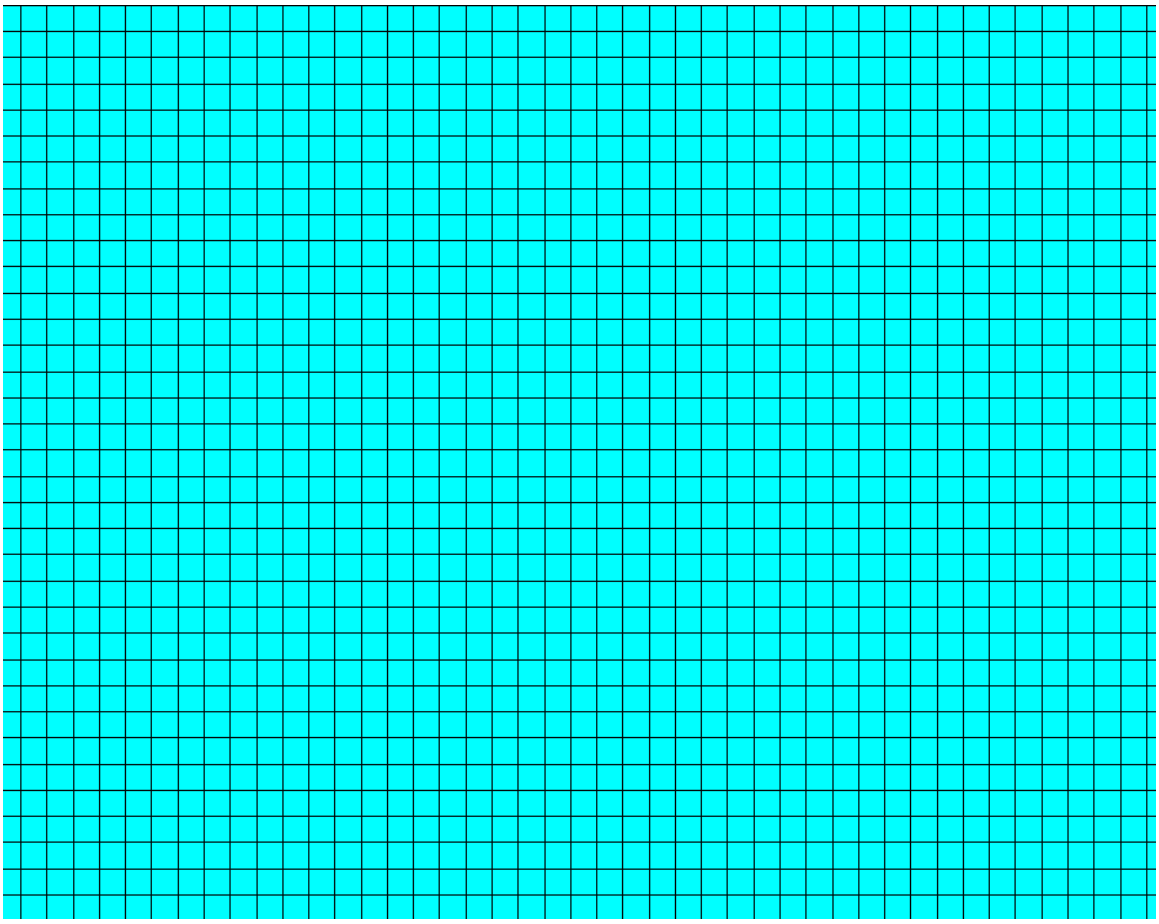

Figure 3.1: Structured mesh

Different element shapes are used in different type of cell. Quadrilateral ele-

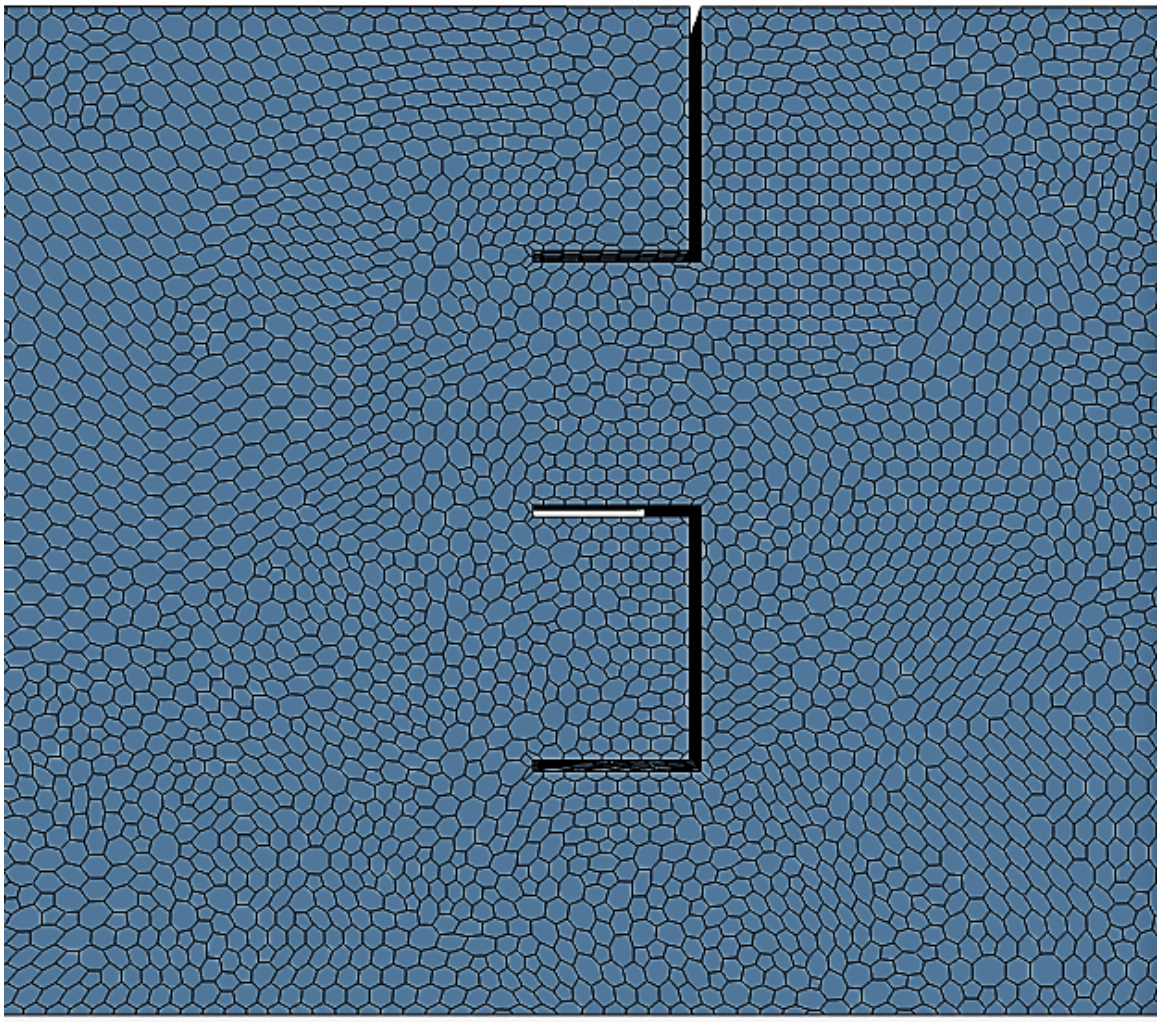

Figure 3.2: Unstructured mesh

ments are used in 2D and hexahedral in 3D for structured grid. For unstructured grid Quadrilateral and triangular for 2D and tetrahedral, pyramid, hexahydral and dedocahydral in 3D. Although structured grid have better numerical accuracy and occupy less memory but it is not always feasible to generate structure grid because of complex geometry. A hybrid grid structure mesh is generated where geometry and simple and unstructured for complex part of the geometry. It is very important to handle the mesh elements near wall to ensure that y+ values are within a range for a particular turbulence model. Mesh quality is measured on the basis of skewness, smoothness and aspect ratio of the cells. Skewness is measured on the basis of nor-

malized equilateral angle, smoothness is based on the gradual change in size of mesh elements and aspect ratio is the ratio of longest to shortest edge length.

3.4 Physical Settings

Solver provides wide range of physics models and methods to simulate single and multi-phase flows for different disciplines, for example, heat transfer, aeroacoustics, and other related phenomena. This step can be further divided into two steps, mathematical modeling and numerical analysis. Mathematical modeling is implementing the governing differential equations (conservation of mass, momentum, and energy) correctly with suitable boundary conditions. It seems very simple and straightforward, but in fact it is most challenging and difficult task when using CFD.

The governing differential equations can be solved using three different numerical methods, finite difference method (FDM), finite element method (FEM) and finite volume method (FVM). FDM is the oldest method to solve PDEs numerically, main disadvantage of it is the limitation of the simple geometry if the flow is complex. Because of this, nowadays most of the commercial software are using FEM and FVM. This FVM transform governing equation to a set of algebraic equation by discretizing these equations in space and time.

Flows are categorized as laminar and turbulent. Turbulent flows are of more interest for engineers and scientist. Flow properties are irregularly fluctuating in turbulent flows. These fluctuations are happening at small scales with high frequencies and resolving these in space and time requires excessive computational costs. To reduce the computational cost, these quantities are solved for averaged or filtered and approximation is made for the impact of the small fluctuating structures. Different turbulent models are available for the approximation of these fluctuating quantities. For example, the turbulence models that are implemented in STAR-CCM+ can be subdivided into two categories: (i) Reynolds-averaged Navier-Stokes (RANS) turbulence models,

and (ii) scale-resolving simulations such as large eddy simulations (LES) and detached eddy simulations (DES).

3.5 Post-processing and Visualization

This is the final step for CFD simulations. In this step, results obtained from the solver are analyzed to get the complete insight of the of these results. Different methods like contour plots, vector plots, streamlines, as well as various data curves/lines or representations are used for appropriate graphical representations and report. Most of the solvers have their own post-processing tool, but if required data can be exported to other tools.

CHAPTER IV

DESCRIPTION OF AIR-MIXER

In literature, less information is available about the dimensions of the air-mixer used for research purpose in the past. Due to this reason, dimensions selected in this study are based on the current industrial and research requirement. Engineering drawings with full dimensions of the geometries are shown in appendix, figures A.1- A.5. Few assumptions have been made to simplify the geometry. For example, in experiments there is a small gap between mixer's wall and duct's wall to move the mixer which is removed for computational purpose. Second assumption is the thickness of the sheet (0.2 inch) which is different from industrial practice. For example, SMACNA used 0.05 inch thickness for duct length of 122 inches. This assumption is made to reduce number of the mesh elements. For meshing, smallest cell size must be equal to the smallest part of the model to capture the details of that part. It not only decrease the mesh size but also the computational time.

4.1 Geometric Models

In the first phase, temperature mixing effectiveness is studied without any mixing device for the Geometry-1 used is shown in figure 4.1. The purpose of the mid wall is to allow both air-streams to get fully developed flow before interacting each other. For further investigations, this geometric dimensions are kept constant. In Geometry-2 as shown in the figure 4.2, louver-baffle mixer is added. For this geometry, parametric study is done to see the see the effect of louver angles on the mixing effectiveness. Another model as shown in figure 4.3 is also investigated, in this model two louver-

baffle mixers are used. In this model, all louvers are at 45° angle. The orientation of the second mixer is at 90 degree to the first mixer. Moreover, second mixer is place at different distance to see the effect of distance between the mixer on the mixing effectiveness. In the fourth model as shown in the figure 4.4, louver-baffles mixer is replaced with louvers mixer. Orifice-target mixer is also modeled as shown in the figure 4.5, in this geometric model orifice diameter is selected as a parametric model to see its effect on the mixing effectiveness. The last geometric model which is used in this study is the removal of target plate from Geometry-5 to see how mixing effectiveness is influenced with the use of perforated plate. This geometric model is shown in figure 4.6.

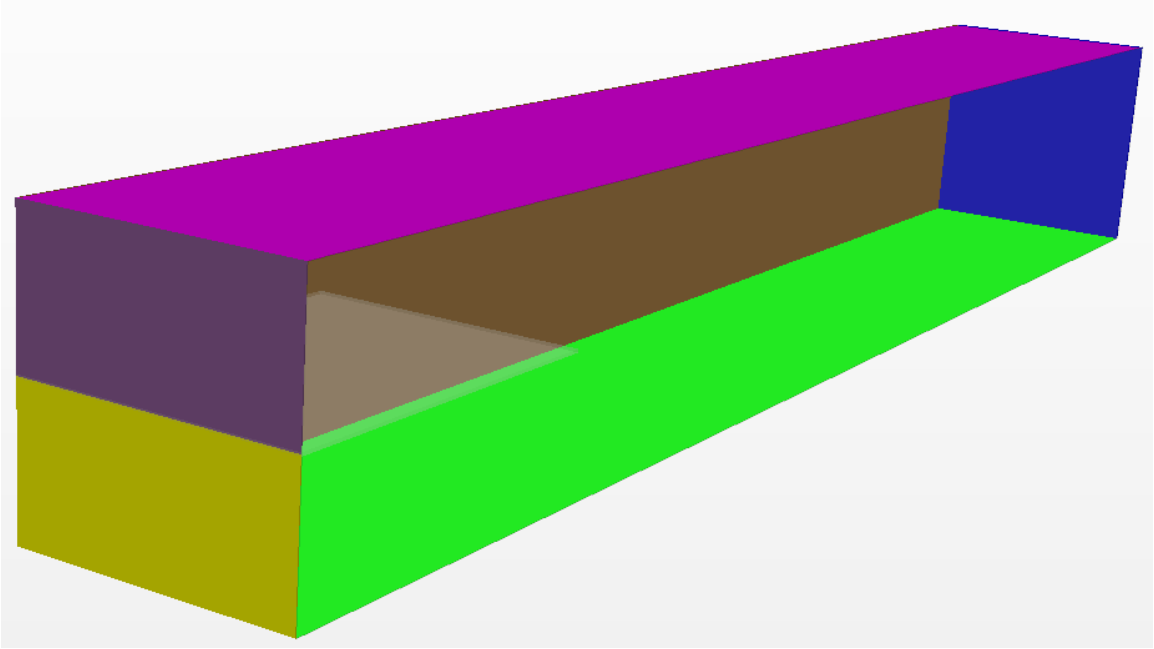

Figure 4.1: Geometry-1: duct with mid-wall

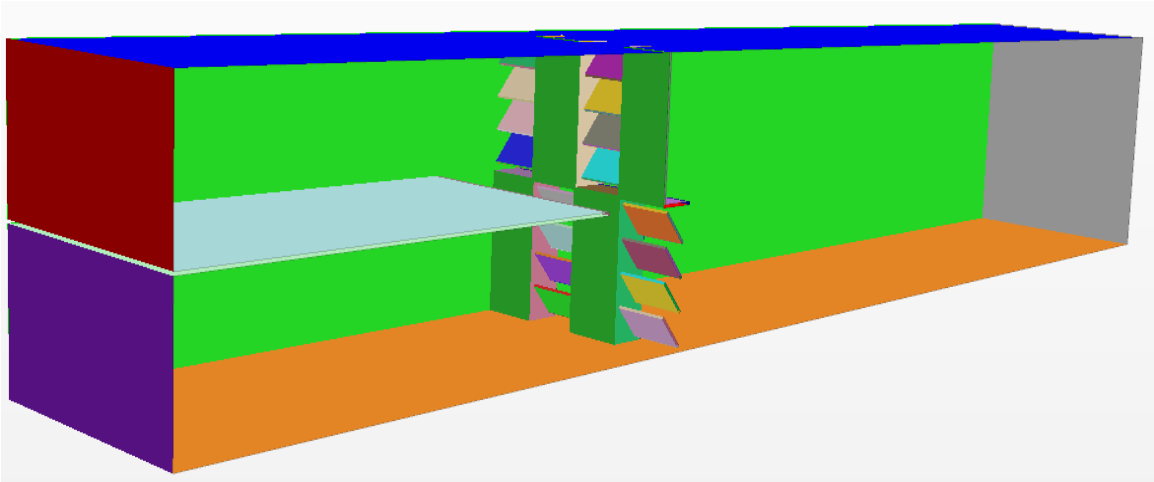

Figure 4.2: Geometry-2: duct with louver-baffle mixer

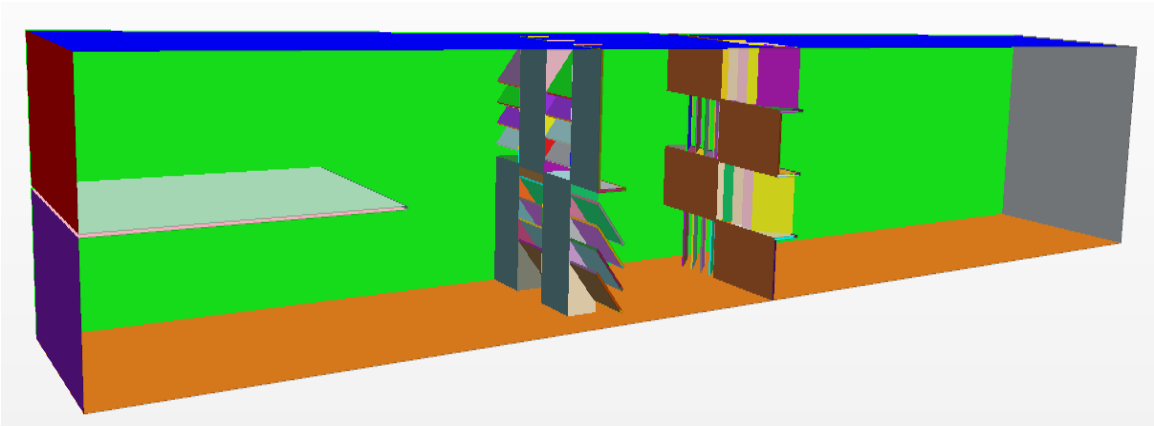

Figure 4.3: Geometry-3: duct with two louver-baffle mixers

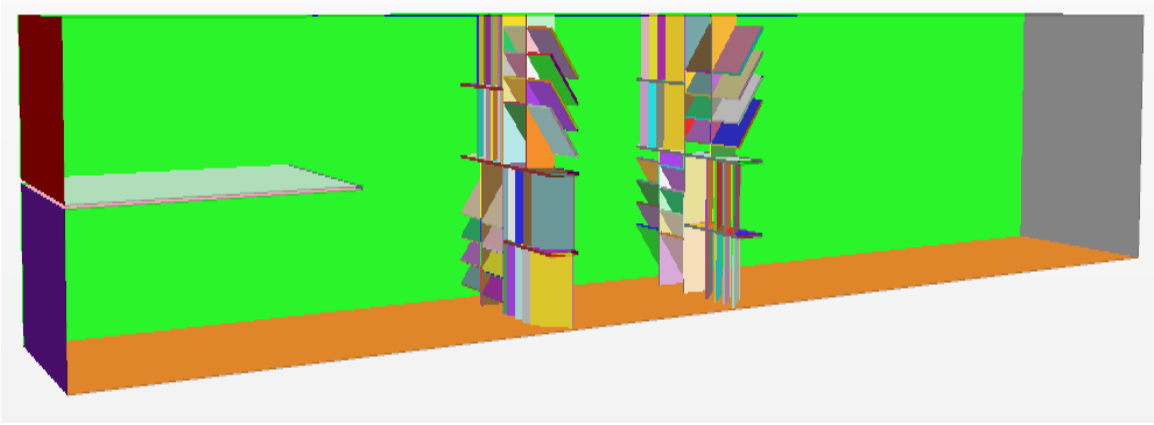

Figure 4.4: Geometry-4: duct with two louver mixers

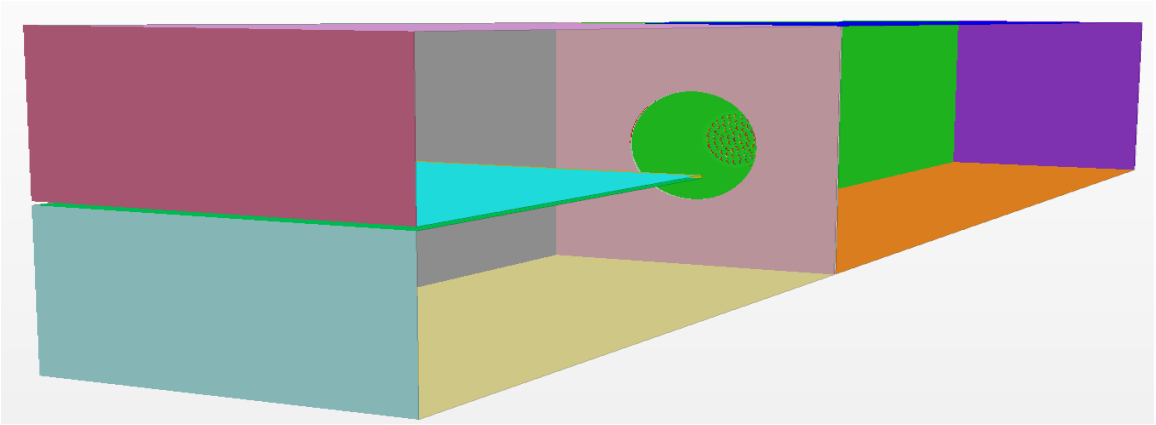

Figure 4.5: Geometry-5: duct with orifice-target mixer

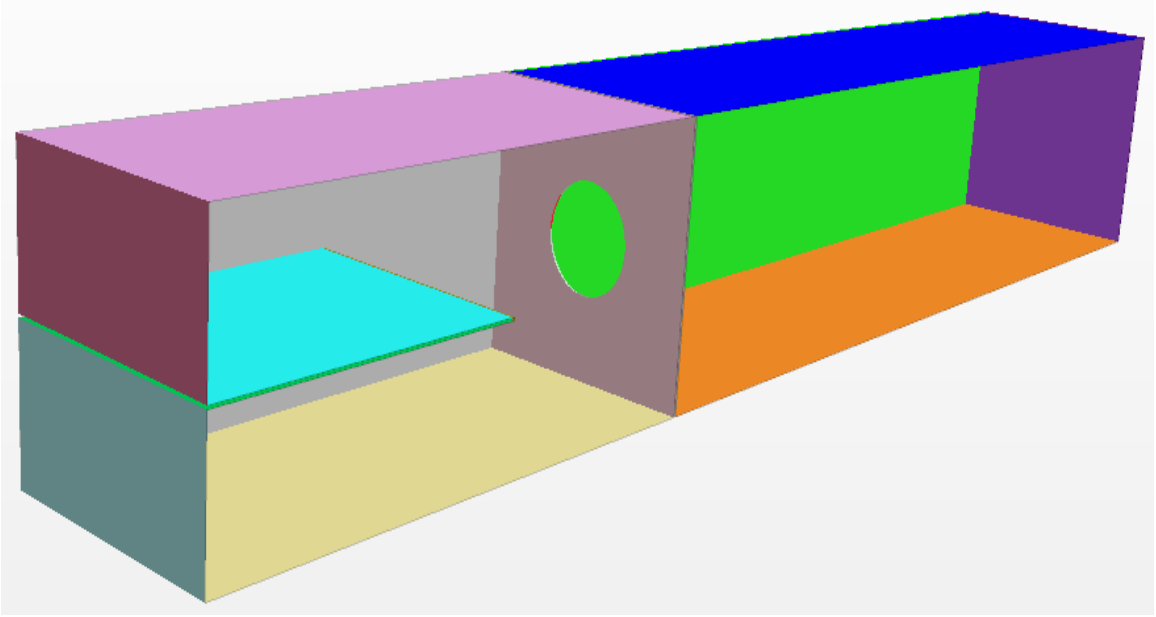

Figure 4.6: Geometry-5: duct with orifice mixer

4.2 Meshing

Due to complex geometries unstructured mesh is used to reduce meshing and computational time. Star-CCM+ software is used for mesh generation and as a solver. Different base sizes, target surface sizes and first prism layer heights are tried for mesh dependence study to get an acceptable Y+ for k-ω turbulence model. The acceptable value of Y+ for k-ω turbulence model is less than 1. For the visual purpose coarse,

medium and fine meshes, those are used for mesh dependence study of Geometry-2 are presented in figures 4.7- 4.9.

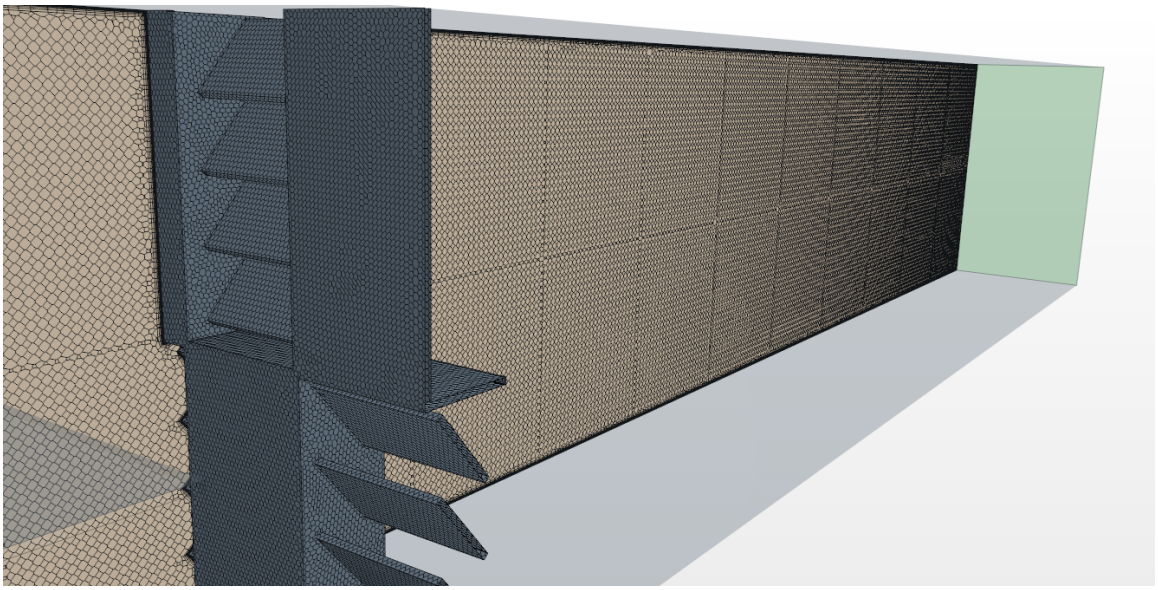

Figure 4.7: Coarse mesh

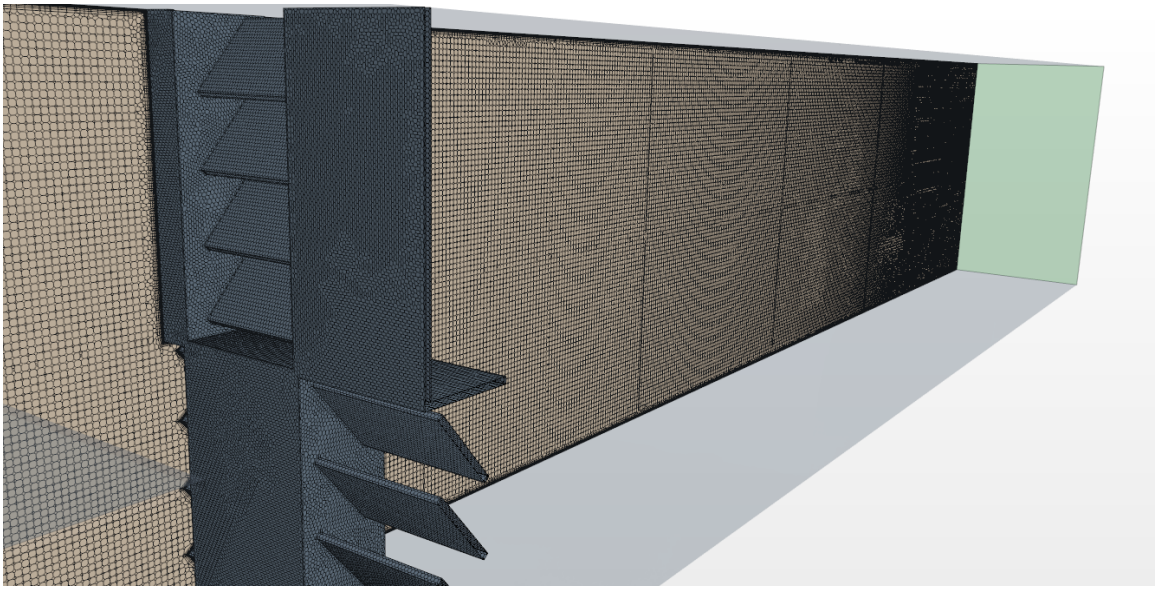

Figure 4.8: Medium mesh

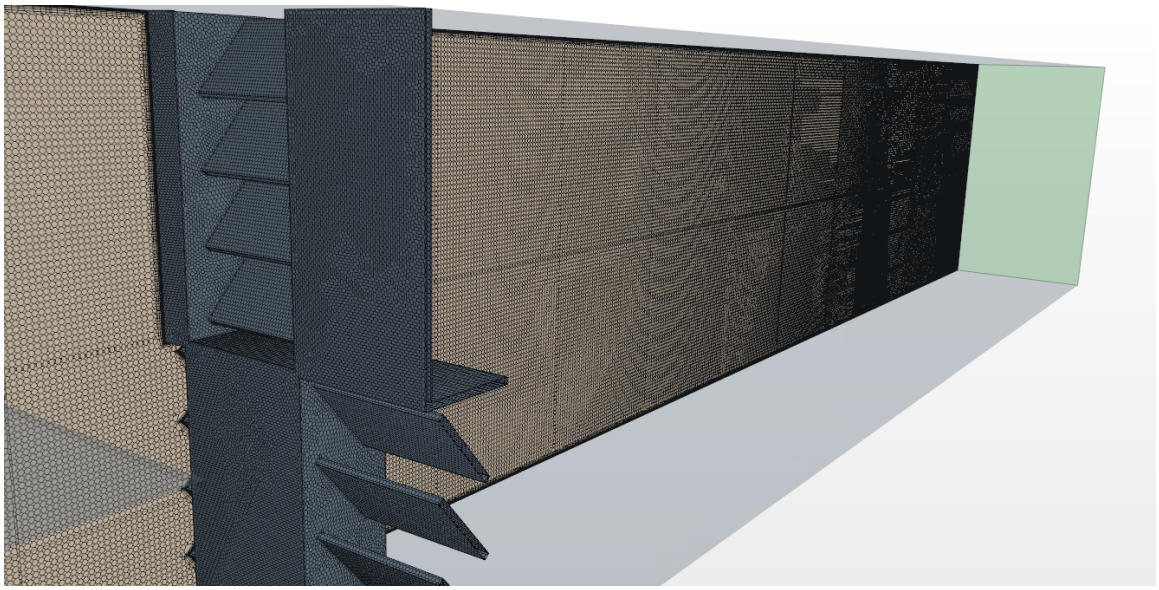

Figure 4.9: Fine mesh

Summary of important meshing parameters those are used for mesh generation for Geometry-1, Geometry-2, and Geometry-5 are mentioned in tables 4.1- 4.3 respectively. The number of mesh cells are different for different geometries, for example, for Geometry-5 total number of cells are approximately equal to 21 million. From mesher selection: surface mesher, polyhedral and prism layer meshers are selected. For prism layer mesher, geometric progression is used as a stretching function and wall thickness is used as a distribution mode. For Geometry-1, surface control mesh is taken at mid-wall. For Geometry-2 and Geometry-5 all surfaces of air mixers are added in surface control mesh. In addition to these settings, custom control settings for mixers are used for example, in case of curves of orifice and target plate, curvature option is enabled which use maximum cells by using the smallest size required to follow the curves during mesh generation. For control volume mesh, a block of 100 inches length is generated which started from 22 inches duct length to outlet of the duct.

Table 4.1: Meshing parameters for Geometry-1.

Mesher	Surface remesher	Default	
	Polyhedral mesher	Default	
	Prism layer mesher	Stretching function	Geometric progression
		Distribution mode	Wall thickness
		Gap fill percentage	25
		Minimum thickness percentage	10
		Layer reduction percentage	50
Default control	Base size		1 inch
	Target surface size	Relative to base	30%
	Minimum surface size		10%
	Surface growth rate		1.1
	Number of prism layer		15
	Prism layer near wall thickness		0.01 mm
	Prism layer total thickness	Absolute	5 mm
Custom control	Surface control	Target surface size(relative to base)	5%

Table 4.2: Meshing parameters for Geometry-2.

Mesher	Surface remesher	Default	
	Polyhedral mesher	Default	
	Prism layer mesher	Stretching function	Geometric progression
		Distribution mode	Wall thickness
		Gap fill percentage	25
		Minimum thickness percentage	2
		Layer reduction percentage	10
Default control	Base size		1 inch
	Target surface size	Relative to base	30%
	Minimum surface size		10%
	Surface growth rate		1.1
	Number of prism layer		15
	Prism layer near wall thickness		0.01 mm
	Prism layer total thickness	Absolute	5 mm
Custom control	Surface control	Target surface size(relative to base)	10%
Volume control	Surface remesher	Relative to base	20%

Table 4.3: Meshing parameters for Geometry-5.

Mesher	Surface remesher		Default
	Polyhedral mesher		Default
	Prism layer mesher	Stretching function	Geometric progression
		Distribution mode	Wall thickness
		Gap fill percentage	25
		Minimum thickness percentage	2
		Layer reduction percentage	10
Default control	Base size		1 inch
	Target surface size	Relative to base	30%
	Minimum surface size		10%
	Surface growth rate		1.1
	Number of prism layer		15
	Prism layer near wall thickness		0.01 mm
	Prism layer total thickness	Absolute	5 mm
Custom control	Surface control	Target surface size(relative to base)	10%
Volume control	Surface remesher	Relative to base	20%

4.3 Solver Settings

All simulations are done as steady state in time. Ideal gas is taken as a fluid. To model fluid energy, segregated fluid temperature approach is selected. This approach calculate the total energy equation with temperature as the solved variable later enthalpy is calculated from temperature with respect to the equation of state. The k-ω turbulence model is selected with all-y+ treatment and exact wall distance options enabled. This all-y+ treatment is a hybrid method that mimic the high-y+ wall treatment for coarse mesh and low-y+ treatment for fine mesh. For boundary conditions, mass flow inlet is chosen for both hot and cold airstreams at both inlets of the duct and pressure outlet boundary condition is taken at outlet the outlet of the duct. No-slip boundary condition is taken for all other surfaces including mid-wall. Gravity effect is not considered in this study.

Quantitative values of different meshes for Geometry-1, 2 and 5 are shown in tables 4.4 - 4.6 respectively and the plots are shown in figures 4.10 - 4.12 respectively. Equation 4.1 is used to calculate the temperature mixing effectiveness.

$$\text{Temperature Mixing Effectiveness} = \left(1 - \frac{S.D._{downstream}}{S.D._{upstream}}\right) \times 100 \tag{4.1}$$

where

$$\text{Standard Deviation (S.D.) of Temperature} = \sqrt{\frac{\sum_i (T_{f,i} - \bar{T})^2 A_{f,i}}{\sum_i A_{f,i}}} \tag{4.2}$$

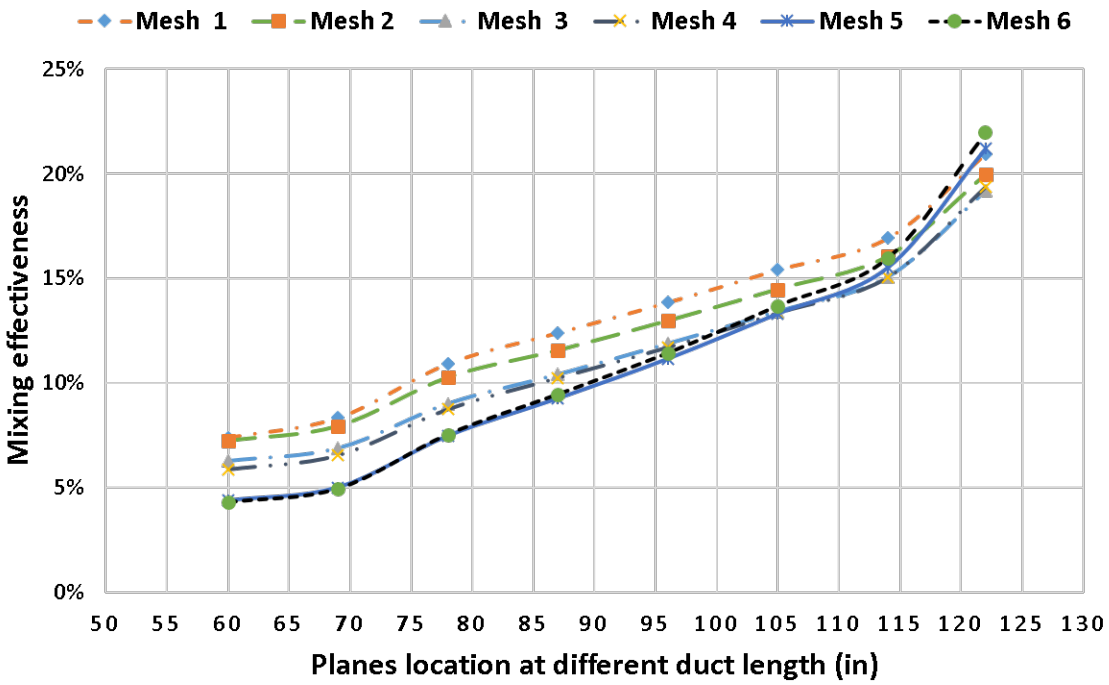

Figure 4.10: Grid independence plot for Geometry-1 with cold airstream at 65 °F and 400 CFM and hot airstream at 85 °F and 1600 CFM.

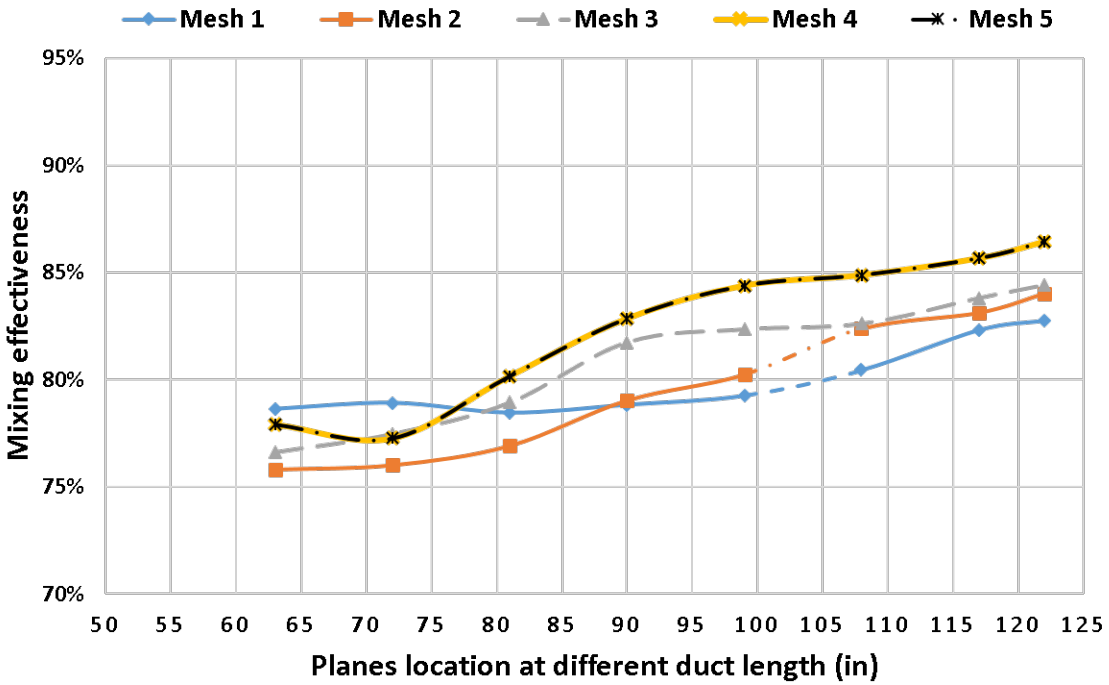

Figure 4.11: Grid independence plot for Geometry-2 with cold airstream at 65 °F and 400 CFM and hot airstream at 85 °F and 1600 CFM. Mixer is located at 42 inches distance from the inlet of the duct

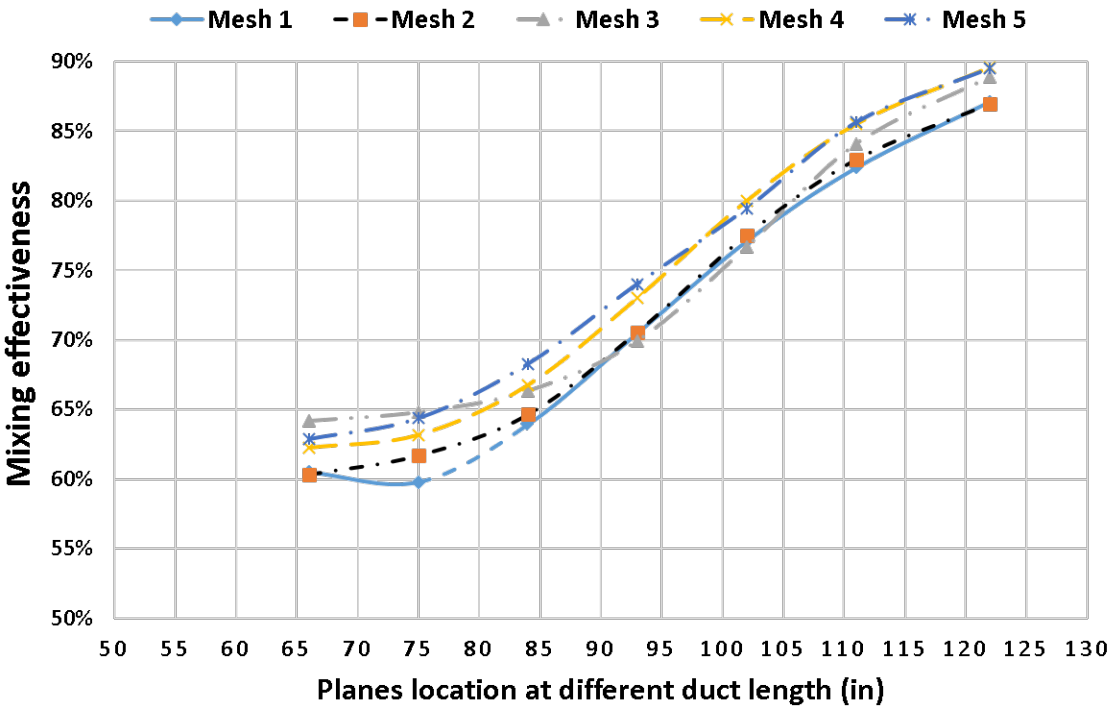

Figure 4.12: Grid independence plot for Geometry-5 with cold airstream at 65 °F and 1000 CFM and hot airstream at 85 °F and 1000 CFM. Orifice is located at 42 inches distance from the inlet of the duct and target plate is at 48 in distance from the duct

Table 4.4: Grid dependence for Geometry-1 (no mixer) with cold airstream at 65 °F and 400 CFM and hot airstream at 85 °F and 1600 CFM.

Name		Inlet	Plane 1	Plane 2	Plane 3	Plane 4	Plane 5	Plane 6	Plane 7	Outlet
	Location of Plane (inch)	0	60	69	78	87	96	105	114	122
Mesh 1	S.D. of Temp. (F)	10.01	9.27	9.17	8.91	8.77	8.62	8.47	8.31	7.91
	Mixing Effectiveness (%)		7.4	8.3	10.9	12.4	13.8	15.4	16.9	20.9
Mesh 2	S.D. of Temp. (F)	10.01	9.28	9.21	8.98	8.85	8.71	8.56	8.40	8.011
	Mixing Effectiveness (%)		7.2	7.9	10.3	11.6	13.0	14.5	16.1	19.9
Mesh 3	S.D. of Temp. (F)	10.01	9.38	9.32	9.11	8.97	8.82	8.67	8.50	8.09
	Mixing Effectiveness (%)		6.3	6.9	9.0	10.4	11.9	13.4	15.1	19.2
Mesh 4	S.D. of Temp. (F)	10.01	9.42	9.35	9.13	8.98	8.84	8.67	8.50	8.07
	Mixing Effectiveness (%)		5.9	6.5	8.7	10.2	11.7	13.3	15.1	19.4
Mesh 5	S.D. of Temp. (F)	10.01	9.57	9.51	9.26	9.08	8.89	8.68	8.46	7.89
	Mixing Effectiveness (%)		4.4	5.0	7.5	9.3	11.1	13.3	15.5	21.2
Mesh 6	S.D. of Temp. (F)	10.01	9.58	9.51	9.25	9.06	8.86	8.64	8.41	7.81
	Mixing Effectiveness		4.3%	4.9%	7.5%	9.5%	11.4%	13.7%	16%	21.9%

Table 4.5: Grid dependence for Geometry-2 with cold airstream at 65 °F and 400 CFM and hot airstream at 85 °F and 1600 CFM. Mixer is located at 42 inches distance from the inlet of the duct

Name		Inlet	Plane 1	Plane 2	Plane 3	Plane 4	Plane 5	Plane 6	Plane 7	Outlet
	Location of Plane (inch)	0	63	72	81	90	99	108	117	122
Mesh 1	S.D. of Temp. (F)	9.92	2.12	2.09	2.14	2.10	2.06	1.94	1.76	1.71
	Mixing Effectiveness (%)		78.6	78.9	78.5	78.8	79.2	80.4	82.3	82.7
Mesh 2	S.D. of Temp. (F)	9.87	2.39	2.37	2.28	2.07	1.95	1.74	1.67	1.58
	Mixing Effectiveness (%)		75.8	76.0	76.9	79.0	80.2	82.4	83.1	84.0
Mesh 3	S.D. of Temp. (F)	9.96	2.33	2.24	2.10	1.82	1.76	1.73	1.61	1.55
	Mixing Effectiveness (%)		76.6	77.5	78.9	81.7	82.3	82.6	83.8	84.4
Mesh 4	S.D. of Temp. (F)	9.89	2.18	2.25	1.96	1.70	1.54	1.50	1.42	1.34
	Mixing Effectiveness (%)		77.9	77.3	80.2	82.8	84.4	84.9	85.7	86.4
Mesh 5	S.D. of Temp. (F)	10.02	2.40	2.24	2.07	1.62	1.56	1.41	1.49	1.50
	Mixing Effectiveness (%)		77.9	77.3	80.2	82.8	84.4	84.9	85.7	86.4

Table 4.6: Grid dependence for Geometry-5 with cold airstream at 65 °F and 1000 CFM and hot airstream at 85 °F and 1000 CFM. Orifice is located at 42 inches distance from the inlet of the duct and target plate is at 48 in distance from the duct.

Name		Inlet	Plane 1	Plane 2	Plane 3	Plane 4	Plane 5	Plane 6	Outlet
	Location of Plane (inch)	0	66	75	84	93	102	111	122
Mesh 1	S.D. of Temp. (F)	10.00	3.95	4.02	3.61	2.95	2.29	1.76	1.29
	Mixing Effectiveness (%)		60.5	59.8	63.9	70.5	77.1	82.4	87.1
Mesh 2	S.D. of Temp. (F)	10.00	3.97	3.83	3.54	2.94	2.25	1.71	1.31
	Mixing Effectiveness (%)		60.3	61.7	64.6	70.6	77.5	82.9	86.9
Mesh 3	S.D. of Temp. (F)	10.00	3.58	3.52	3.37	3.01	2.33	1.59	1.11
	Mixing Effectiveness (%)		64.2	64.8	66.3	69.9	76.7	84.1	88.9
Mesh 4	S.D. of Temp. (F)	10.00	3.77	3.68	3.33	2.70	2.00	1.45	1.04
	Mixing Effectiveness (%)		62.3	63.2	66.7	73.0	80.0	85.5	89.6
Mesh 5	S.D. of Temp. (F)	10.00	3.71	3.56	3.17	2.60	2.06	1.44	1.05
	Mixing Effectiveness (%)		62.9	64.4	68.3	74.0	79.4	85.6	89.5

CHAPTER V

RESULTS

In this study, we have investigated four different models of air mixers with different geometric configurations and flow parameters to see their effect on the temperature, mixing effectiveness, and pressure loss. From the past research as discussed in chapter 2, some of these parameters have more impact on the performance of these devices as compared to others. For example, the geometric configuration has a remarkable influence on the temperature mixing effectiveness and the pressure drop. Among the flow parameters, difference between flowrates of two airstreams is very important. Results of CFD simulations will be presented next in this chapter.

A complete simulation plan is shown in the table 5.1. From the simulation plan, readers can see the parameters used for each simulation. In the results, cold air means airstream at 65 °F and hot air means airstream at 85 °F unless otherwise mentioned. Mixing effectiveness is calculated at different locations in the duct as shown in figure 5.3 to provide maximum insight for the different duct length used in the industry and experimental purpose. Location of each plane is specified when the values of mixing effectiveness are presented in the tables. Residual convergence is always seen below 1×10^{-3} as can be seen in figure 5.2.

Geometry	Mixer type	Test Name	Total Flowrate (CFM)	Flowrate Bottom (CFM)	Flowrate Top (CFM)	Bottom inlet temp [F]	Top inlet temp [F]	Louver Angle (Degree)	Orifice Diameter (inches)	Distance between mixers (inches)	Description
Geometry-1	None	2000-1c4h-00	2000	400	1600	65	85	-	-	-	These will be the reference cases for the rest of simulation for respective flow ratio for total flowrate of 2000 CFM at inlet temperatures 65F for cold and 85 F for hot airstream.
		2000-1c1h-00		1000	1000	65	85	-	-	-	
Geometry-2	Louver Baffles, Single Mixer	2000-1c4h-Lb-45		400	1600	65	85	45	-	-	Comparison of mixing effectiveness at different louver angles will be studied in louver-baffles mixer. Only the varying parameter is louver angle
		2000-1c4h-Lb-50				65	85	50	-		
		2000-1c4h-Lb-55				65	85	55	-		
		2000-1c4h-Lb-60				65	85	60	-		
		2000-1c4h-Lb-65				65	85	65	-		
Geometry-3	Louver Baffles, Pair in series	2000-1c4h-Lb-45-2		400	1600	65	85	45	-	2	Mixer distance will be 2 in , mixing effectiveness will be studied with the difference in flow ratio
		2000-1c1h-Lb-45-2		1000	1000	65	85		-		
		2000-1c4h-Lb-45-18		400	1600	65	85		-	18	Mixer distance will remain same in this study which is D_h, mixing effectiveness will be studied with the difference in flow ratio
		2000-1c1h-Lb-45-18		1000	1000	65	85		-		
Geometry-4	Louver, Pair in series	2000-1c4h-L-45-2		400	1600	65	85	45	-	2	Mixer distance will be 2 in , mixing effectiveness will be studied with the difference in flow ratio
		2000-1c1h-L-45-2		1000	1000	65	85		-		
		2000-1c4h-L-45-6		400	1600	65	85		-	6	Mixer distance will remain same in this study which is 1/3D_h, mixing effectiveness will be studied with the difference in flow ratio
		2000-1c1h-L-45-6		1000	1000	65	85		-		
		2000-1c4h-L-45-18		400	1600	65	85		-	18	Mixer distance will remain same in this study which is D_h, mixing effectiveness will be studied with the difference in flow ratio
		2000-1c1h-L-45-18		1000	1000	65	85		-		
Geometry-5	Orifice with Target	2000-1c1h-OT		1000	1000	65	85	-	7.2	-	Comparison of missing effectiveness with different orifice diameter in orifice target type mixer will be studied for same flow ratio for all cases
		2000-1c1h-OT				65	85	-	8.1		
		2000-1c1h-OT				65	85	-	9		
		2000-1c1h-OT				65	85	-	9.9		
		2000-1c1h-OT				65	85	-	10.8		
Geometry-6	Orifice	2000-1c1h-O				65	85	-	7.2		Mixing effectivess will be observed for orifice arrangment only.
Geometry-3	Louver Baffles	200-1c1h-Lb-45-18	200	100	100	65	85	45	-	18	Effect of low flowrate will be seen with both louver-baffles and mixer with only louvers for keeping all other parameters same.
Geometry-4	Louver	200-1h1C-L-45-18	200	100	100	85	65				
TBD	TBD	2000-1H1C-BM	2000	1000	1000	80.5	79.5	TBD	TBD	TBD	Best mixer from the previous study will be chosen and mixing effectiveness will be seen for inlet temperatures 79.5 F and 80.5 F. Intent of the study to see the effect on mixing effectivenss for small temperature difference between two air streams.
TBD	TBD	2000-1c1h-BM	200	100	100	85	65	TBD	TBD	TBD	Hot and cold inlets swapped to determine effect of stratification on mixing effectiveness

Figure 5.1: Simulation Plan

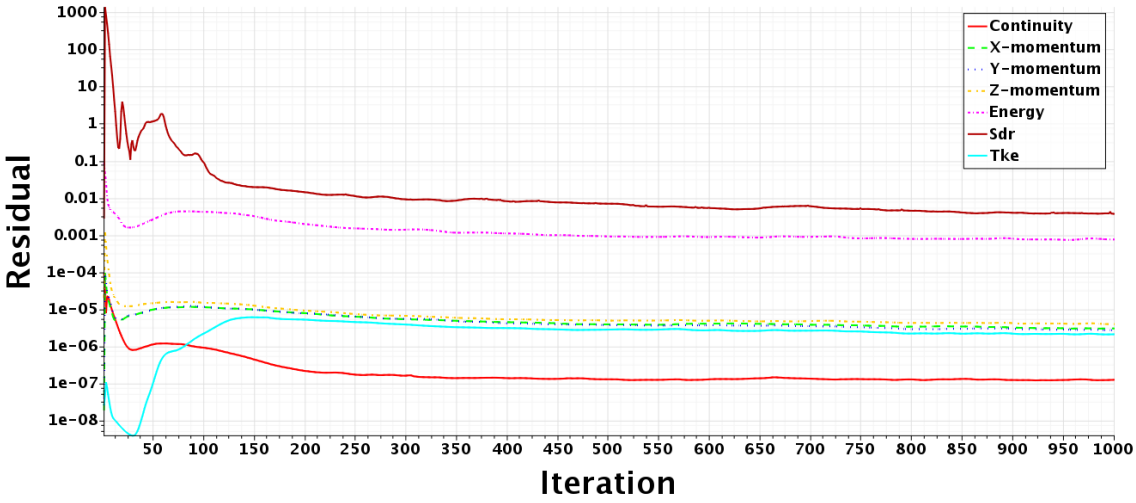

Figure 5.2: Residual convergence

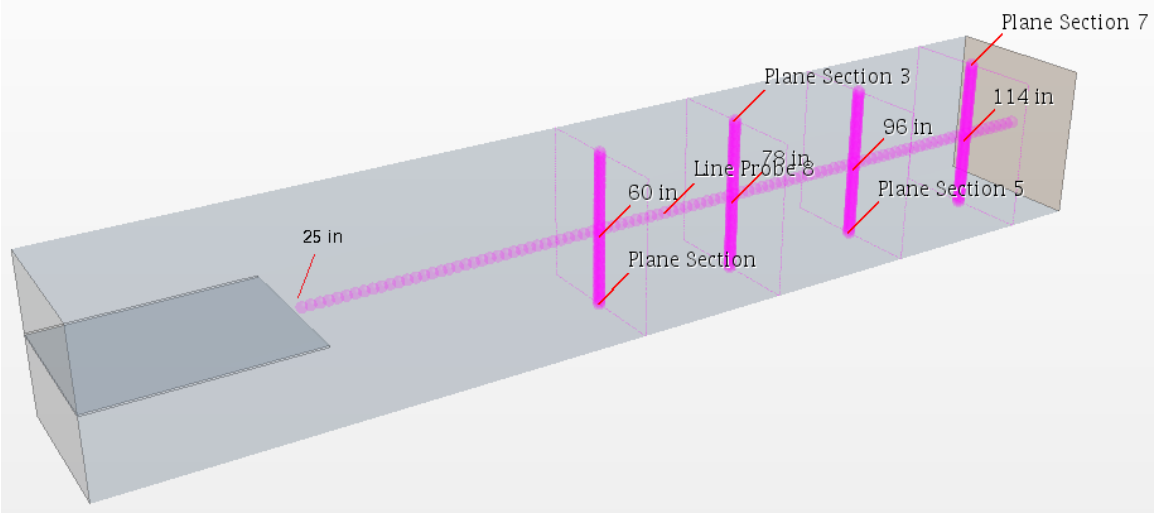

Figure 5.3: Visual understanding for planes and probes

5.1 Geometry-1: Baseline Case without Mixer

In this case, the investigation is done without any mixer. In all simulations the flow is turbulent, and we know that turbulence enhances mixing. The purpose of this case is to serve as a baseline to see the change in mixing effectiveness when both airstreams have different flowrate ratio compared to when these have same flowrate. Mixing effectiveness is 21.2% when the flowrate is 400 CFM for cold airstream and 1600 CFM for hot airstream as shown in table 5.1. When the flowrate (1000 CFM) is same for both airstreams, less mixing effectiveness is achieved which is 7.7% as presented in table 5.1.

One of the reasons of the difference in mixing effectiveness is that, in case of 1600 CFM the Reynolds number is high which mean more turbulence. Airstream which is at higher velocity transfers its momentum to the low velocity airstream inducing more air movement in the low velocity airstream and enhances the mixing. When both airstreams have same flowrate (1000 CFM), there is less transfer of momentum among two airstreams which is the reasons of less mixing. The temperature and velocity profiles profiles for different flowrate are presented in figures 5.10 - 5.11

respectively. By looking at these profiles, inference can be made for the exchange of momentum and temperature at the interface of two airstreams.

Within the same case, the mixing effectiveness increases along the duct, the temperature change along the duct can be seen from temperature contours presented in figure 5.4 for same flowrate and figure 5.9 for different flowrate.

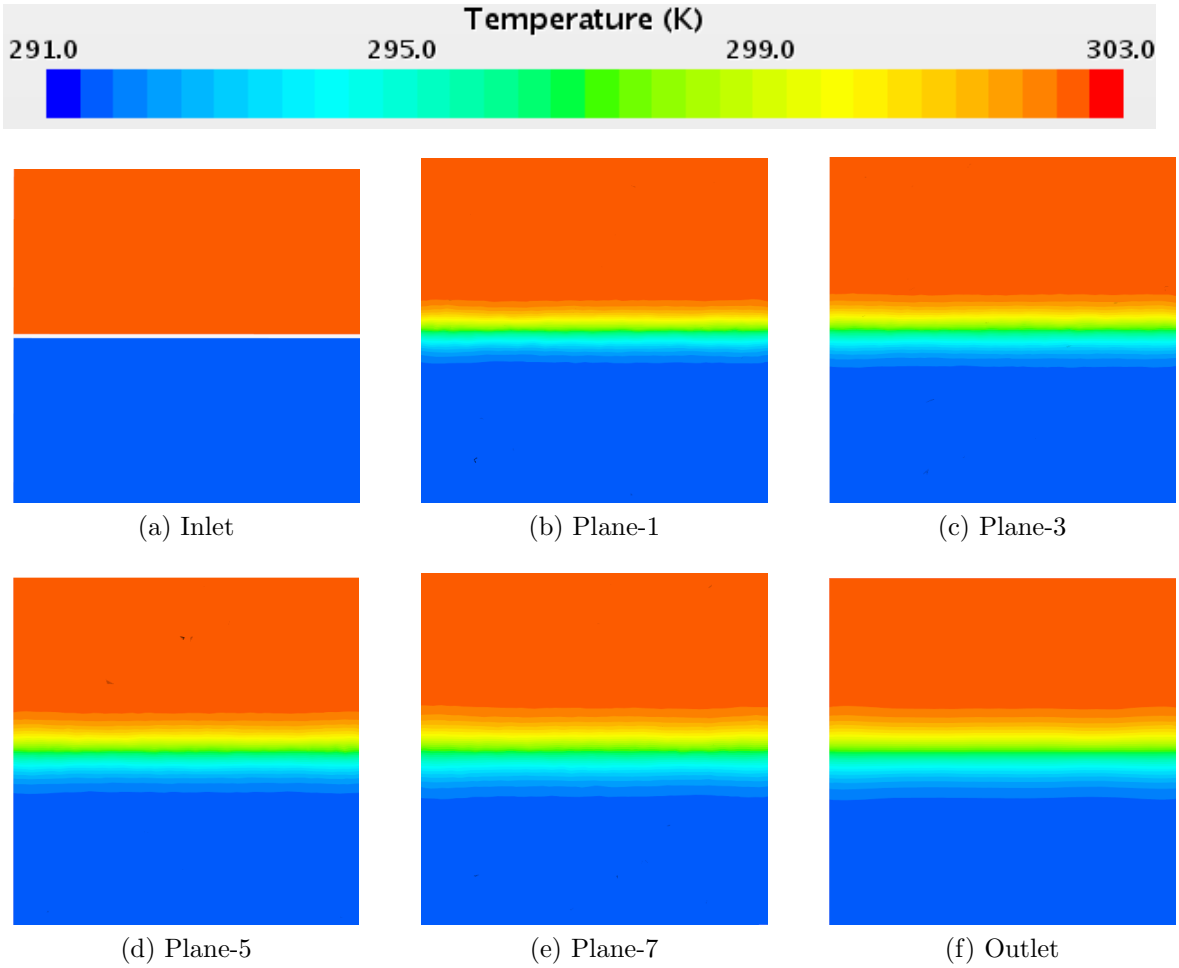

(a) Inlet (b) Plane-1 (c) Plane-3

(d) Plane-5 (e) Plane-7 (f) Outlet

Figure 5.4: Temperature contours for cold airstream at 65°F and 1000 CFM and hot airstream at 85°F and 1000 CFM.

Static pressure field for a plane located at the middle of the duct for both cases have been presented in figures 5.5 and 5.8 for visual understanding of how the pressure is decreasing along the duct. Velocity vector contours for a plane located at the middle of the duct for both cases have been presented in figures 5.6 and 5.9 to see the flow behaviour in the duct. Just by looking at these contours it is not possible to see tiny

vortices, which are present in the flow because of turbulence.

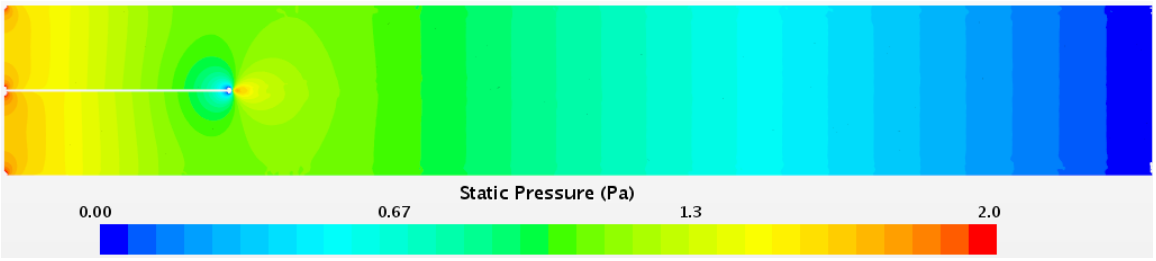

Figure 5.5: Static pressure for cold airstream at 65°F and 1000 CFM and hot airstream at 85°F and 1000 CFM

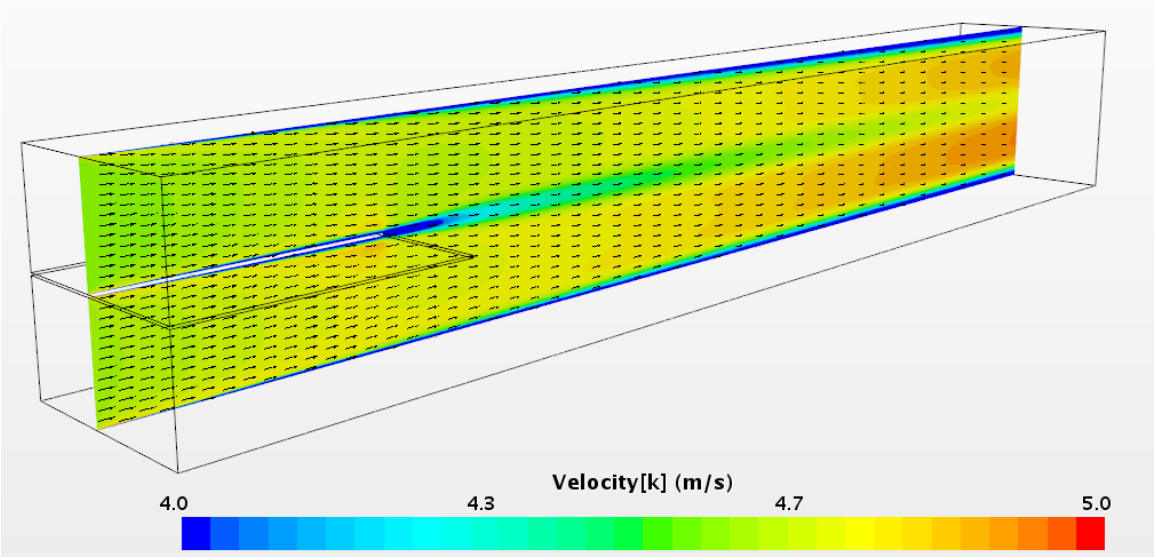

Figure 5.6: Velocity vector contour for cold airstream at 65°F and 1000 CFM and hot airstream at 85°F and 1000 CFM

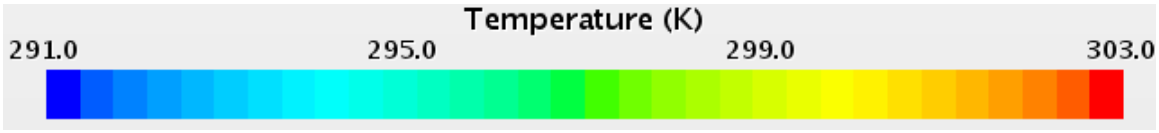

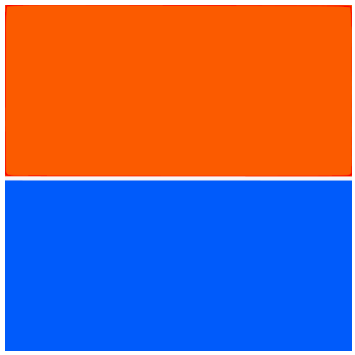

(a) Inlet

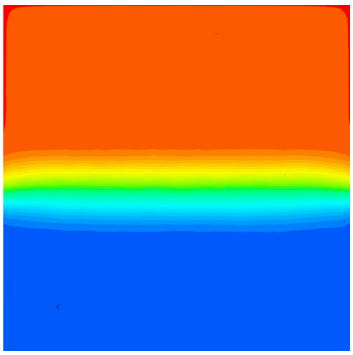

(b) Plane-1

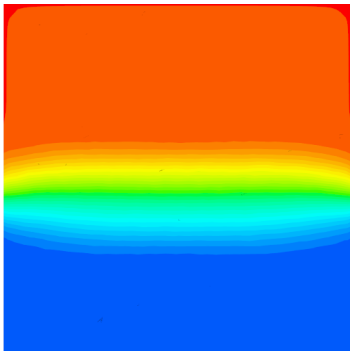

(c) Plane-3

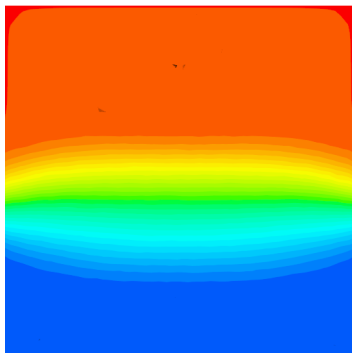

(d) Plane-5

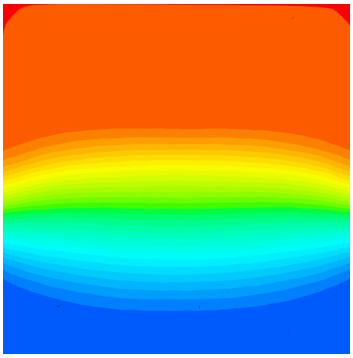

(e) Plane-7

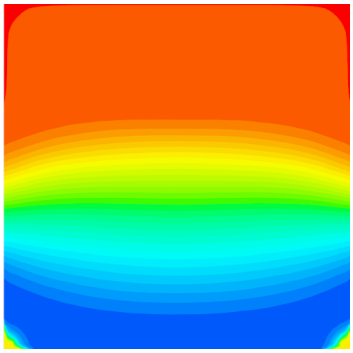

(f) Outlet

Figure 5.7: Temperature contours for cold airstream at 65°F and 400 CFM and hot airstream at 85°F and 1600 CFM.

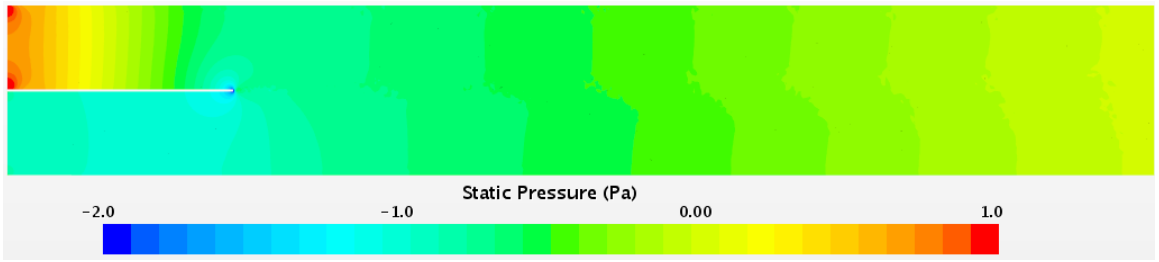

Figure 5.8: Static pressure for cold airstream at 65°F and 400 CFM and hot airstream at 85°F and 1600 CFM

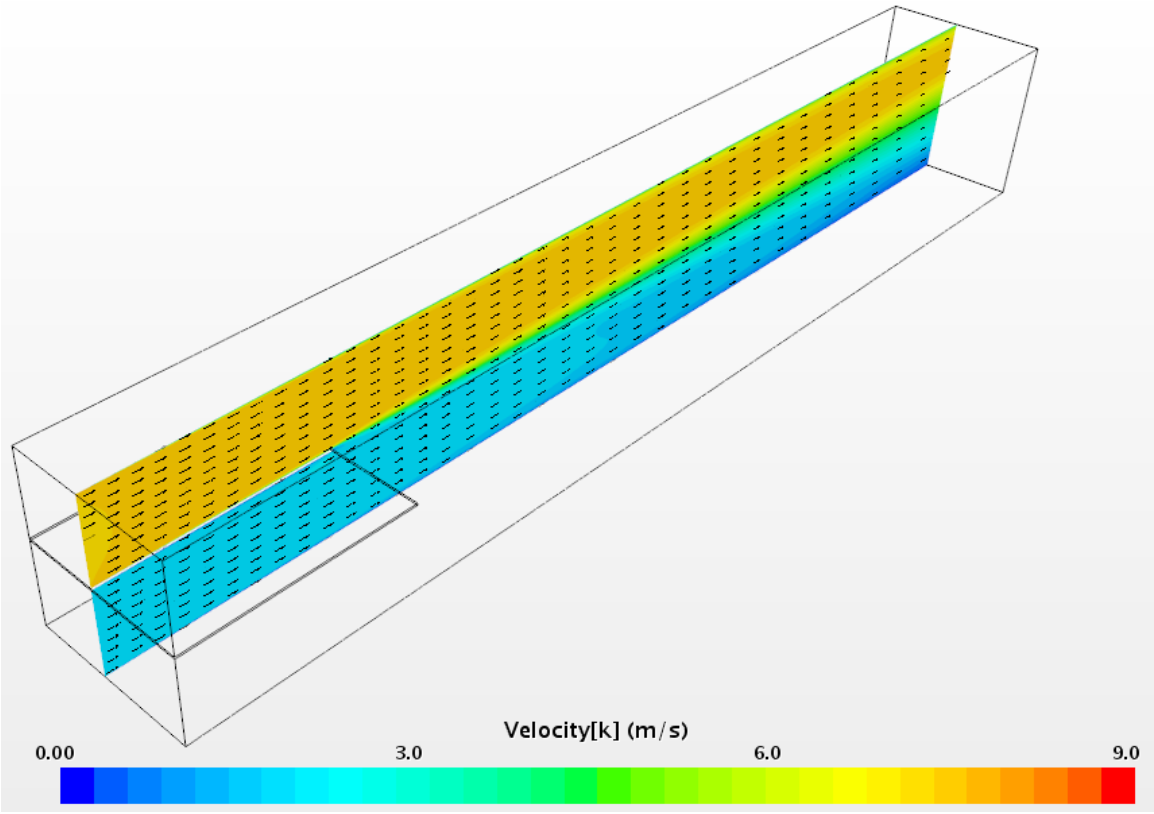

Figure 5.9: Velocity vector contour for cold airstream at 65°F and 400 CFM and hot airstream at 85°F and 1600 CFM

Temperature and the velocity profiles along the height of the duct at different locations are shown in the figure 5.10 and 5.11 respectively. From these profiles, it is observed that temperature decreases more in the cold region of the duct and increase in the hot region along the duct when the flowrates are different. At the airstream interface velocity is high as compared to the velocity of cold air and low in the hot region as compared to the inlet conditions.

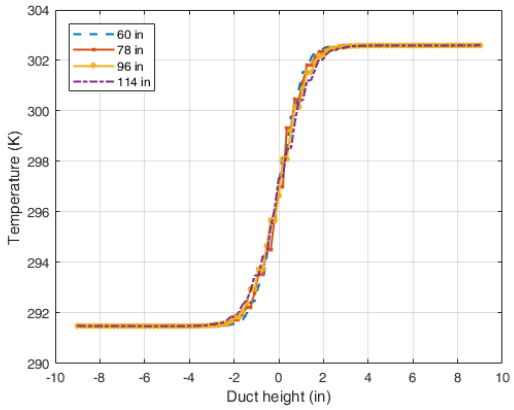

(a)

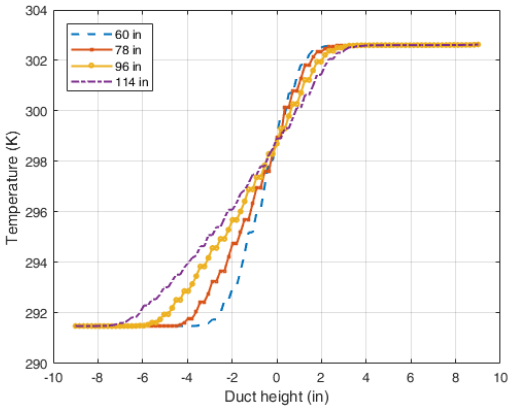

(b)

Figure 5.10: Temperature profile at different location of duct (a) flowrates of cold air (1000 CFM) and hot air (1000 CFM) (b) flowrates of cold air (400 CFM) and hot air (1600 CFM)

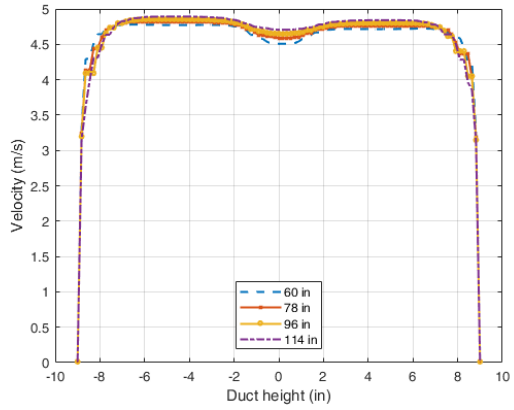

(a)

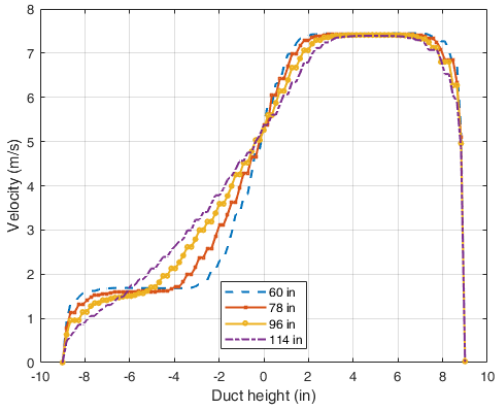

(b)

Figure 5.11: Velocity profile at different location of duct (a) flowrates of cold air (1000 CFM) and hot air (1000 CFM) (b) flowrates of cold air (400 CFM) and hot air (1600 CFM)

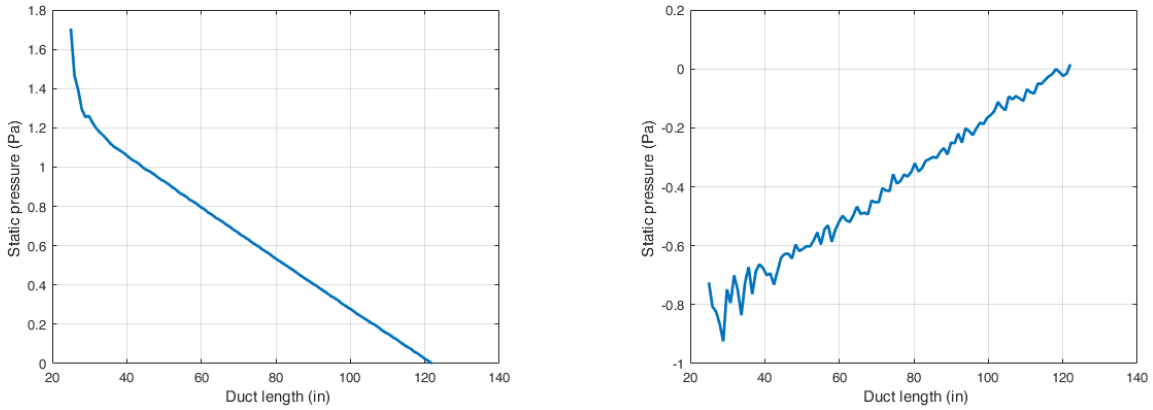

(a) (b)

Figure 5.12: Static pressure profile along the duct (a) flowrates of cold air (1000 CFM) and hot air (1000 CFM) (b) flowrates of cold air (400 CFM) and hot air (1600 CFM)

Mixing effectiveness for both cases at different planes is shown in table 5.1 and figure 5.13. Mixing effectiveness is calculated using equation 4.1.

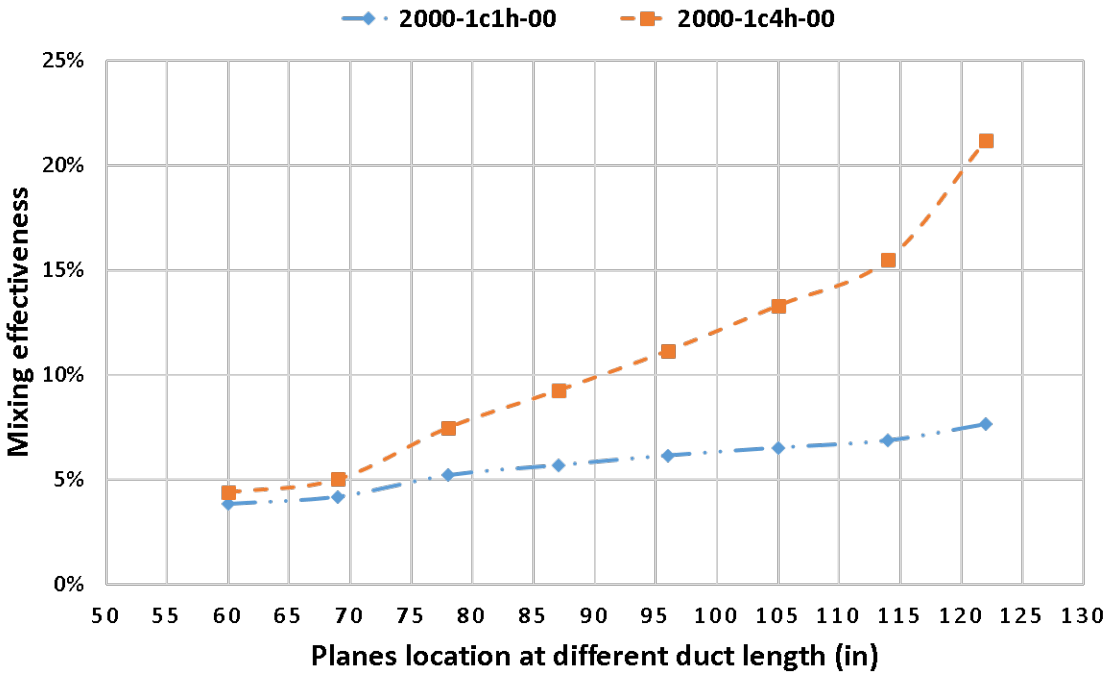

Figure 5.13: Plot of mixing effectiveness at different location for Geometry-1 for when both airsteams with same flowrate (1000 CFM) and when airstreams are at different flowrate with cold air at 400 CFM and hot air at 1600 CFM

Table 5.1: Mixing effectiveness comparison for two different inlet conditions. In one case, flowrates of cold air (400 CFM) and hot air (1600 CFM) and in the second case, both airstreams have same flowrate (1000 CFM).

Name		Inlet	Plane-1	Plane-2	Plane-3	Plane-4	Plane-5	Plane-6	Plane-7	Outlet
	Location of Plane (inch)	0	60	69	78	87	96	105	114	122
2000-1c4h-00	S.D. of Temp. (F)	10.01	9.57	9.51	9.26	9.08	8.89	8.68	8.46	7.89
	Mixing Effectiveness (%)		4.4	5.0	7.5	9.3	11.1	13.3	15.5	21.2
2000-1c1h-00	S.D. of Temp. (F)	10.00	9.62	9.58	9.48	9.43	9.38	9.35	9.31	9.23
	Mixing Effectiveness (%)		3.8	4.2	5.2	5.7	6.2	6.5	6.9	7.7

5.2 Geometry-2: Single Louver-Baffle Mixer

In this section, simulation results for Geometry-2 are presented. For Geometry-2, investigations are done on louver-baffle type air-mixer for different louvers angles. In this case, flowrate for cold airstream is 400 CFM and hot airstream is 1600 CFM. The length of the middle wall is 36 inches and the distance between the mixer and the midwall is 6 inches. From the Geometry-1 results, it is observed that only the turbulence due to flow is not enough to get uniform mixing. To increase mixing, it is important to have large vortices in the flow instead of small vortices. To generate large vortices louver-baffle air-mixer is placed in the duct. Louver angle is varied from 45° to 65° angle with an increment of 5°. For understanding of the flow behaviour, the results are presented for louver at 65° angle.

In figure 5.14, temperature contours for different planes along the duct are shown to see the variation of temperature along the duct. From the streamlines, presented in figure 5.17, it can be seen that high velocity and high temperature airstream are diverging towards lower part of the duct which has cold airstream and low velocity. In addition to this when the flow is striking the baffles, it is producing large vortices in the lower part of the duct which causes premixing prior to the mixer. Relatively small vortices can be seen on the upper part of the duct and as there is no cold air present in the upper part so there is no mixing. Flow behaviours can also be seen from velocity vectors contours presented in the figure 5.16. As the flow passes through louvers, louvers are directing both airstream towards their adjacent walls,

due to which there is very less mixing of fluid at the upper wall and relatively high mixing towards the lower wall. The reason of relatively high mixing is that high temperature fluid is coming to the lower part of the duct when it passes the mixer. Large vortices are responsible for improved mixing.

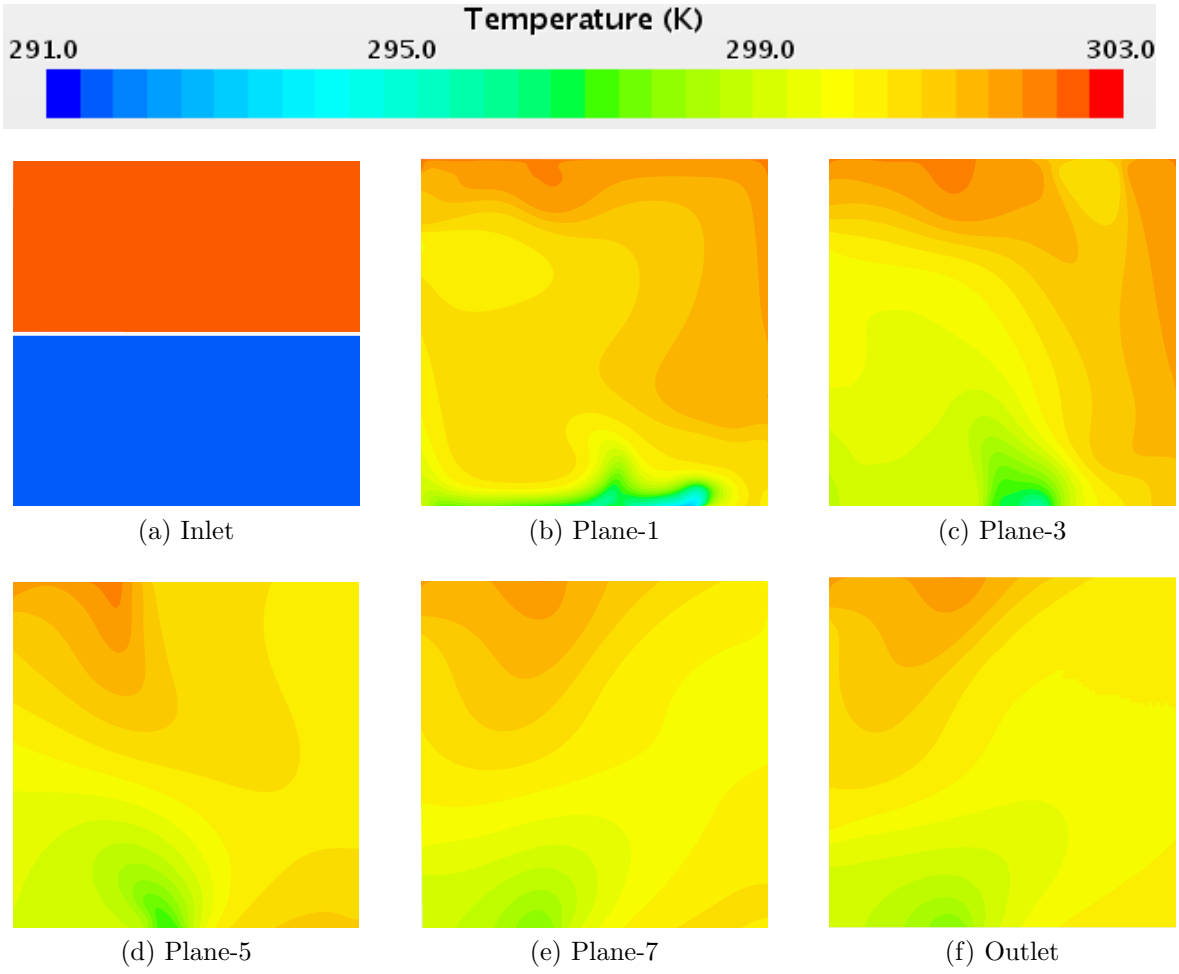

(a) Inlet (b) Plane-1 (c) Plane-3

(d) Plane-5 (e) Plane-7 (f) Outlet

Figure 5.14: Temperature contours for Geometry-2 when louver at 65° angle and flowrate of cold air (400 CFM) and hot air (1600 CFM). Mixer is located at 42 inches distance from the inlet of the duct

There is large pressure drop across the air-mixers which can be seen from the static pressure profile in figure 5.20. Static pressure contour is also presented along the duct in figure 5.15. Negative pressure region is present after the baffles which is causing flow re-circulation in this region which enhances mixing. Temperature difference is reducing not only along the height of the duct but also reducing along the length of

the duct as the flow is going towards the outlet. This can be seen in the temperature profile presented in figure 5.18. In figure 5.19, velocity profiles are shown. From these profiles, it can be seen that as the flow is approaching towards outlet velocity profile is becoming more stable and the velocity difference in the upper and lower airstream is reducing.

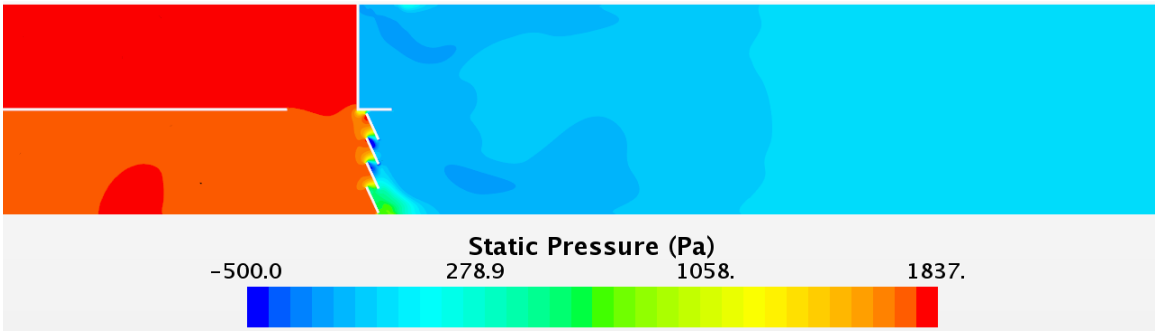

Figure 5.15: Static pressure for Geometry-2 when louver at 65° angle and flowrate of cold air (400 CFM) and hot air (1600 CFM). Mixer is located at 42 inches distance from the inlet of the duct

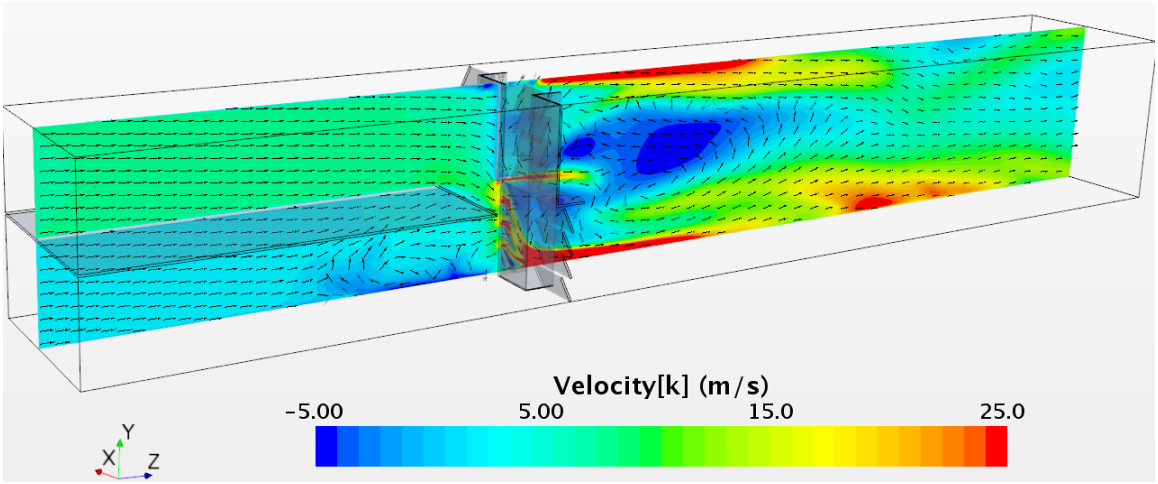

Figure 5.16: Velocity vector contour for Geometry-2 when louver at 65° angle and flowrate of cold air (400 CFM) and hot air (1600 CFM). Mixer is located at 42 inches distance from the inlet of the duct

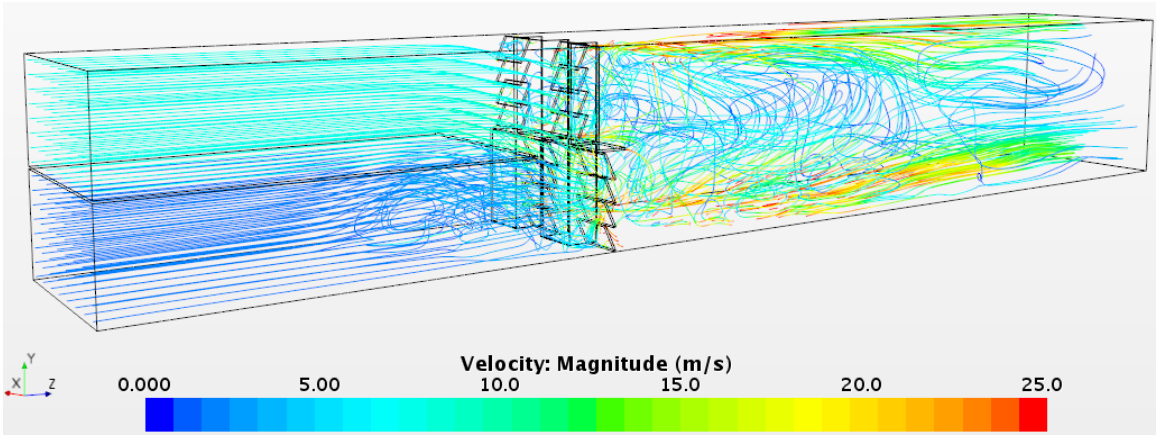

Figure 5.17: Velocity streamlines for Geometry-2 when louver at 65° angle and flowrate of cold air (400 CFM) and hot air (1600 CFM). Mixer is located at 42 inches distance from the inlet of the duct

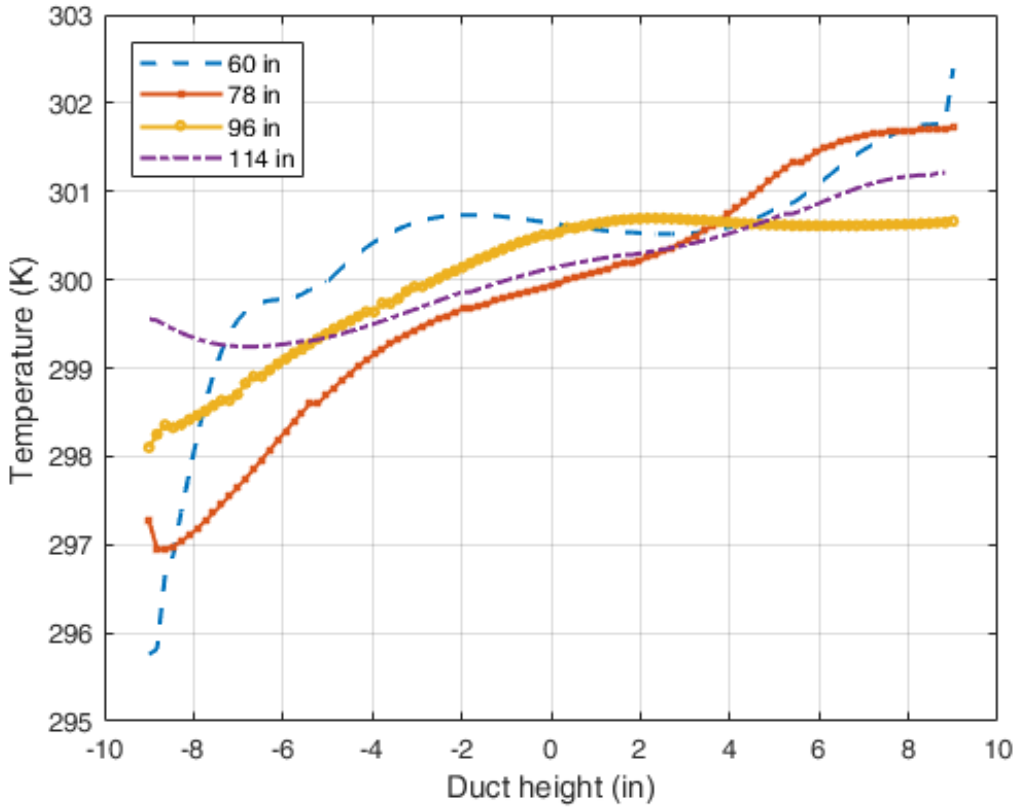

Figure 5.18: Temperature profile at different location of duct for Geometry-2 when louver at 65° angle and flowrate of cold air (400 CFM) and hot air (1600 CFM). Mixer is located at 42 inches distance from the inlet of the duct (0 inch)

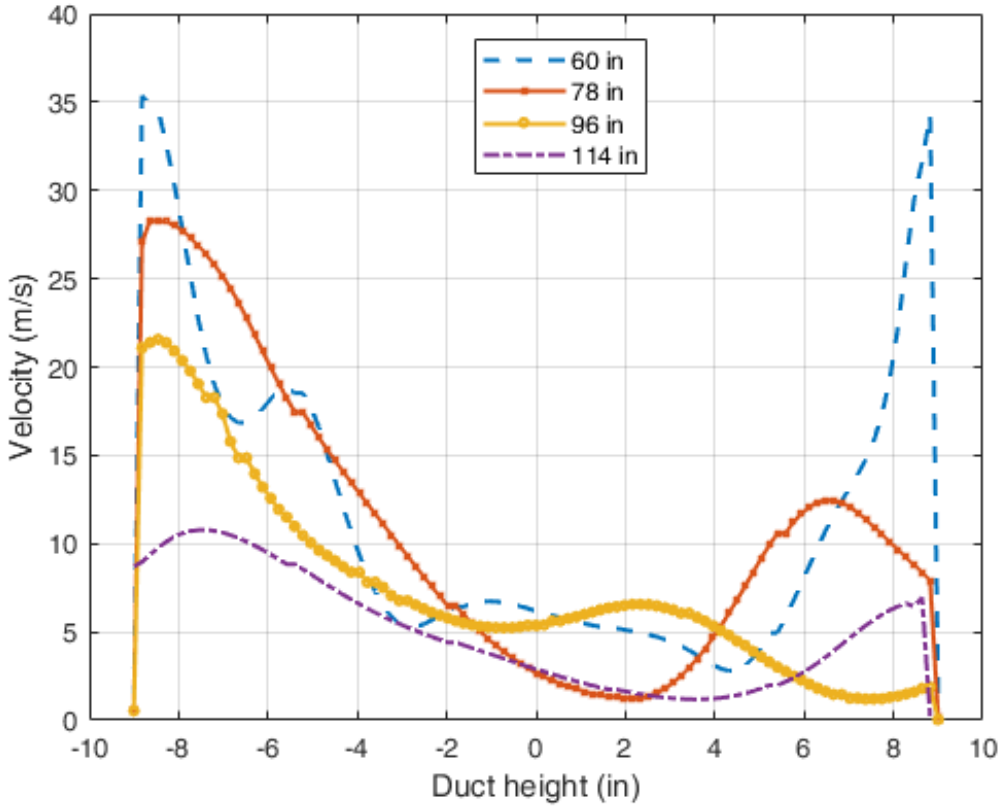

Figure 5.19: Velocity profile at different location of duct for Geometry-2 when louver at 65° angle and flowrate of cold air (400 CFM) and hot air (1600 CFM). Mixer is located at 42 inches distance from the inlet of the duct

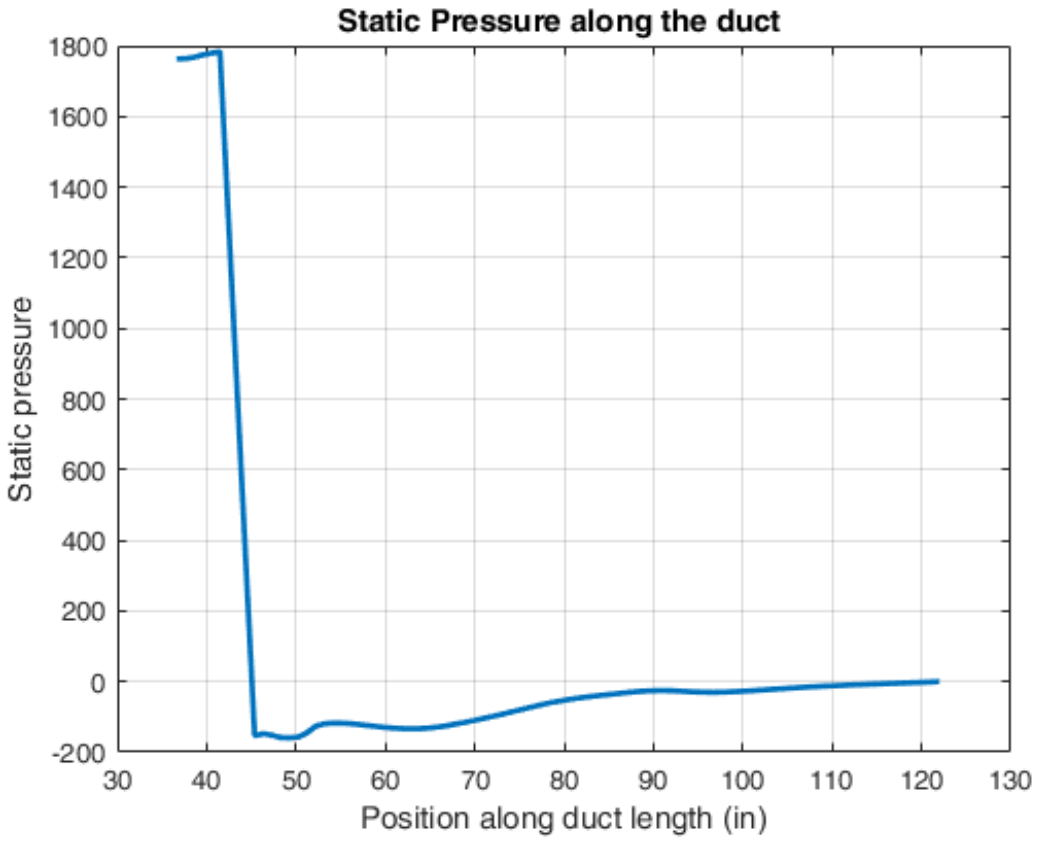

Figure 5.20: Static Pressure profile at different location of duct for Geometry-2 when louver at 65° angle and flowrate of cold air (400 CFM) and hot air (1600 CFM). Mixer is located at 42 inches distance from the inlet of the duct(0 inch)

In table 5.2, values of temperature mixing effectiveness are presented for each plane. For all 5 cases, it can be seen that mixing effectiveness decreases at plane-2 and again starts to increase. By looking at streamlines, it seems that the plane-1 has more circulation regions of hot and cold airstream as compared to the plane-2. After plane-2 the flow from upper part of the duct is coming towards the center, roughly near plane-3, so mixing again starts to increase from this region till the outlet of the duct. Mixing effectiveness for different louvers angles are presented in table 5.2 and figure 5.21. Mixing effectiveness first increases from 45° to 50° angle and then decrease at angle 55° and again starts to increase which is a different trend than reported in the literature. The results were obtained based on metrics described in the NIST report Faison et al. (1970). In general, the effectiveness increased initially as the angle is increased from 45° to 55°, then a slight decrease in mixing effectiveness was seen for the louver angle of 60°. The difference in trend could be because of different geometric configurations and flow conditions.

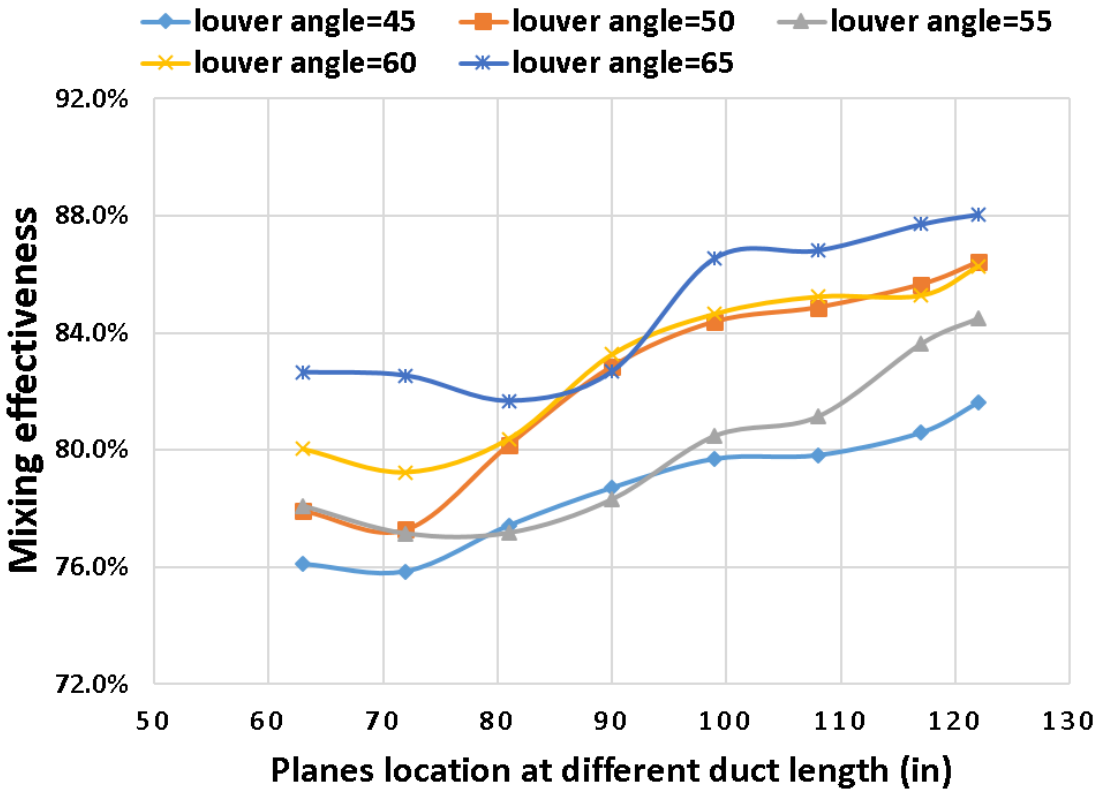

Figure 5.21: Plot of mixing effectiveness for Geometry-2 with different louver angles with flowrate of cold air (400 CFM) and hot air (1600 CFM). Mixer is located at 42 inches distance from the inlet of the duct

Table 5.2: Mixing effectiveness for Geometry-2 with different louver angles with flowrate of cold air (400 CFM) and hot air (1600 CFM) at different location of the duct. Mixer is located at 42 inches distance from the inlet of the duct.

Name		Inlet	Plane-1	Plane-2	Plane-3	Plane-4	Plane-5	Plane-6	Plane-7	Outlet
	Location of Plane (inch)	0	63	72	81	90	99	108	117	122
2000-1c4h-Lb-45	S.D. of Temp. (F)	9.97	2.38	2.41	2.25	2.12	2.03	2.01	1.94	1.83
	Mixing Effectiveness (%)		76.1	75.8	77.4	78.7	79.7	79.8	80.6	81.6
2000-1c4h-Lb-50	S.D. of Temp. (F)	10.02	2.40	2.24	2.07	1.62	1.56	1.41	1.49	1.50
	Mixing Effectiveness (%)		77.9	77.3	80.2	82.8	84.4	84.9	85.7	86.4
2000-1c4h-Lb-55	S.D. of Temp. (F)	9.87	2.16	2.26	2.25	2.14	1.93	1.86	1.62	1.53
	Mixing Effectiveness (%)		78.1	77.1	77.2	78.3	80.5	81.1	83.6	84.5
2000-1c4h-Lb-60	S.D. of Temp. (F)	9.97	1.99	2.07	1.96	1.67	1.53	1.47	1.46	1.37
	Mixing Effectiveness (%)		80.0	79.2	80.4	83.3	84.7	85.2	85.3	86.3
2000-1c4h-Lb-65	S.D. of Temp. (F)	9.98	1.73	1.74	1.83	1.73	1.34	1.32	1.23	1.19
	Mixing Effectiveness (%)		82.6	82.5	81.7	82.7	86.6	86.8	87.7	88

5.3 Geometry-3: Orthogonal Pair of Louver-Baffle Mixer

In this section, results for different simulations for Geometry-3 are presented. In this geometry, two louver-baffle mixers are used, second mixer is placed at 90° angle to the first mixer for all cases. Louver angle is 45° for all cases. This geometry is not only analyzed by varying distance between the mixers but also the effect of low total flowrate (200 CFM) is studied. Visual results for low flowrate are shown in figures 5.22 - 5.24 and the quantitative values for all cases are shown in tables 5.3 - 5.5. From the temperature contours shown in 5.22 for different planes at different locations of the duct, temperature variation along the duct can be seen. In these contours high temperature zone can be seen at upper right corner of the duct, and low temperature zone is present at the the lower left corner of the duct. These zones are because of the geometric arrangement of both mixer. When cold air passes the first mixer the louvers directs the air downward and when the same airstream passes the second mixer it directs these streams towards the left corner of the wall due to which relatively cold region at the left in temperature contours is observed. Same phenomenon is happening for hot air zone.

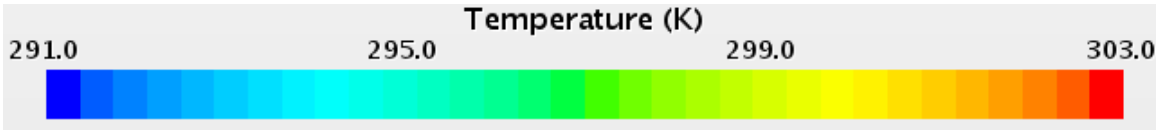

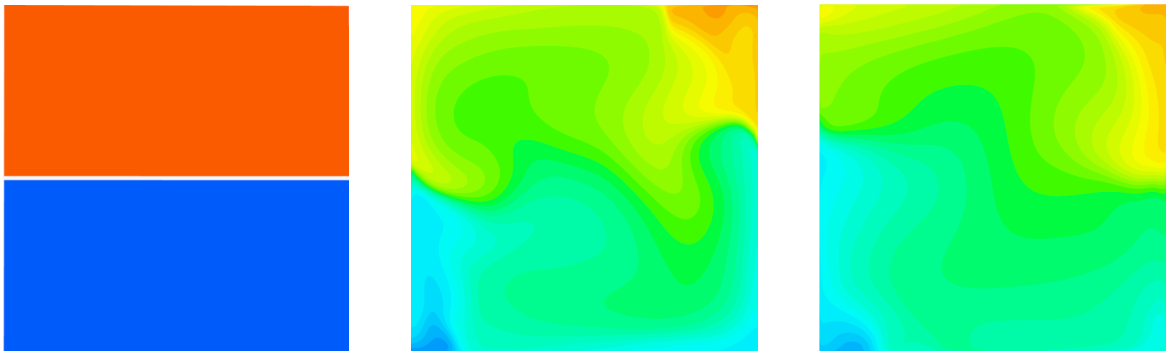

(a) Inlet (b) Plane-1 (c) Plane-3

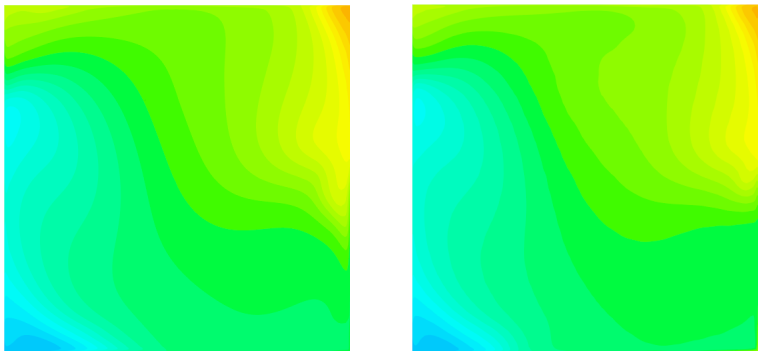

(d) Plane-5 (e) Outlet

Figure 5.22: Temperature contours for Geometry-3 when distance between mixers is 18 inches when both hot and cold airstream have same flowrates equal to 100 CFM. First mixer is located at 42 inches distance from the inlet of the duct

Static pressure contour is presented in figure 5.23 to see how the pressure is changing along the duct. From the static pressure plot presented in figure 5.24 pressure drops from approx. 10.2 Pa to 4.3 Pa at 42 inches duct length where the first mixer is placed then it regains to 5 Pa and again decreases at 63 inches where the second mixer is located. Due to the second mixer pressure decreases from 5 Pa to -1 Pa and then it starts to recover/regain till the outlet of the duct.

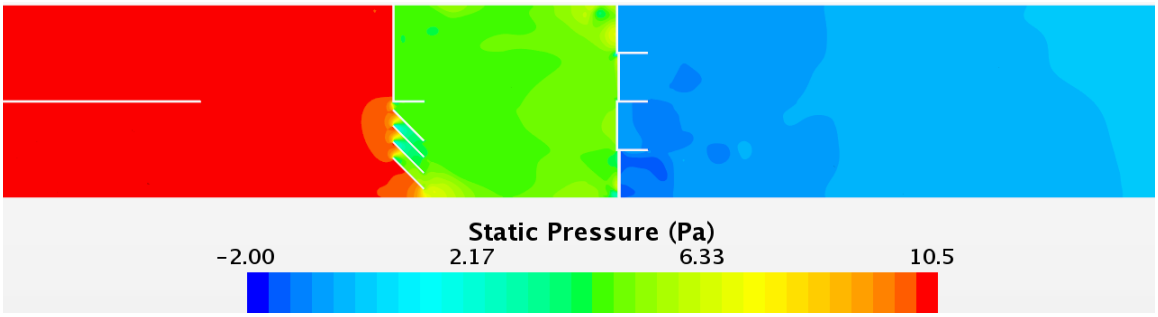

Figure 5.23: Static pressure for Geometry-3, when distance between mixers is 18 inches and both hot and cold airstream have same flowrates equal to 100 CFM. First mixer is located at 42 inches distance from the inlet of the duct

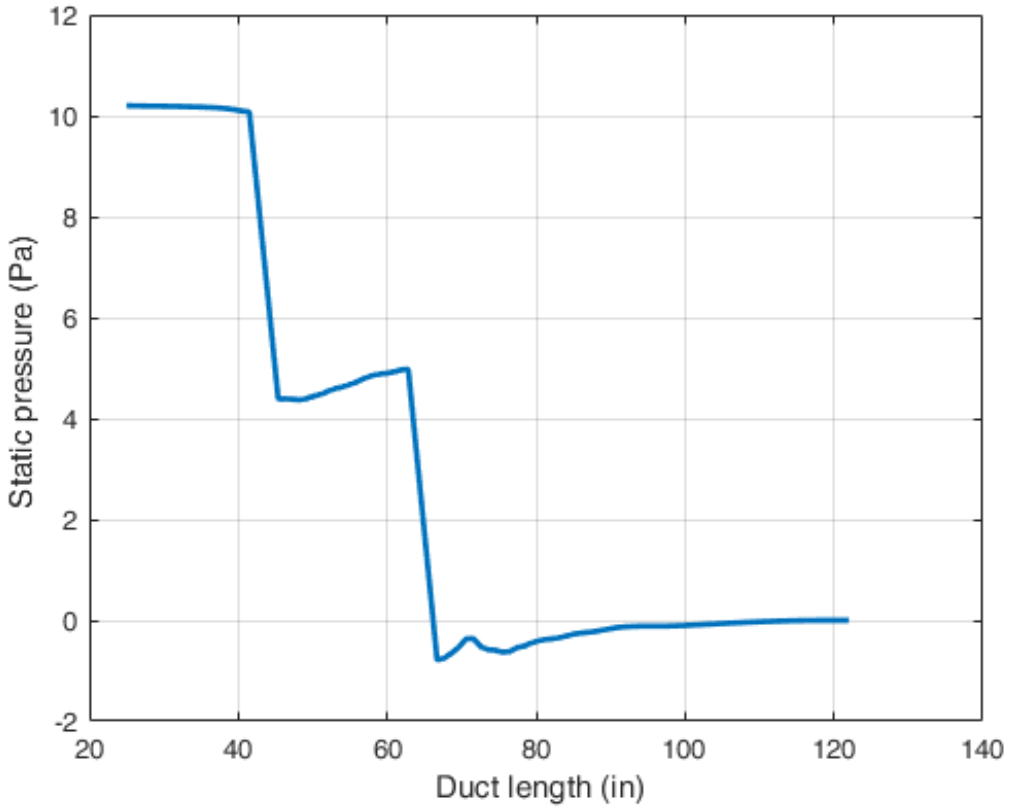

Figure 5.24: Velocity profile at different location of duct when distance between mixers is 18 inches mixer at 65° cold airstream at 65°F and 100 CFM and hot airstream at 85°F and 100 CFM. First mixer is located at 42 inches distance from the inlet of the duct

From figure 5.26 of streamlines, very large vortices can be seen starting from the outlet of the first which are responsible for good mixing even at low flowrate. Velocity

vector field is also presented in figure 5.25 at the plane along the duct to give more understanding of the flow direction.

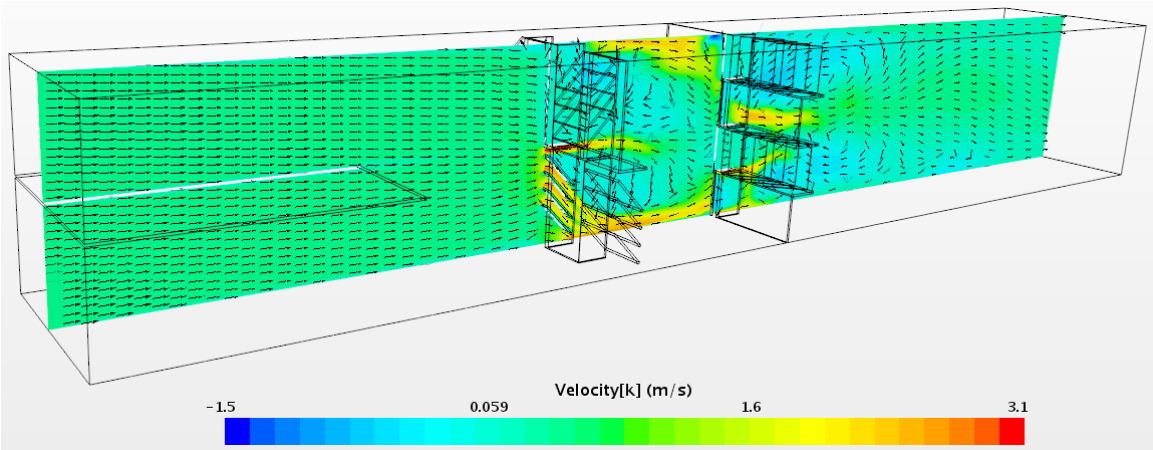

Figure 5.25: Velocity vector contour for Geometry-3 when distance between mixers is 18 inches when both hot and cold airstream have same flowrates equal to 100 CFM. First mixer is located at 42 inches distance from the inlet of the duct

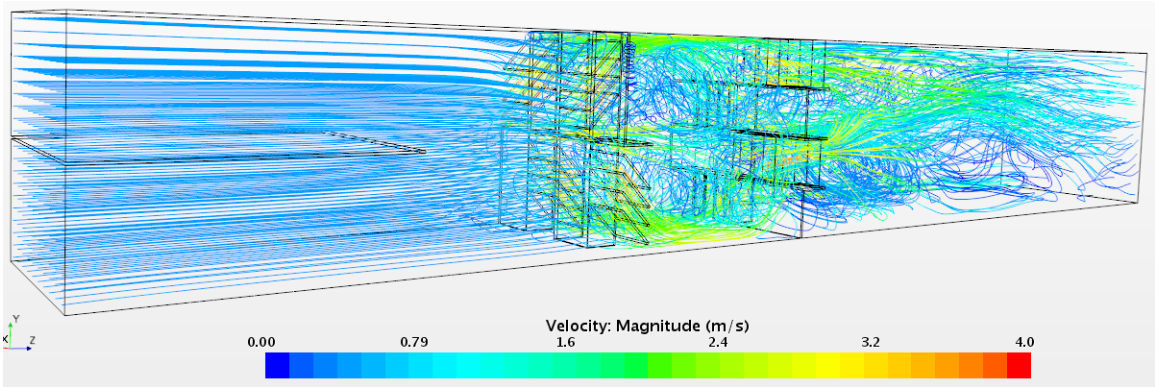

Figure 5.26: Velocity streamlines for Geometry-3 when distance between mixers is 18 inches when both hot and cold airstream have same flowrates equal to 100 CFM. First mixer is located at 42 inches distance from the inlet of the duct

To see the change in temperature along the height at different locations of the duct, temperature profiles are presented in figure 5.27. It can be seen that temperature variation reduces as the flow reaches the outlet. From the velocity profile presented in figure 5.28, it can be seen that the velocity is more irregular in the lower half of the duct because of more vortices in the lower half near the outlet of the duct which can also be seen in the streamlines figure 5.26.

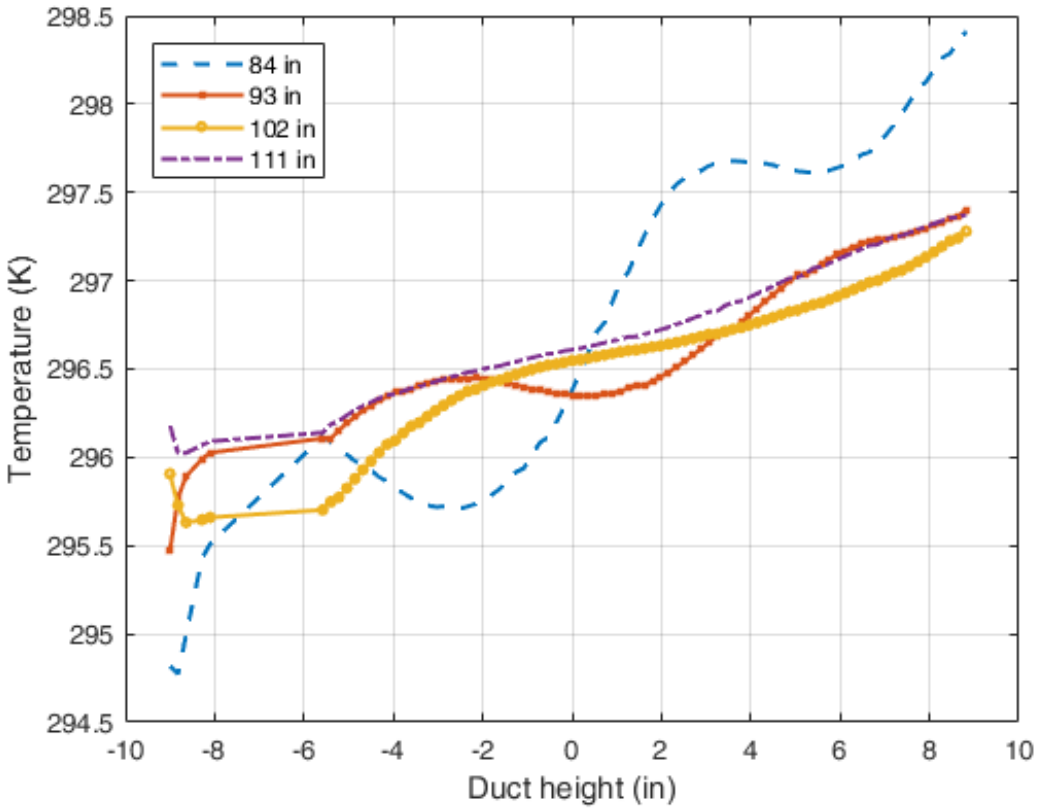

Figure 5.27: Temperature profile at different location of duct for louver mixer when distance between mixers is 18 inches with cold airstream is at 65°F and 100 CFM and hot airstream at 85°F and 100 CFM. First mixer is located at 42 inches distance from the inlet of the duct

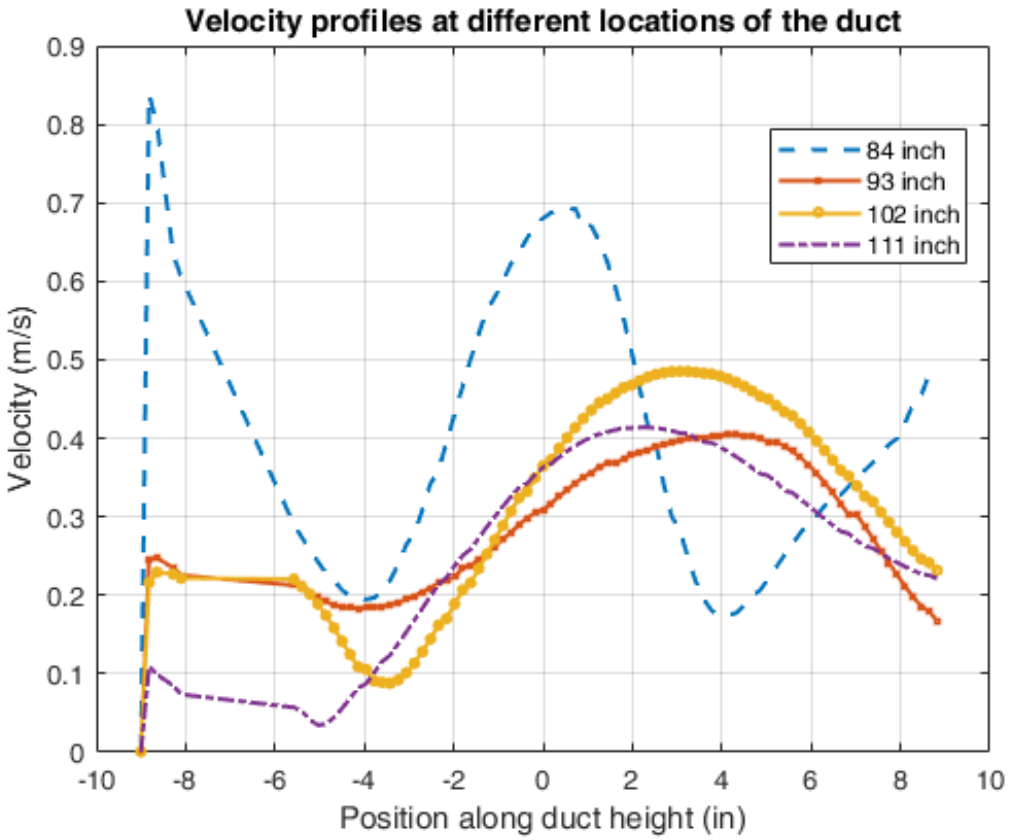

Figure 5.28: Velocity profile at different location of duct when distance between mixers is 18 inches mixer at 65° cold airstream at 65°F and 100 CFM and hot airstream at 85°F and 100 CFM. First mixer is located at 42 inches distance from the inlet of the duct

Values of mixing effectiveness for different simulations using different geometric configurations and flowrates at different planes of the duct are shown in tables 5.3 - 5.5. Lowest mixing effectiveness is seen with total flowrate 200 CFM case with same flow ratio of hot and cold airstreams. The mixing effectiveness in this case is 77.4% at the outlet. When the total flowrate is 2000 CFM lowest mixing effectiveness is seen for the case with same flow ratios for both streams and the distance between the two mixers is 2 inches. Highest mixing effectiveness is seen for the case with different flow ratio and the distance between the mixers is 18 inches. Mixing effectiveness decreases with the decrease in distance between the mixer. Similar conclusion is made by the experimental study done at NIST (Faison et al., 1970).

Table 5.3: Comparison of mixing effectiveness for Geometry-3 when the total flowrate is 200 CFM and both airstream have same flowrate (100 CFM) and distance between the mixers is 18 inches. First mixer is located at 42 inches distance from the inlet of the duct.

Name		Inlet	Plane-1	Plane-2	Plane-3	Plane-4	Plane-5	Outlet
	Location of Plane (inch)	0	84	93	102	111	120	122
200-1c1h-LB-45-18	S.D. of Temp. (F)	10.0	3.08	2.89	2.64	2.54	2.32	2.26
	Mixing Effectiveness (%)		69.2	71.1	73.6	74.6	76.8	77.4

Table 5.4: Comparison of mixing effectiveness for Geometry-3 when flowrates are same and different and distance between the mixers is 2 inches. First mixer is located at 42 inches distance from the inlet of the duct

Name		Inlet	Plane-1	Plane-2	Plane-3	Plane-4	Plane-5	Plane-6	Outlet
	Location of Plane (inch)	0	68	77	86	95	104	113	122
2000-1c4h-LB-45-2	S.D. of Temp. (F)	9.87	2.07	2.05	2.03	2.04	2.01	1.82	1.70
	Mixing Effectiveness (%)		79.0	79.2	79.4	79.3	79.7	81.5	82.8
2000-1c1h-LB-45-2	S.D. of Temp. (F)	10.0	3.34	2.92	2.70	2.61	2.50	2.44	2.44
	Mixing Effectiveness (%)		66.6	70.8	73.0	73.9	75.0	75.6	75.6

Table 5.5: Comparison of mixing effectiveness for Geometry-3 when flowrates are same and different and distance between the mixers is 18 inches. First mixer is located at 42 inches distance from the inlet of the duct

Name		Inlet	Plane-1	Plane-2	Plane-3	Plane-4	Plane-5	Outlet
	Location of Plane (inch)	0	84	93	102	111	120	122
2000-1c4h-LB-45-18	S.D. of Temp. (F)	9.93	1.71	1.50	1.18	1.24	1.26	1.30
	Mixing Effectiveness (%)		82.8	84.9	88.1	87.6	87.3	86.9
2000-1c1h-LB-45-18	S.D. of Temp. (F)	10.0	2.50	2.27	2.18	2.00	1.90	1.89
	Mixing Effectiveness (%)		75.0	77.3	78.2	80.0	81.0	81.1

5.4 Geometry-4: Orthogonal Pair of Louver Mixer

In this section, results of different simulations for Geometry-4 are shown. In this geometry, two louver mixers are used, second mixer is placed at 90° angle to the first mixer for all cases. As compared to the previous case in this case, 6 inches distance between the mixers is also analyzed to see either it follow the same trend or not. Again louver angle is 45° for all cases. For visual understanding, results for total flowrate (2000 CFM) with different flow ratios (1:4) and the distance between the mixer is 18 inches, are shown in figures 5.29 - 5.31 and the quantitative values for all cases are shown in tables 5.6 - 5.9. From the temperature contours shown in figure 5.29 for different planes at different locations of the duct, temperature variation along the duct can be seen. When compared these contours with same case of louver-baffle mixer temperature patterns are entirely different, for example, in this case at first plan high temperature zone are slightly in the middle but in case of louver-baffle high temperature zones are at the top. In this case, the high temperature regions are present at the right side of the duct as flow is moving to the outlet but in case of louver-baffle mixer high temperature regions are seen from plane-5 to the outlet. But as compared to the louver mixers, more uniform pattern is seen in the case of louver-baffles mixer.

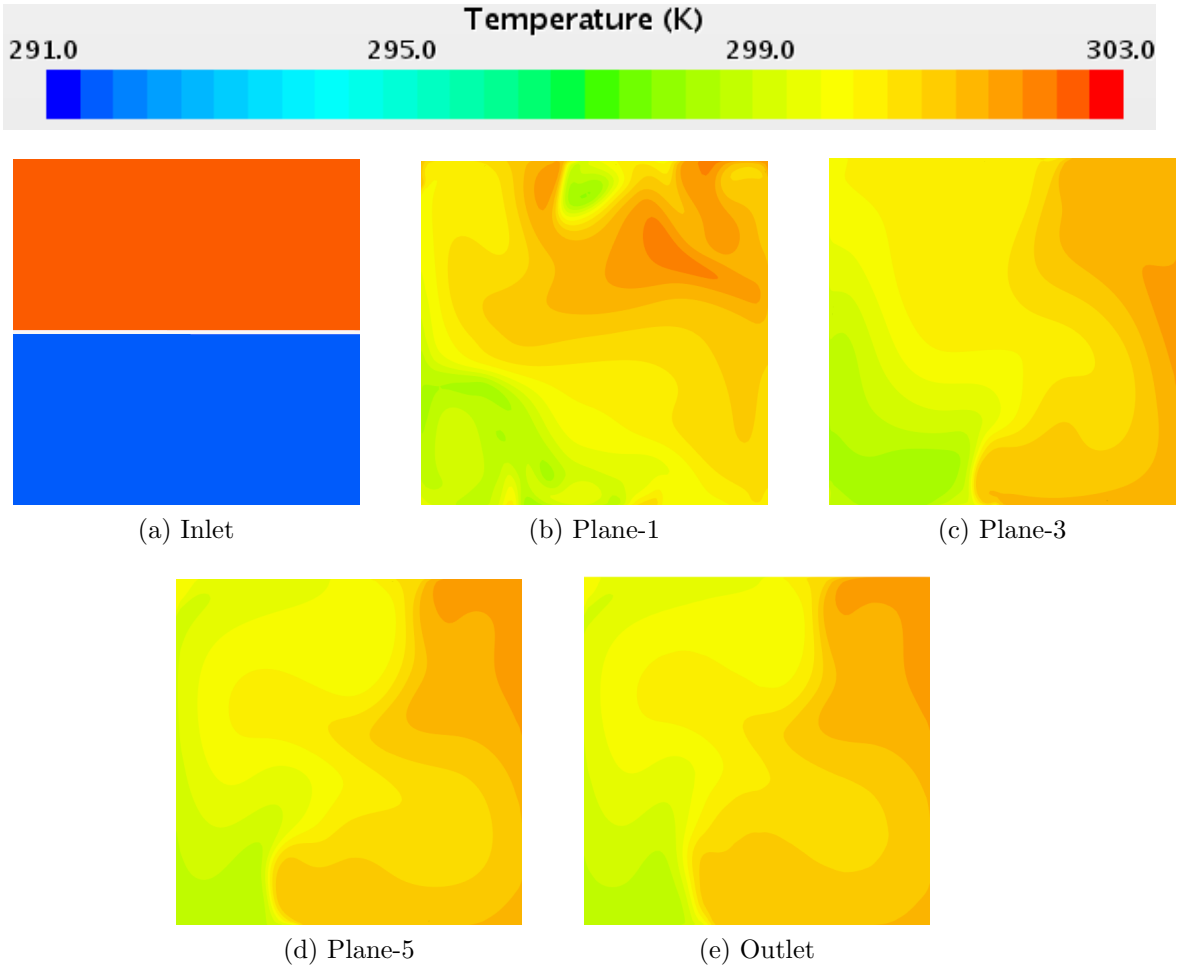

(a) Inlet (b) Plane-1 (c) Plane-3

(d) Plane-5 (e) Outlet

Figure 5.29: Temperature contours for Geometry-4 when distance between mixers is 18 inches when flowrate of hot airstream is 1600 CFM and cold airstream is 400 CFM. First mixer is located at 42 inches distance from the inlet of the duct

Static pressure contours are presented in figure 5.30 to see how the pressure is changing along the duct. From the plot presented in figure 5.31, pressure drops from approx. 190 Pa to 60 Pa at 42 inches duct length where the first mixer is placed and then it regains a pressure of 75 Pa and again decreases at 63 inches where the second mixer is located. Due to the second mixer pressure decreases from 40 Pa to -25 Pa and then it starts to regain till the outlet of the duct. Comparing the pressure drop for the same case with louver-baffles mixer, high pressure drop is observed in louver-baffle case, across the first mixer it dropped from 980 Pa to 420 Pa and across the second mixer it dropped from approx. 480 Pa to -85 Pa. Due to the baffles, more

pressure drop is expected in louver-baffles combination.

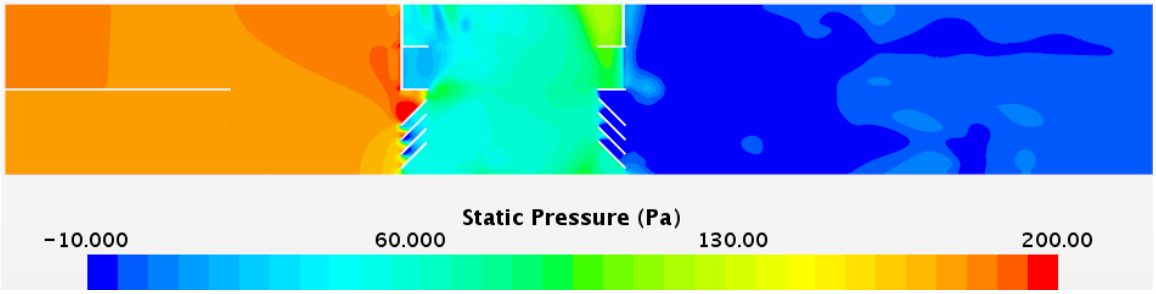

Figure 5.30: Static pressure for Geometry-4 when distance between mixers is 18 inches when flowrate of hot airstream is 1600 CFM and cold airstream is 400 CFM. First mixer is located at 42 inches distance from the inlet of the duct

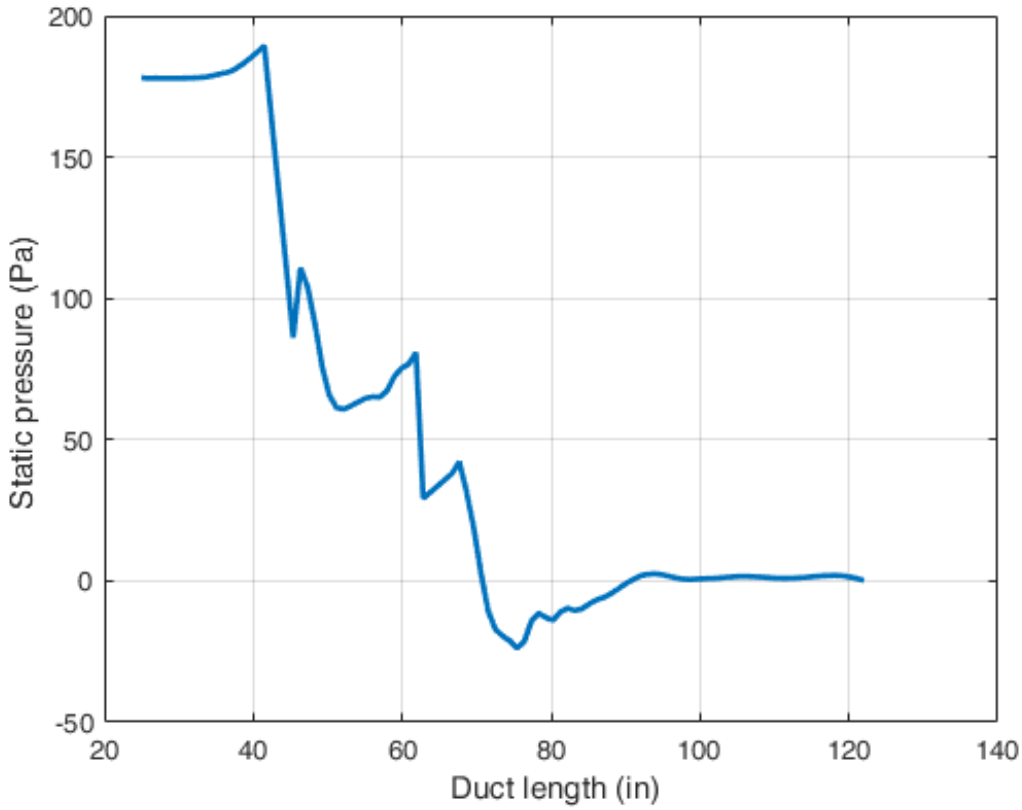

Figure 5.31: Velocity profile at different location of duct for Geometry-4 when distance between mixers is 18 inches when flowrate of hot airstream is 1600 CFM and cold airstream is 400 CFM. First mixer is located at 42 inches distance from the inlet of the duct

In figure 5.32, relatively small vortices are seen between the mixers and after the second mixer when compared with the louver-baffles mixer. Because in this case,

we have only louvers those are directing the flow instead of blocking it, which is happening in case of louver-baffle mixer due to baffles. So small vortices are expected in this case. Velocity vector contour are also presented in figure 5.33 at the plane along the duct to give more understanding of the flow direction in different sections of the duct.

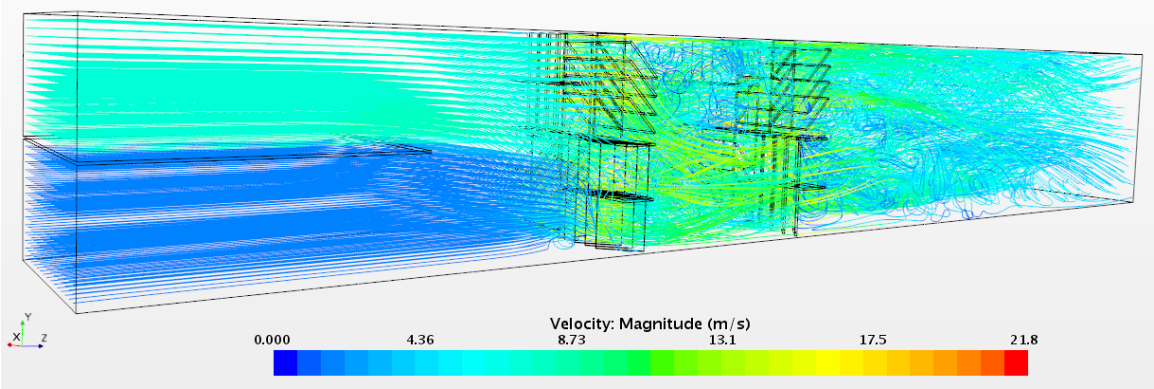

Figure 5.32: Velocity streamlines for Geometry-4 when distance between mixers is 18 inches when flowrate of hot airstream is 1600 CFM and cold airstream is 400 CFM. First mixer is located at 42 inches distance from the inlet of the duct

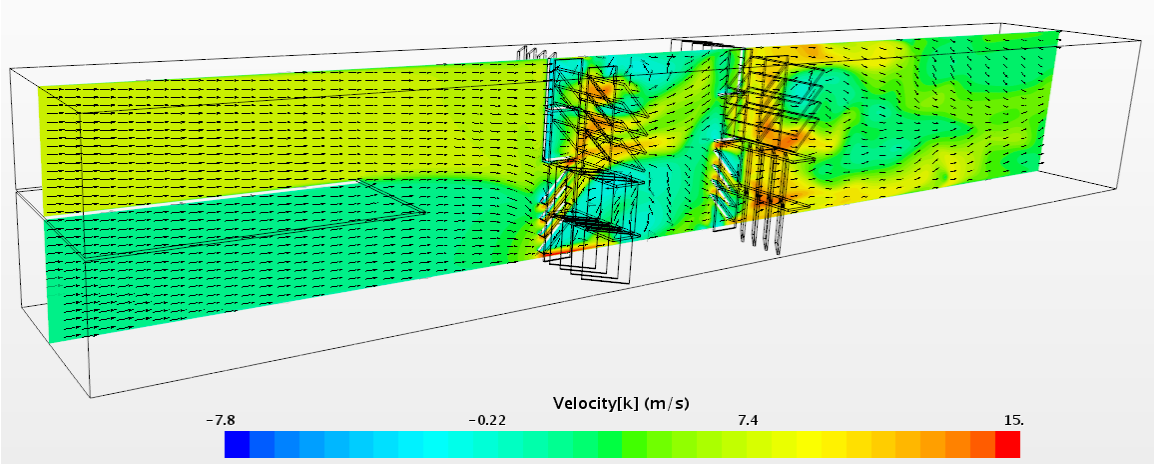

Figure 5.33: Velocity vector contour for Geometry-4 when distance between mixers is 18 inches when flowrate of hot airstream is 1600 CFM and cold airstream is 400 CFM. First mixer is located at 42 inches distance from the inlet of the duct

To see the change in temperature along the height at different locations of the duct, temperature profiles are presented in figure 5.34. It can be seen that temperature variation reduces in the middle of the duct as flow approaches the outlet. In this

case, the trend of the profile is different for high temperature as is seen at the lower half of the duct and lower temperature is seen the upper half of the duct. From the velocity profile presented in figure 5.35, it can be seen that velocity profile is more irregular but the magnitude of the fluctuations is less near the outlet of the duct.

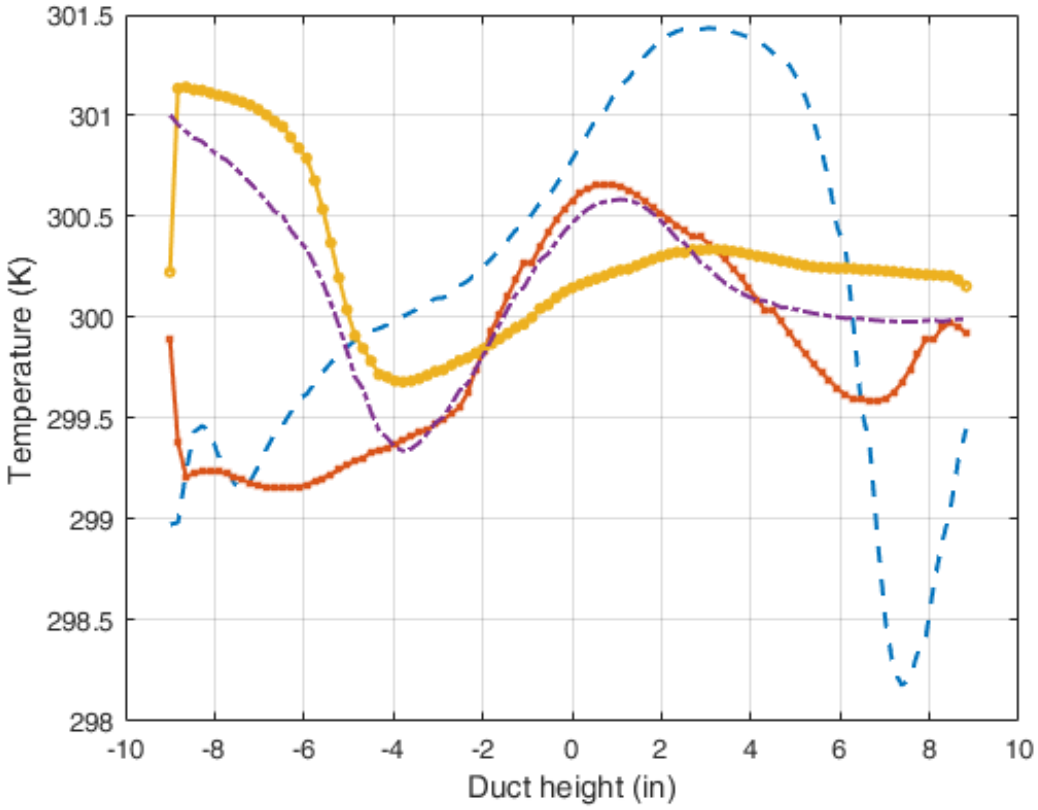

Figure 5.34: Temperature profile at different location of duct for Geometry-4 when distance between mixers is 18 inches when flowrate of hot airstream is 1600 CFM and cold airstream is 400 CFM. First mixer is located at 42 inches distance from the inlet of the duct

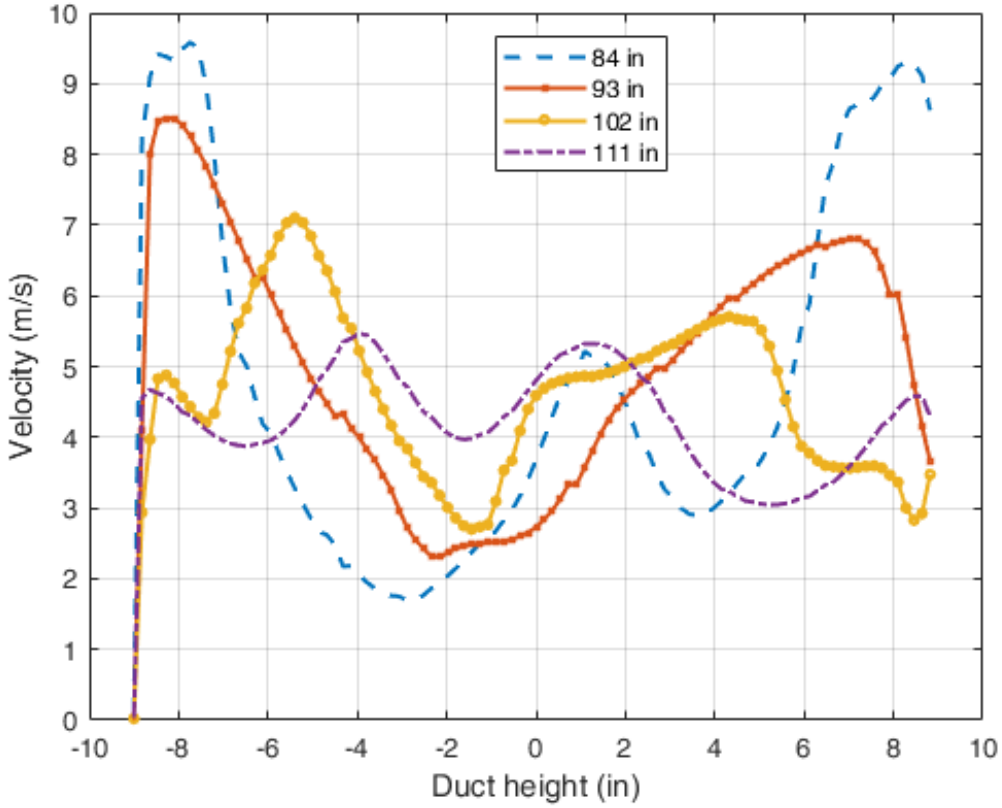

Figure 5.35: Velocity profile at different location of duct for Geometry-4 when distance between mixers is 18 inches when flowrate of hot airstream is 1600 CFM and cold airstream is 400 CFM. First mixer is located at 42 inches distance from the inlet of the duct

Values of mixing effectiveness for different simulations using different geometric configurations and flowrates at different planes of the duct are shown in tables 5.6 - 5.9. Lowest mixing effectiveness of 49.3% at the outlet is seen for case with total low flowrate (2000 CFM), the flow ratio of hot and cold airstreams are same and the distance between mixers is 2 inches. When the total flowrate is 200 CFM and the flow ratios are same, mixing effectiveness is 81.7%. This trend is different when comparison is made with louver-baffle mixer. Highest mixing effectiveness is seen for the case with different flow ratio and the distance between the mixers is 18 inches. From tables 5.6 - 5.9, it can also be seen that mixing effectiveness is decreased with decreasing distance between mixer.

Table 5.6: Comparison of mixing effectiveness for Geometry-4 when distance between mixers is 2 inches for different flow ratio (1:4) and the same flow ratio (1:1) keeping total flowrate (2000 CFM). First mixer is located at 42 inches distance from the inlet of the duct

Name		Inlet	Plane-1	Plane-2	Plane-3	Plane-4	Plane-5	Plane-6	Outlet
	Location of Plane (inch)	0	68	77	86	95	104	113	122
2000-1c4h-L-45-2	S.D. of Temp. (F)	9.86	4.32	4.03	4.04	3.89	3.61	3.45	3.07
	Mixing Effectiveness (%)		56.2	59.1	59.1	60.5	63.4	65.0	68.9
2000-1c1h-L-45-2	S.D. of Temp. (F)	10.0	6.00	5.55	5.72	5.79	5.72	5.38	5.07
	Mixing Effectiveness (%)		40.0	44.5	42.8	42.1	42.8	46.2	49.3

Table 5.7: Comparison of mixing effectiveness for Geometry-4 when distance between mixers is 6 inches for different flow ratio (1:4) and the same flow ratio (1:1) keeping total flowrate (2000 CFM). First mixer is located at 42 inches distance from the inlet of the duct

Name		Inlet	Plane-1	Plane-2	Plane-3	Plane-4	Plane-5	Plane-6	Outlet
	Location of Plane (inch)	0	72	81	90	99	108	117	122
2000-1c4h-L-45-6	S.D. of Temp. (F)	10.03	3.38	3.14	3.23	3.07	2.47	2.29	2.15
	Mixing Effectiveness (%)		66.3	68.7	67.8	69.3	75.4	77.2	78.6
2000-1c1h-L-45-6	S.D. of Temp. (F)	10.0	4.62	4.23	4.13	4.10	3.93	3.74	3.54
	Mixing Effectiveness (%)		53.8	57.7	58.7	59.0	60.7	62.6	64.6

Table 5.8: Comparison of mixing effectiveness for Geometry-4 when distance between mixers is 18 inches for different flow ratio (1:4) and the same flow ratio (1:1) keeping total flowrate (2000 CFM). First mixer is located at 42 inches distance from the inlet of the duct

Name		Inlet	Plane-1	Plane-2	Plane-3	Plane-4	Plane-5	Outlet
	Location of Plane (inch)	0	84	93	102	111	120	122
2000-1c4h-L-45-18	S.D. of Temp. (F)	9.87	1.64	1.60	1.59	1.54	1.40	1.40
	Mixing Effectiveness (%)		83.4	83.8	83.9	84.4	85.8	85.8
2000-1c1h-L-45-18	S.D. of Temp. (F)	10.0	2.87	2.40	2.25	2.16	2.12	2.05
	Mixing Effectiveness (%)		71.3	76.0	77.5	78.4	78.8	79.5

Table 5.9: Comparison of mixing effectiveness for Geometry-4 when distance between mixers is 18 inches for the same flow ratio (1:1) keeping total flowrate (200 CFM) when position of the hot and cold is swapped. First mixer is located at 42 inches distance from the inlet of the duct

Name		Inlet	Plane-1	Plane-2	Plane-3	Plane-4	Plane-5	Outlet
	Location of Plane (inch)	0	84	93	102	111	120	122
200-1h1c-L-45-18	S.D. of Temp. (F)	10.0	2.65	2.22	2.09	2.06	1.88	1.83
	Mixing Effectiveness (%)		73.5	77.8	79.1	79.4	81.2	81.7

5.5 Geometry-5: Orifice-Target Mixer

In this section, results of different simulations for Geometry-5 are presented. In this geometry, orifice-target mixer is used, orifice is located at 42 inches and target plate is placed at 48 inches in the duct. There is uniform distribution of holes in the target plate, the size of each hole is 0.325 inch. Location of the target plate is same for all simulations. This geometry is analyzed by varying orifice diameter, with different flowrate and temperature difference between two airstreams. Visual results for low temperature gradient when cold air is at 79.5°F and hot air is at 80.5°F are shown in figures 5.36 - 5.37 and the quantitative values for all simulations are shown in tables 5.10 - 5.12. From the temperature contours shown in figure 5.36 for different planes at different locations of the duct, temperature variation along the duct can be seen. In these contours low temperature zone can be seen at center of the duct, which is reducing as the flow is approaching the duct outlet. At the outlet, very small size high temperature zone can be seen at the right corner other then that temperature is uniform at the outlet.

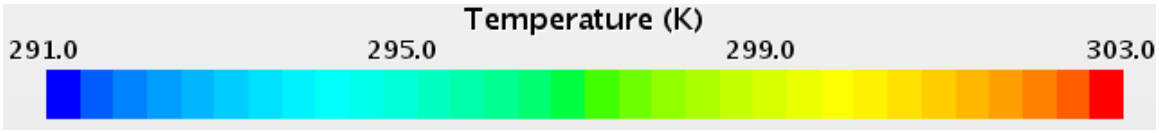

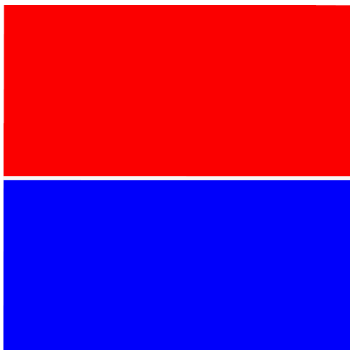

(a) Inlet

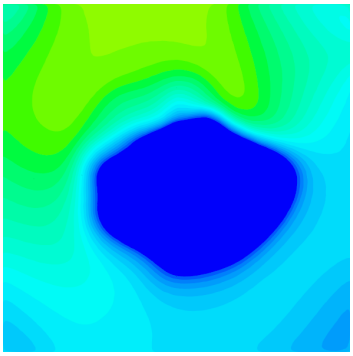

(b) Plane-1

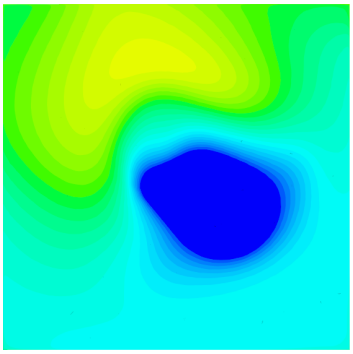

(c) Plane-3

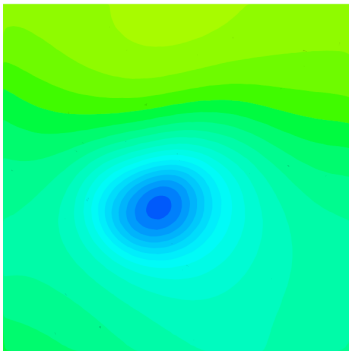

(d) Plane-5

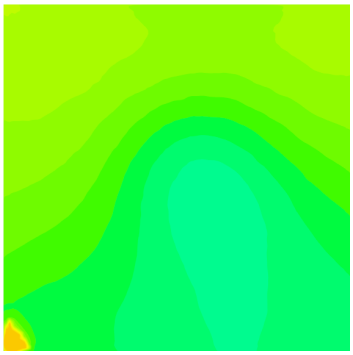

(e) Outlet

Figure 5.36: Temperature contours for orifice-target mixer with orifice diameter of 7.2 inches cold airstream at 79.5°F and 1000 CFM and hot airstream at 80.5°F and 1000 CFM. Orifice is located at 42 inches distance from the inlet of the duct and target plate is located at 48 inches from the inlet of the duct

Static pressure contour is presented in figure 5.38 to see how the pressure is changing along the duct. From the plot presented in figure 5.37 pressure drops from approx. 1932 Pa to 300 Pa at 42 inches duct length where the orifice is placed then it regains to 1200 Pa and again decreases at 48 inches where the target plate is located. Due to the target plate pressure decreases from 1200 Pa to -1500 Pa and then it starts to regain till the outlet of the duct. In this case a high pressure drop is experienced.

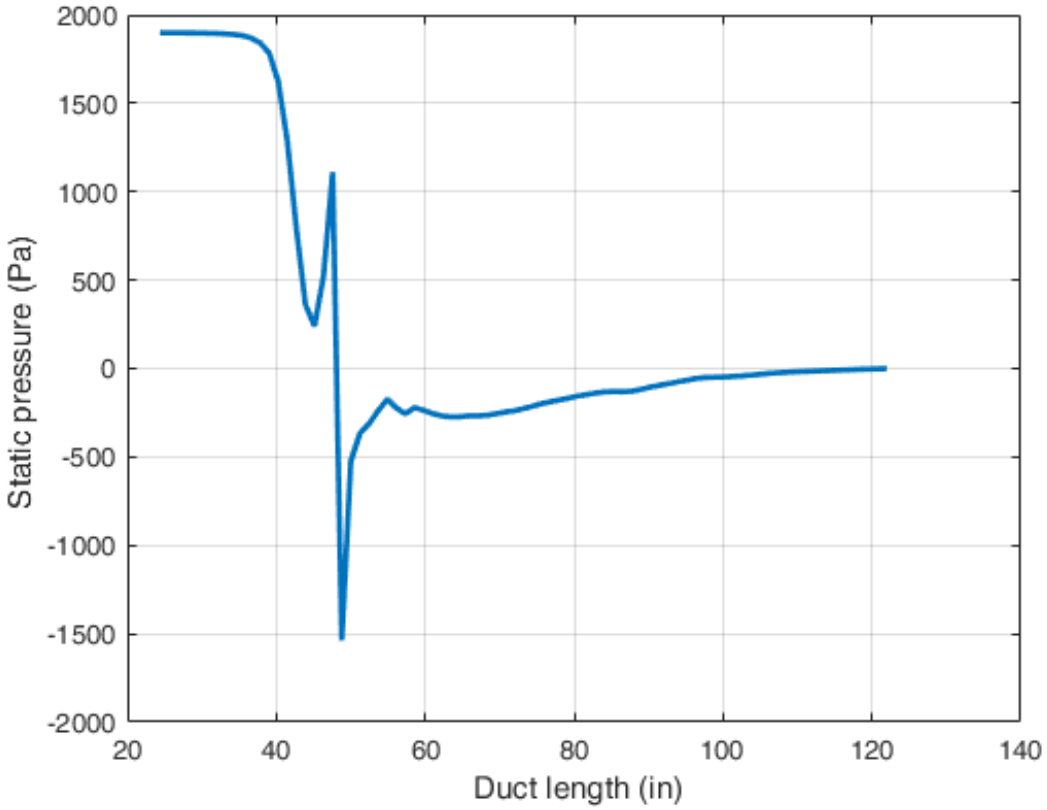

Figure 5.37: Velocity profile at different location of duct for orifice-target mixer with orifice diameter of 7.2 inches cold airstream at 79.5°F and 1000 CFM and hot airstream at 80.5°F and 1000 CFM. Orifice is located at 42 inches distance from the inlet of the duct and target plate is located at 48 inches from the inlet of the duct

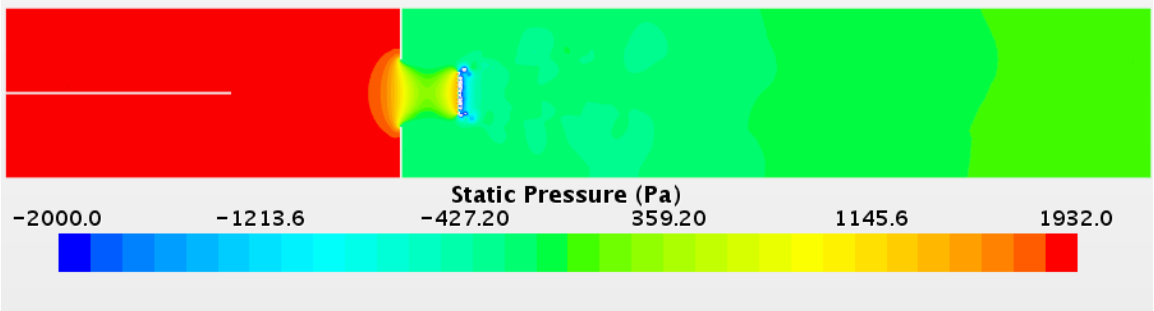

Figure 5.38: Static pressure for orifice-target mixer with orifice diameter of 7.2 inches cold airstream at 79.5°F and 1000 CFM and hot airstream at 80.5°F and 1000 CFM. Orifice is located at 42 inches distance from the inlet of the duct and target plate is located at 48 inches from the inlet of the duct

From figure 5.39 small vortices are seen above and below the duct before the orifice. When both flow passes the orifice, these form a jet of high velocity. More

vortices are seen inches the lower region of the duct as compared to the upper region. As jet strikes the target plate, it diverges after the target plate few vortices can be seen which helps in mixing of airstreams. From figure 5.40 of velocity field flow re-circulations can be seen in the duct.

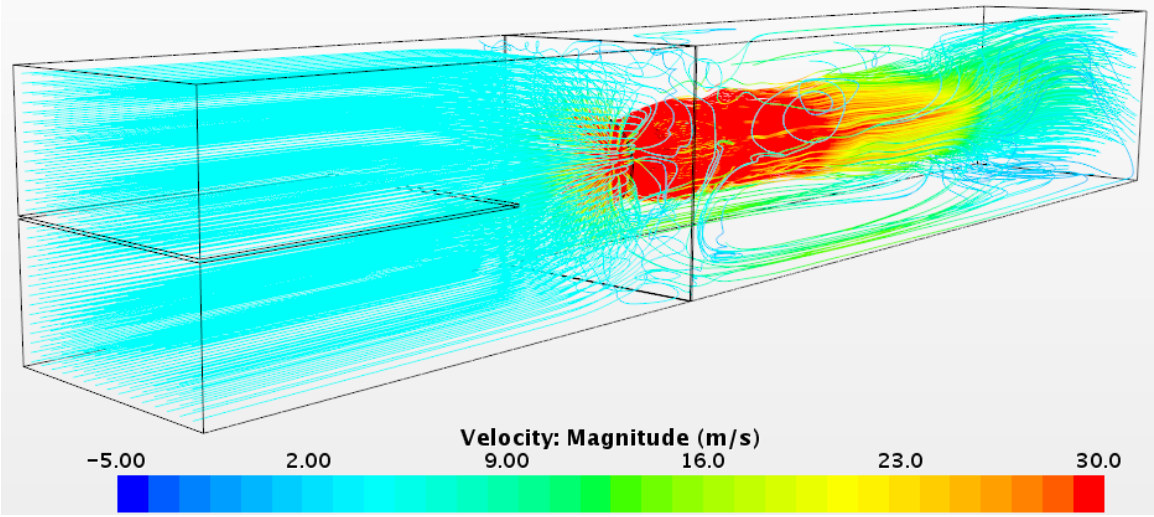

Figure 5.39: Velocity streamlines for orifice-target mixer with orifice diameter of 7.2 inches cold airstream at 79.5°F and 1000 CFM and hot airstream at 80.5°F and 1000 CFM. Orifice is located at 42 inches distance from the inlet of the duct and target plate is located at 48 inches from the inlet of the duct

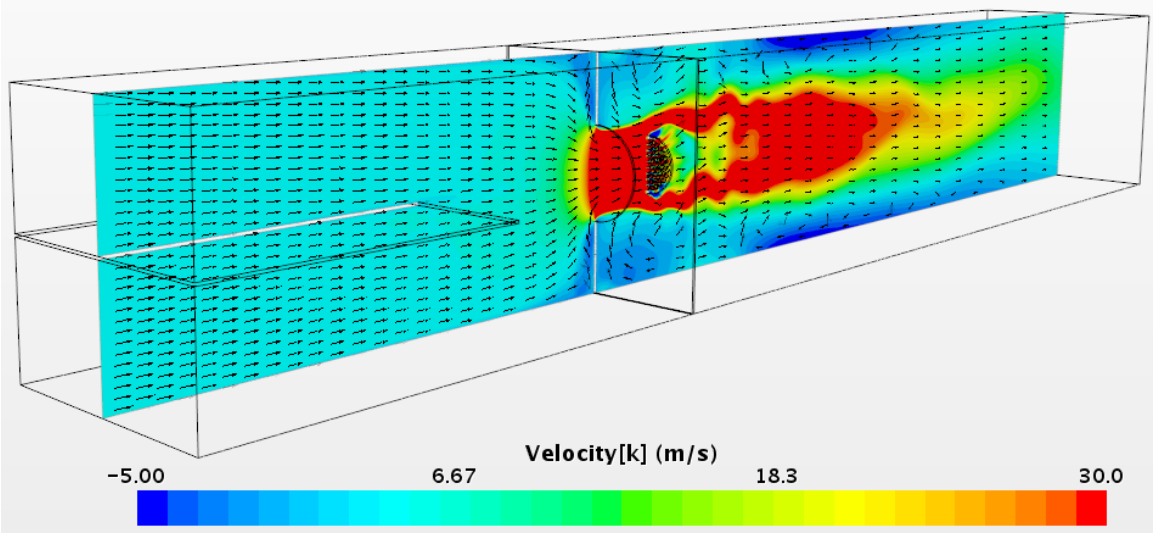

Figure 5.40: Velocity vector contour for orifice-target mixer with orifice diameter of 7.2 inches cold airstream at 79.5°F and 1000 CFM and hot airstream at 80.5°F and 1000 CFM. Orifice is located at 42 inches distance from the inlet of the duct and target plate is located at 48 inches from the inlet of the duct

To see the change in temperature along the height at different locations of the duct, temperature profiles are presented in figure 5.41. It can be seen that temperature was less in the middle of the duct recorded by probes located at 66 inches but later this difference reduced as flow approaches the outlet. Bi-modal shape of the profile is seen at 66 inches with very high velocity in the middle which is presented in figure 5.35, later this velocity reduces as the flow approaches the outlet of the duct but remains high at the center when compared to velocities at the lower and upper half of the duct.

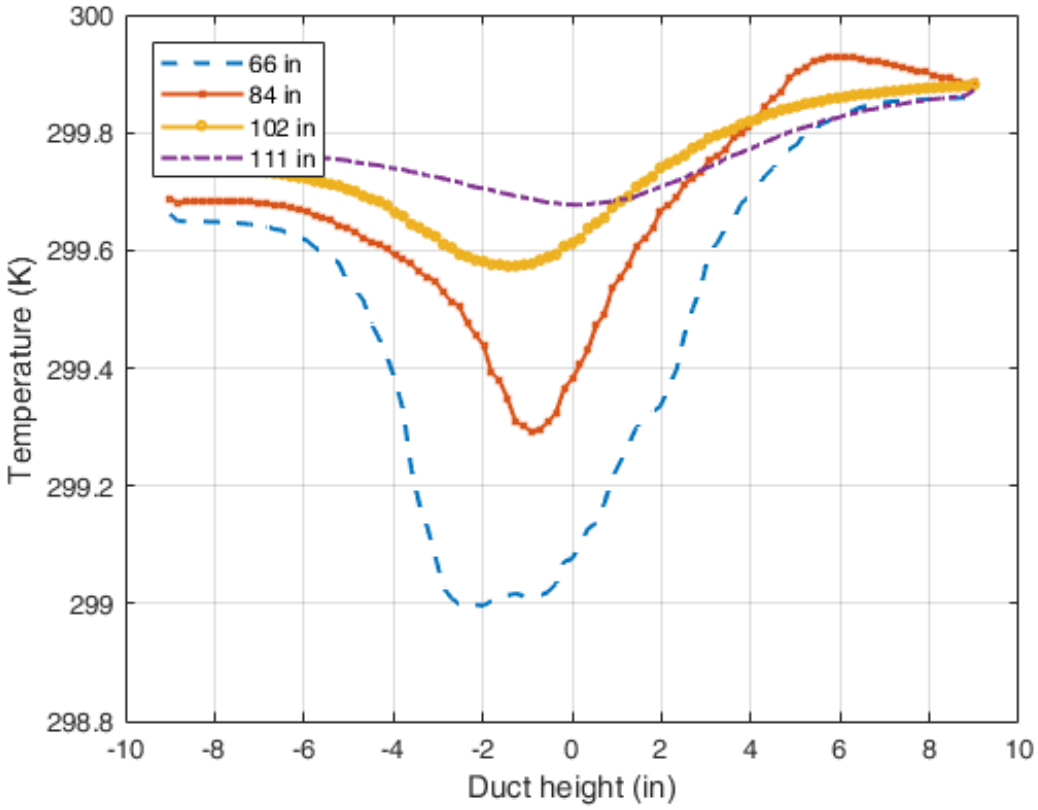

Figure 5.41: Temperature profile at different location of duct for orifice-target mixer with orifice diameter of 7.2 inches cold airstream at 79.5°F and 1000 CFM and hot airstream at 80.5°F and 1000 CFM. Orifice is located at 42 inches distance from the inlet of the duct and target plate is located at 48 inches from the inlet of the duct

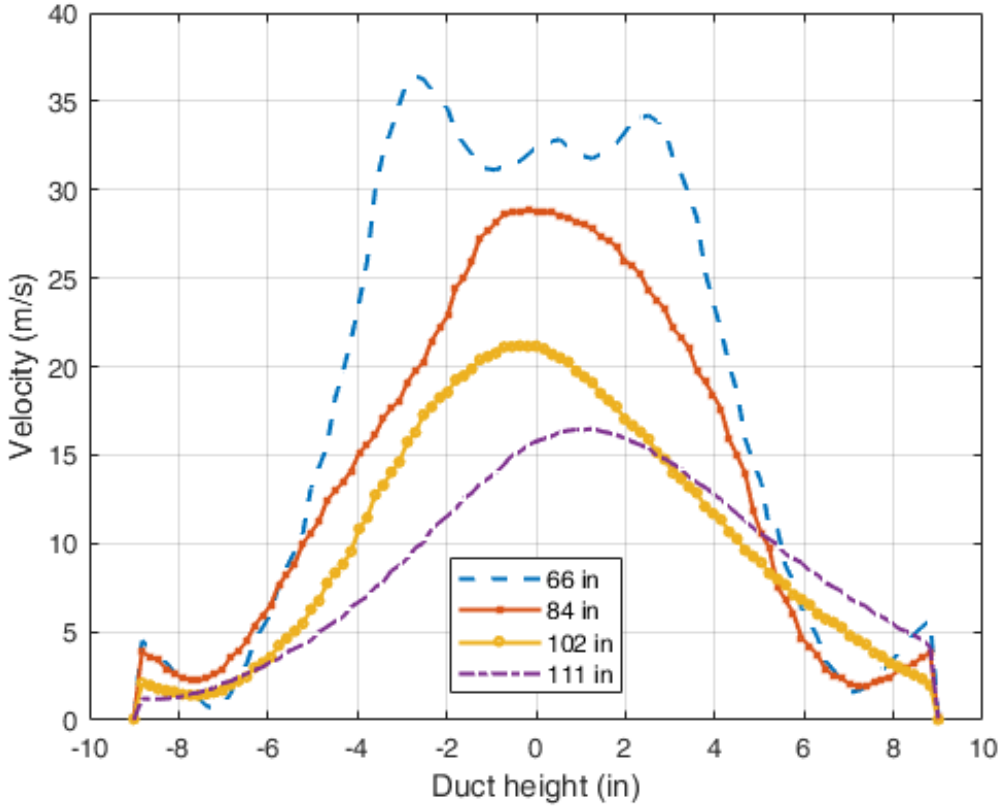

Figure 5.42: Velocity profile at different location of duct for orifice-target mixer with orifice diameter of 7.2 inches cold airstream at 79.5°F and 1000 CFM and hot airstream at 80.5°F and 1000 CFM. Orifice is located at 42 inches distance from the inlet of the duct and target plate is located at 48 inches from the inlet of the duct

Values of mixing effectiveness for different simulations with different orifice diameters at different planes of the duct are shown in tables 5.10 and comparison can also be seen in figure 5.43. From this data it can be easily concluded that maximum effectiveness is achieved with the smallest orifice which indicate that the interface area between the cold and hot airstream contributes to the improvement of the effectiveness. Similar conclusion is made by experimental study done at NIST Faison et al. (1967). Values of mixing effectiveness are also presented in table 5.11 for the small temperature gradient case. In this case, hot air is entered in the duct from bottom and cold air from top. Overall, mixing effectiveness deceases when compared with the large temperature gradient flow while keeping all other parameters constant.

When compared the results of low temperature gradient simulations by swapping inlets at different planes trend is different, for example, at plane-1 mixing effectiveness is better when the cold air is at upper part on the other hand, at plane-3 high mixing effectiveness is seen when cold air is at lower part and also more mixing effectiveness is seen at the outlet for this case. This geometry is also studied when the total flowrate is 200 CFM and cold airstream at 65 °F and 100 CFM and hot airstream at 85 °F and 100 CFM. In this case, 87.7% mixing effectiveness is achieved.

Table 5.10: Mixing effectiveness for Geometry-5 with different orifice size when cold airstream at 65 °F and 1000 CFM and hot airstream at 85 °F and 1000 CFM. Orifice is located at 42 inches distance from the inlet of the duct and target plate is located at 48 inches from the inlet of the duct

Name		Inlet	Plane-1	Plane-2	Plane-3	Plane-4	Plane-5	Plane-6	Outlet
	Location of Plane (inch)	0	66	75	84	93	102	111	122
2000-1c1h-OT-7.2	S.D. of Temp. (F)	10.00	3.77	3.68	3.33	2.70	2.00	1.45	1.04
	Mixing Effectiveness (%)		62.3	63.2	66.7	73.0	80.0	85.5	89.6
2000-1c1h-OT-8.1	S.D. of Temp. (F)	10.00	4.91	4.49	4.47	3.99	3.47	3.20	3.17
	Mixing Effectiveness (%)		50.9	55.1	55.3	60.1	65.3	68.0	68.3
2000-1c1h-OT-9.0	S.D. of Temp. (F)	10.00	5.04	5.38	5.17	4.80	4.72	4.60	4.34
	Mixing Effectiveness (%)		49.6	49.2	48.3	52.0	52.8	54.0	56.6
2000-1c1h-OT-9.9	S.D. of Temp. (F)	10.00	5.29	5.65	5.38	5.17	5.08	4.86	4.54
	Mixing Effectiveness (%)		47.1	43.5	46.2	48.3	49.2	51.4	54.6
2000-1c1h-OT-10.8	S.D. of Temp. (F)	10.00	5.08	5.15	5.05	5.47	5.75	5.15	4.91
	Mixing Effectiveness (%)		49.2	48.5	49.5	45.3	42.5	48.5	50.9

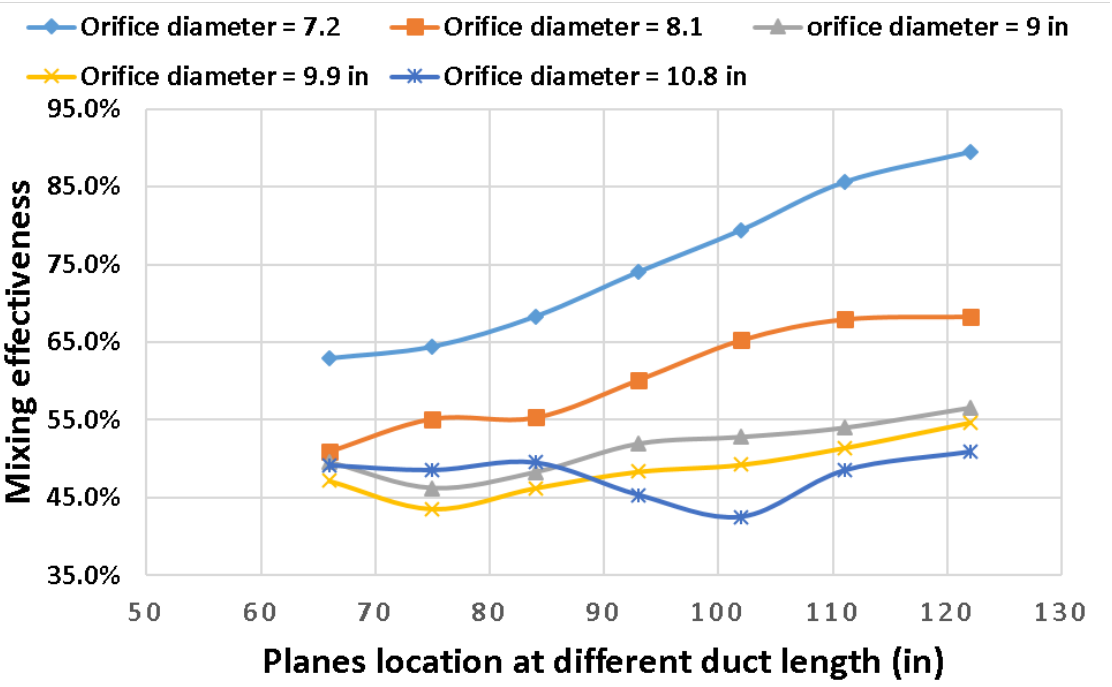

Figure 5.43: Mixing effectiveness at different location of duct for for different orifice diameters for geometry-5 cold airstream at 79.5°F and 1000 CFM and hot airstream at 80.5°F and 1000 CFM. Orifice is located at 42 inches distance from the inlet of the duct and target plate is located at 48 inches from the inlet of the duct

Table 5.11: Mixing effectiveness for Geometry-5 with orifice diameter 7.2 inches when cold airstream at 79.5 °F and 1000 CFM and hot airstream at 80.5 °F and 1000 CFM and the position of the hot and cold airstreams are swapped. Orifice is located at 42 inches distance from the inlet of the duct and target plate is located at 48 inches from the inlet of the duct

Name		Inlet	Plane-1	Plane-2	Plane-3	Plane-4	Plane-5	Plane-6	Outlet
	Location of Plane (inch)	0	66	75	84	93	102	111	122
2000-1c1h-OT-7.2	S.D. of Temp. (F)	0.50	0.36	0.31	0.24	0.17	0.12	0.08	0.07
	Mixing Effectiveness (%)		27.3	38.5	51.2	65.8	75.8	83.7	86.5
2000-1h1c-OT-7.2	S.D. of Temp. (F)	0.50	0.33	0.30	0.25	0.19	0.12	0.07	0.08
	Mixing Effectiveness (%)		33.5	39.7	49.7	62.9	75.9	86.8	84.3

Table 5.12: Mixing effectiveness for Geometry-5 with orifice diameter 7.2 inches when cold airstream at 65 °F and 100 CFM and hot airstream at 85 °F and 100 CFM. location of hot and cold inlets are swapped. Orifice is located at 42 inches distance from the inlet of the duct and target plate is located at 48 inches from the inlet of the duct

Name		Inlet	Plane-1	Plane-2	Plane-3	Plane-4	Plane-5	Plane-6	Outlet
	Location of Plane (inch)	0	66	75	84	93	102	111	122
200-1h1c-OT-7.2	S.D. of Temp. (F)	10.0	4.24	4.21	3.93	3.28	2.53	1.87	1.23
	Mixing Effectiveness (%)		57.6	57.9	60.7	67.2	74.7	81.3	87.7

5.6 Geometry-6: Orifice Mixer

In this section results for Geometry-6 will be discussed. The only difference is the removal of target plate from the geometry-5. This case is studied with orifice diameter 7.2 inches and total flowrate 2000 CFM for same flow ratio for hot and cold air. From the temperature contours presented in figure 5.44, the low and high temperature zones in the middle of the duct those are because of high and low temperature airstreams jet after the orifice. When compared these results with the orifice-target combination for same flowrate. At plane-1, high temperature zone was larger in orifice-case but smaller zone is seen in low temperature region. In this case, at the outlet high temperature zone is seen which decreases the mixing effectiveness at the outlet. In case of orifice-target combination temperature is very uniform at the outlet. By carefully examining this results, it is seen that relatively high temperature air is striking at one side of the outlet in the figure 5.44(e).

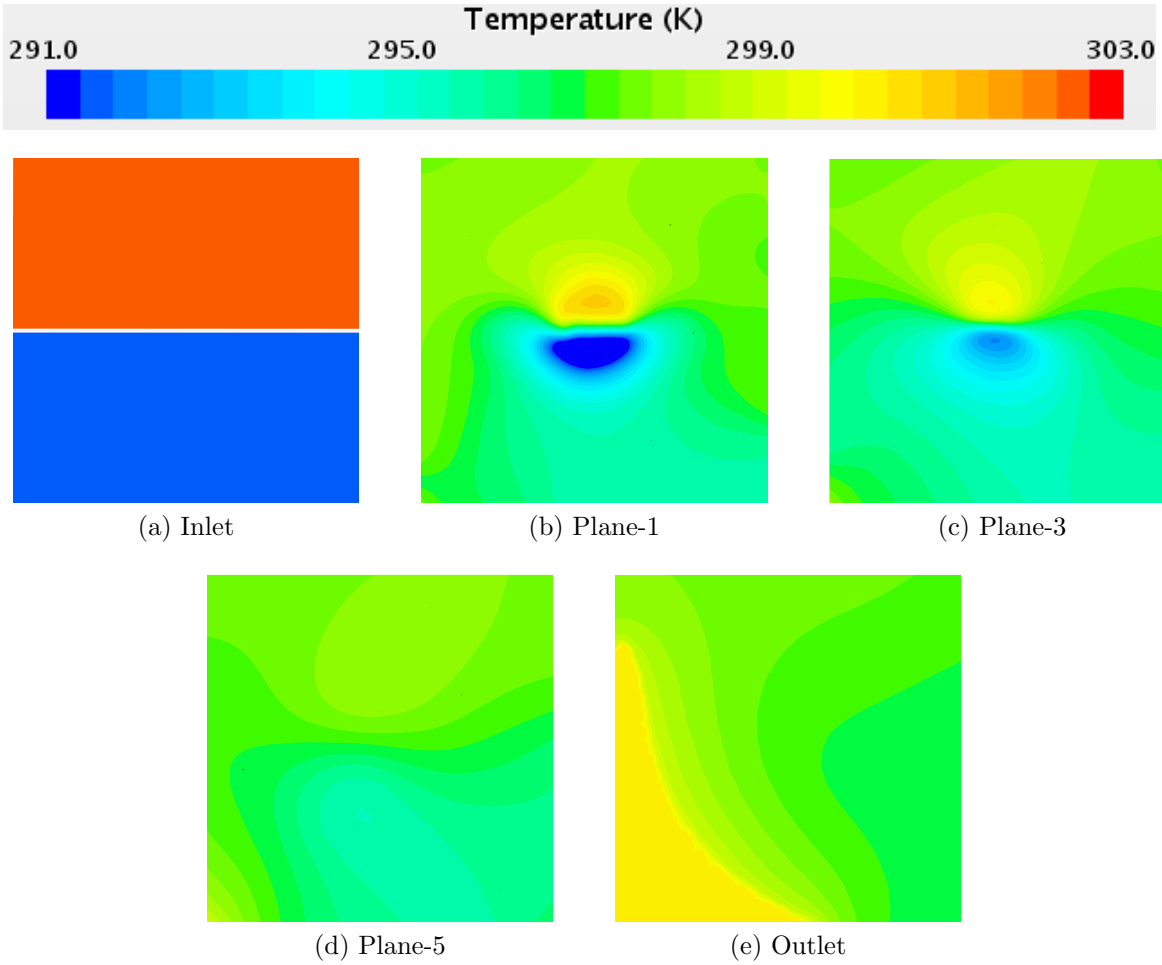

(a) Inlet (b) Plane-1 (c) Plane-3

(d) Plane-5 (e) Outlet

Figure 5.44: Temperature contours for orifice mixer with orifice diameter of 7.2 inches when cold airstream at 65°F and 1000 CFM and hot airstream at 85°F and 1000 CFM. Orifice is located at 42 inches distance from the inlet of the duct

Static pressure contour is presented in figure 5.45 to see how the pressure is changing along the duct. From the plot presented in figure 5.46 pressure drops from approx. 1900 Pa to approx. -250 Pa at 42 inches duct length where the orifice is placed then it starts to regains till the outlet of the duct. When compared with the orifice-target mixer pressure drop is less in this case.

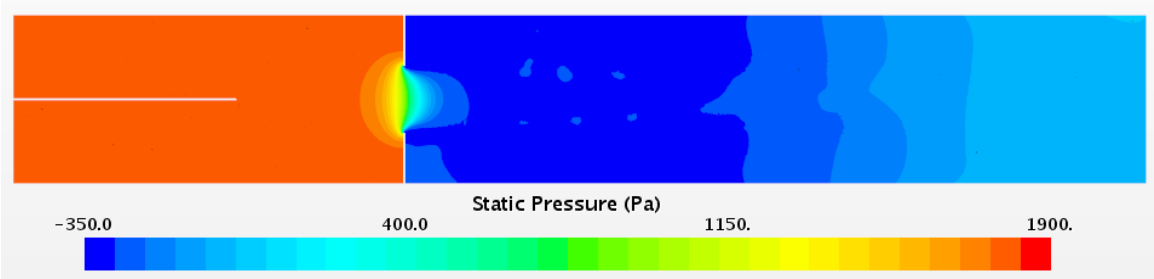

Figure 5.45: Static Pressure for orifice mixer with orifice diameter of 7.2 inches when cold airstream at 65°F and 1000 CFM and hot airstream at 85°F and 1000 CFM

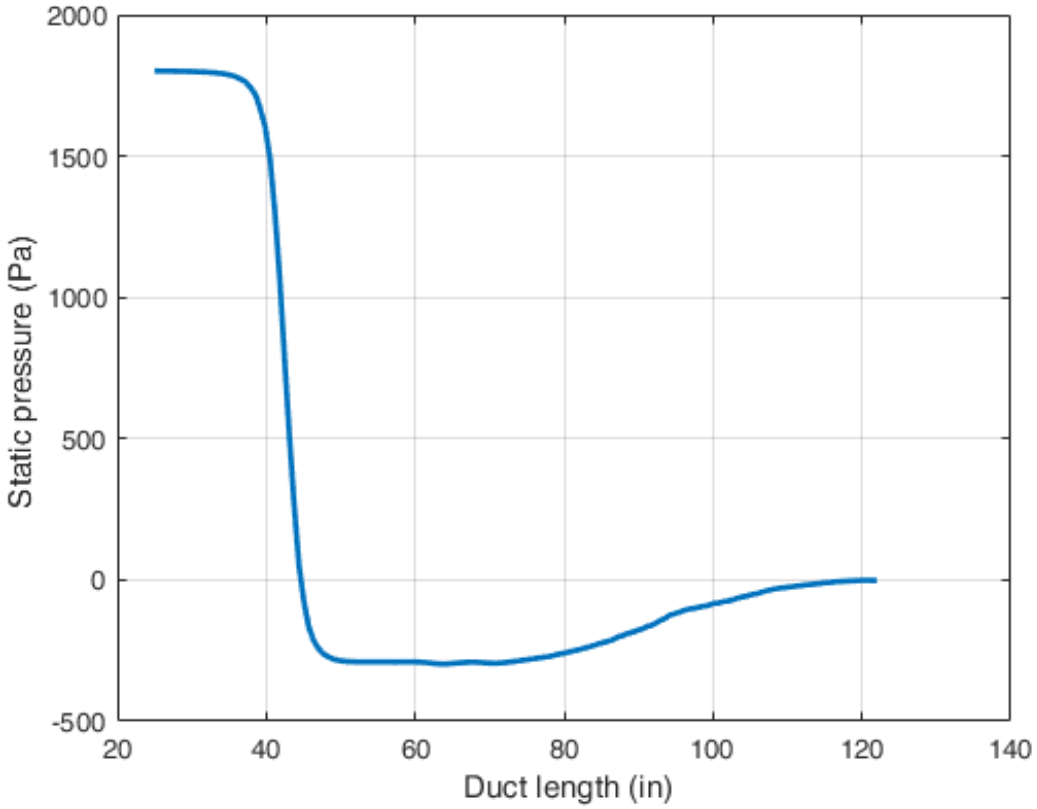

Figure 5.46: Velocity profile at different location of duct for orifice mixer with orifice diameter of 7.2 inches when cold airstream at 65°F and 1000 CFM and hot airstream at 85°F and 1000 CFM. Orifice is located at 42 inches distance from the inlet of the duct

From figure 5.47 of streamlines with small vortices are seen above and below the duct before the orifice. When both flow passes the orifice these form a jet of high velocity. More vortices are seen in the lower region of the duct as compared to the upper region. Diameter of the jet started to increase nearly 90 inches duct length

and after 102 inches length the flow spreads because of this it can be seen that the flow is not uniform or developed at the side where high temperature zone is seen at the outlet. For this study, one understanding is that duct length should be extended to get developed flow. This behaviour could be due to the boundary condition at the outlet. In figure 5.48, velocity contour is presented, many re-circulation regions can be seen in the duct at that plane espeicualy nearly the outlet.

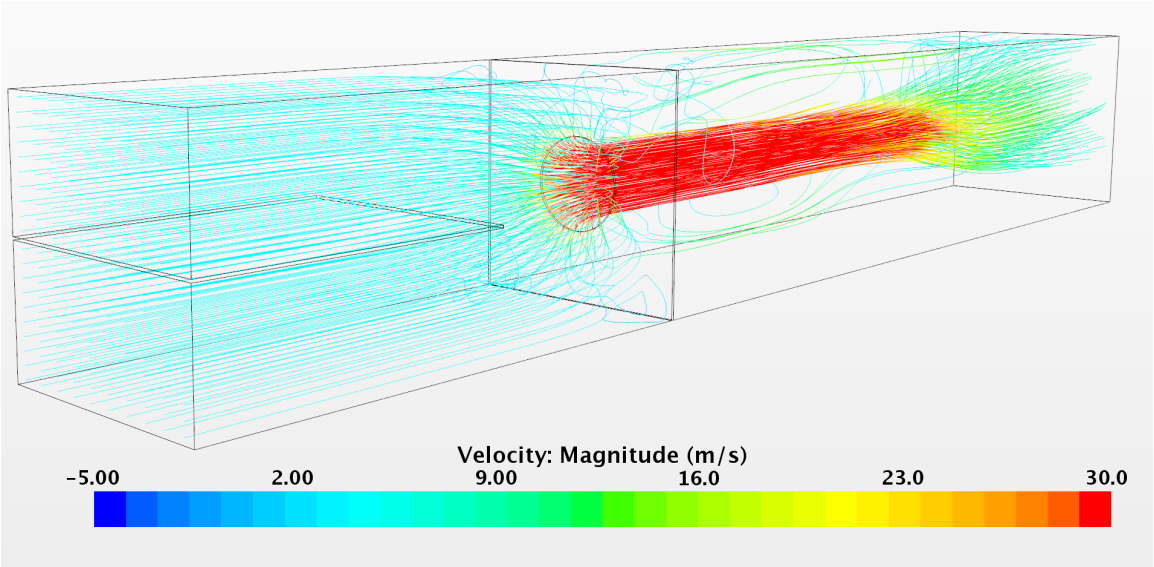

Figure 5.47: Velocity streamlines for orifice mixer with orifice diameter of 7.2 inches when cold airstream at 65°F and 1000 CFM and hot airstream at 85°F and 1000 CFM. Orifice is located at 42 inches distance from the inlet of the duct

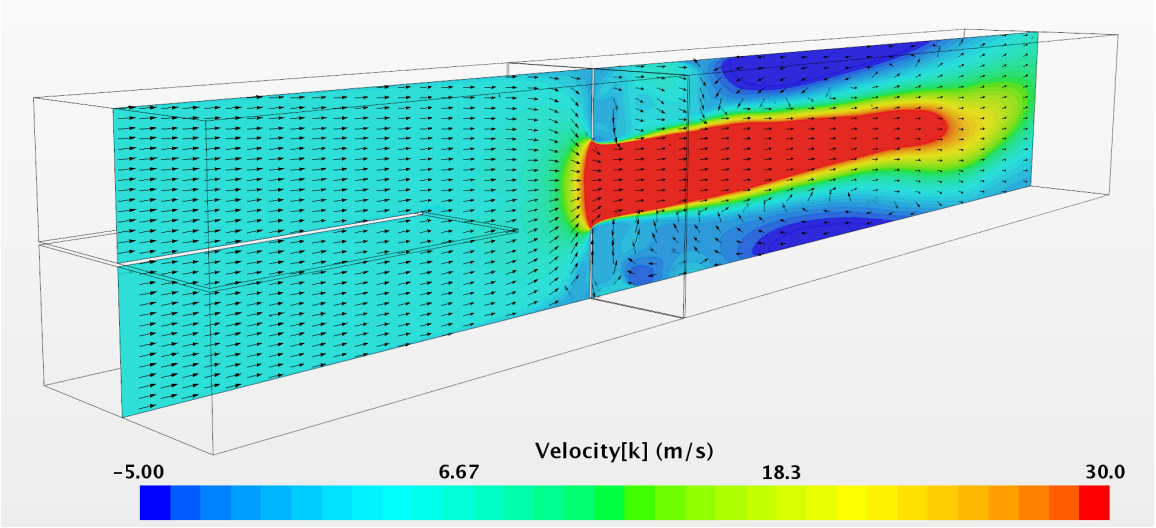

Figure 5.48: Velocity vector contour for orifice mixer with orifice diameter of 7.2 inches when cold airstream at 65°F and 1000 CFM and hot airstream at 85°F and 1000 CFM. Orifice is located at 42 inches distance from the inlet of the duct

To see the change in temperature along the height at different locations of the duct, temperature profiles are presented in figure 5.49. It can be seen that temperature at the probe lines placed at 102 inches temperature is quite uniform and then at 111 inches length fluctuation are high, which shows that flow is not stable yet. Very high velocity is seen in the middle of the duct which is presented in figure 5.49, later this velocity reduces as the flow approaches the outlet of the duct but remains relatively high at the center when compared to velocities at the lower and upper half of the duct.

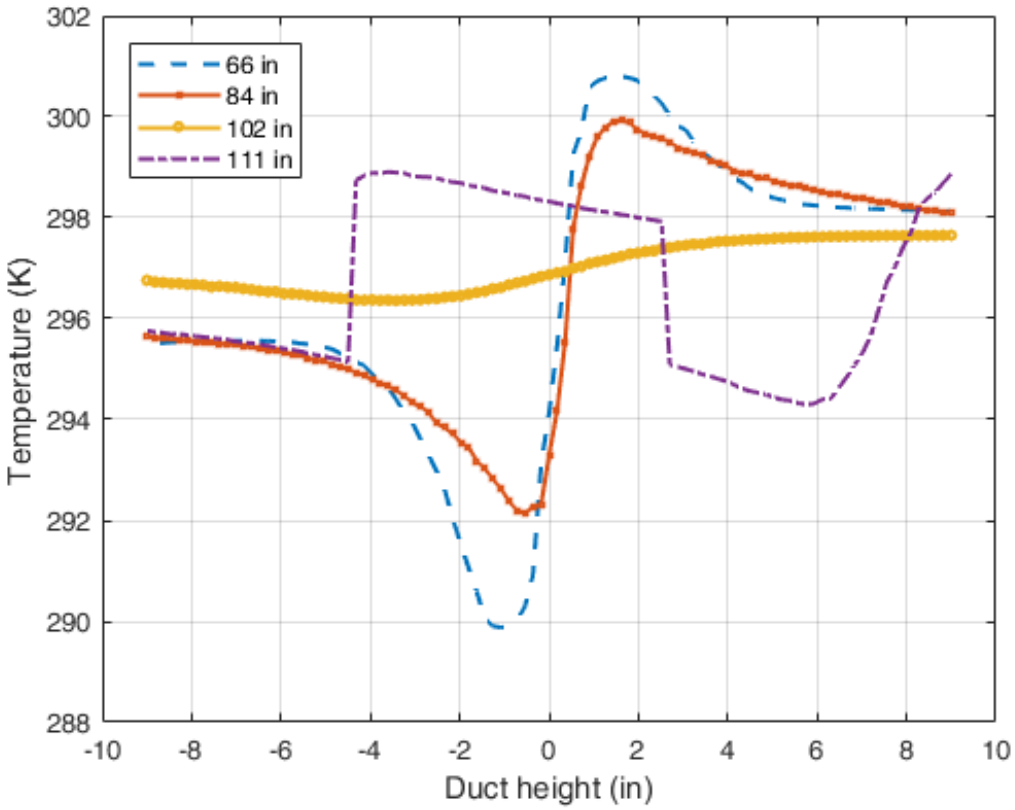

Figure 5.49: Temperature profile at different location of duct for orifice mixer with orifice diameter of 7.2 inches when cold airstream at 65°F and 1000 CFM and hot airstream at 85°F and 1000 CFM. Orifice is located at 42 inches distance from the inlet of the duct

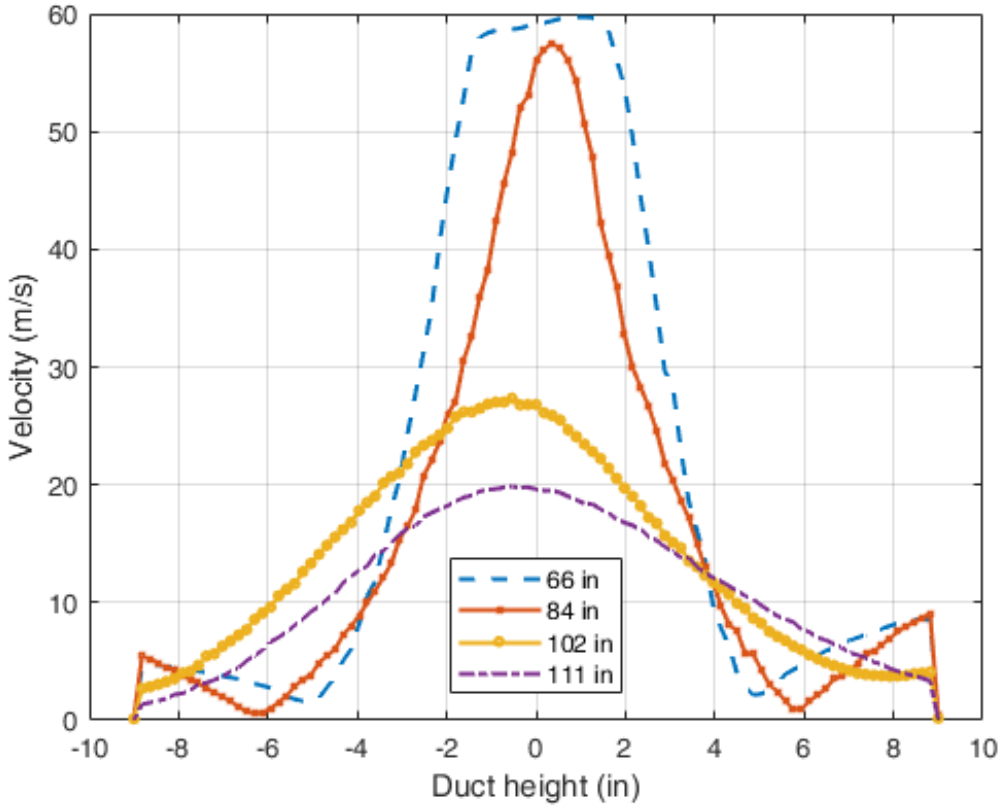

Figure 5.50: Velocity profile at different location of duct for orifice mixer with orifice diameter of 7.2 inches when cold airstream at 65°F and 1000 CFM and hot airstream at 85°F and 1000 CFM. Orifice is located at 42 inches distance from the inlet of the duct

Mixing effectiveness at different planes for this case has been reported in table 5.13. Highest mixing effectiveness which is 90.1% is seen in this case when compared with other cases till 111 inches duct length and then suddenly mixing effectiveness decreases to 80.9%. This unexpected trend may be a result of constant pressure outlet boundary condition imposed at the outlet; see also re-circulation, figure 5.47, from outlet of the duct to the mixer plane for different mixer case . To investigate it more, the same geometry is analyzed for an increase duct length of 244 inches by keeping all other parameters as constant. Quantitative values of mixing effectiveness with the extended duct length are shown in table 5.13. From table 5.14, it can be seen that at duct length of 122 inches mixing effectiveness is 96.3%, where as at the same length it was 80.9% when the total length of the duct was 122 inches, table 5.13. This result supports suspicion of the outlet boundary condition affecting the result, see figure 5.51 and 5.52. Static pressure becomes zero approximately at 180 inch duct length.

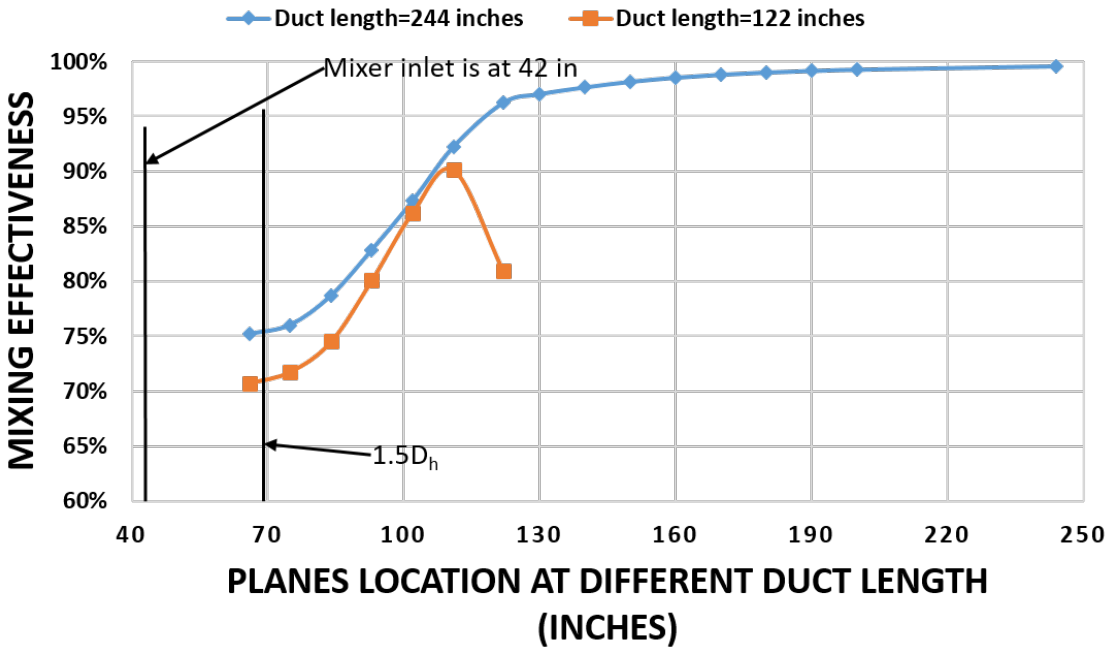

Figure 5.51: Comparison of mixing effectiveness for Geometry-6 when cold airstream at 65 °F and 1000 CFM and hot airstream at 85 °F and 1000 CFM. Orifice is located at 42 inches distance from the inlet of the duct. When duct length is 122 inches and 244 inches

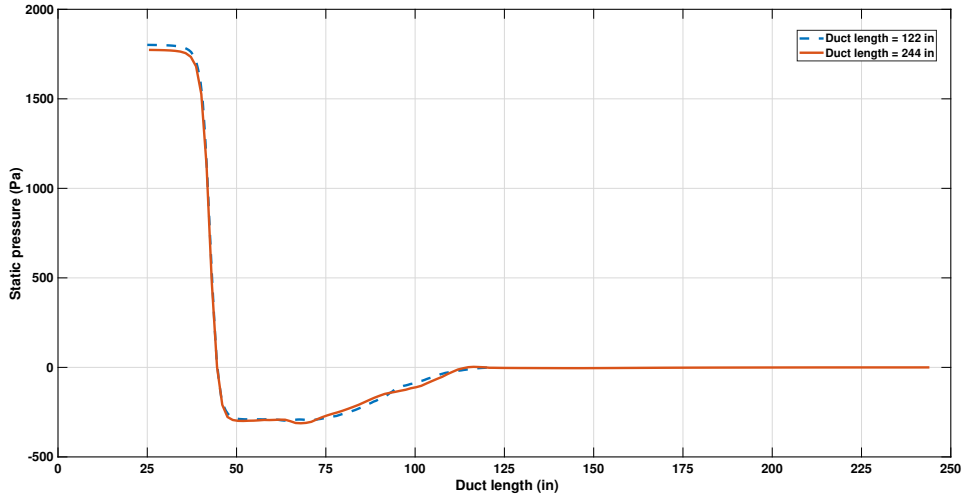

Figure 5.52: Comparison of static pressure for Geometry-6 when cold airstream at 65 °F and 1000 CFM and hot airstream at 85 °F and 1000 CFM. Orifice is located at 42 inches distance from the inlet of the duct. When duct length is 122 inches and 244 inches

Table 5.13: Mixing effectiveness for Geometry-6 when cold airstream at 65 °F and 1000 CFM and hot airstream at 85 °F and 1000 CFM. Orifice is located at 42 inches distance from the inlet of the duct. Duct length 122 inches, default for all other cases.

Name		Inlet	Plane-1	Plane-2	Plane-3	Plane-4	Plane-5	Plane-6	Outlet
	Location of Plane (inch)	0	66	75	84	93	102	111	122
2000-1c1h-O-7.2	S.D. of Temp. (F)	10.0	2.93	2.82	2.55	1.99	1.38	0.99	1.91
	Mixing Effectiveness (%)		70.7	71.8	74.5	80.1	86.2	90.1	80.9

Table 5.14: Mixing effectiveness for Geometry-6 when cold airstream at 65 °F and 1000 CFM and hot airstream at 85 °F and 1000 CFM. Orifice is located at 42 inches distance from the inlet of the duct. Duct length 244 inches.

Name		Inlet	Plane-1	Plane-2	Plane-3	Plane-4	Plane-5	Plane-6	Plane-7
	Location of Plane (inch)	0	66	75	84	93	102	111	122
2000-1c1h-O-7.2	S.D. of Temp. (F)	10.0	2.48	2.40	2.13	1.71	1.27	0.78	0.37
	Mixing Effectiveness (%)		75.2	76.0	78.7	82.9	87.3	92.2	96.3

5.7 Summary

This research is a part of ASHRAE RP-1733 *Develop Design Criteria for Psychrometric Air Sampler and Mixer Apparatus for Use in ASHRAE Test Standards.* Air sampler is used to sample air and measure average properties. Air mixer is used to provide uniform (mixed) air conditions to the air sampler, increasing accuracy. This allows more accurate performance measurements of HVAC systems then single point sampling. This thesis focuses specifically on the air mixer apparatus; five different air mixers are modeled using SolidWorks. The performance of these models is then investigated using CFD technique for different flow conditions in a square duct(18" x 18"). Star-CCM+ is used as a CFD package. A total duct length of 122 inches is used to see the distance required to reach 80% mixing effectiveness with different mixers under different flow conditions. The result for this study for all simulations are shown in sections 5.2 to 5.6.

Mixing effectiveness at the outlet of the duct for all cases is presented in table 5.15. Five best mixers are colored in green and the density of the color is reducing with the decrease in mixing effectiveness.

Table 5.15: Mixing effectiveness for all simulations

Setup	Mixer type	Test name	Total flowrate (CFM)	Flowrate bottom (CFM)	Flowrate top (CFM)	Bottom inlet temp [F]	Top inlet temp [F]	Louver angle (Degree)	Orifice diameter (inches)	Distance between mixers (inches)	Mixing effectiveness at outlet (%)
Geometry-1	None	2000-1c4h-00	2000	400	1600	65	85	-	-	-	21.2
		2000-1c1h-00		1000	1000	65	85	-	-	-	7.7
Geometry-2	Louver Baffles, Single Mixer	2000-1c4h-Lb-45		400	1600	65	85	45	-	-	81.6
		2000-1c4h-Lb-50				65	85	50	-		86.4
		2000-1c4h-Lb-55				65	85	55	-		84.5
		2000-1c4h-Lb-60				65	85	60	-		86.3
		2000-1c4h-Lb-65				65	85	65	-		88.0
Geometry-3	Louver Baffles, Pair in Series	2000-1c4h-Lb-45-2		400	1600	65	85	45	-	2	82.8
		2000-1c1h-Lb-45-2		1000	1000	65	85		-		75.6
		2000-1c4h-Lb-45-18		400	1600	65	85		-	18	86.9
		2000-1c1h-Lb-45-18		1000	1000	65	85		-		81.1
Geometry-4	Louver, Pair in Series	2000-1c4h-L-45-2		400	1600	65	85	45	-	2	49.3
		2000-1c1h-L-45-2		1000	1000	65	85		-		68.9
		2000-1c4h-L-45-6		400	1600	65	85		-	6	78.6
		2000-1c1h-L-45-6		1000	1000	65	85		-		64.6
		2000-1c4h-L-45-18		400	1600	65	85		-	18	85.8
		2000-1c1h-L-45-18		1000	1000	65	85		-		79.5
Geometry-5	Orifice with Target	2000-1c1h-OT		1000	1000	65	85	-	7.2	-	89.5
		2000-1c1h-OT				65	85	-	8.1		68.3
		2000-1c1h-OT				65	85	-	9		56.6
		2000-1c1h-OT				65	85	-	9.9		54.6
		2000-1c1h-OT				65	85	-	10.8		50.9
Geometry-6	Orifice	2000-1c1h-O				65	85	-	7.2		80.9
Geometry-3	Louver Baffles	200-1c1h-Lb-45-18	200	100	100	65	85	45	-	18	77.4
Geometry-4	Louver	200-1h1c-L-45-18	200	100	100	85	65				81.7
Geometry-5	Orifice with Target	2000-1h1c-OT	2000	1000	1000	80.5	79.5	-	7.2	-	84.3
		200-1h1c-OT	200	100	100	85	65	-	7.2	-	87.7

5.7.1 Duct length for 80% mixing effectiveness and pressure drop

It is observed that mixing effectiveness and the pressure drop are more influenced by geometric parameters as compared to the flow conditions. Among all these tests, Geometry-5 (orifice-target) performs best but at the expense of high pressure drop. One notable point is that Geometry-6 (orifice) showed highest mixing effectiveness until plane-6 which is located at 111 inches duct length, but after that it shows around 10% decrease in mixing effectiveness at the outlet. One of the reasons of this drop could be that the flow was not fully developed, this geometry could be examined in future with extended duct length to see its effect on mixing effectiveness. Another reason could be the outlet boundary conditions. It was also seen in additional analysis, orifice type mixer is better than the orifice-target combination for short duct lengths. From this analysis, one can conclude that, there is no benefit to use the orifice-target mixers for short ducts, when we consider the trade-off between mixing performance

and difficulties in manufacturing and modelling.

Second highest mixing effectiveness is seen for Geometry-2 (louver-baffle) with louvers at 65° angle, with different flow ratios. From the analysis of Geometry-1 (without mixer), it is seen that difference of airflow ratio (i.e, using different flowrates for hot and cold airstream) also enhances the mixing. However, relatively high pressure drop is seen in this case, which is approximately equal to the pressure drop in Geometry-5 and Geometry-6. When Geometry-2 is compared for louver angle of 45° with Geometry-3 (louver-baffle) in which louvers are also at 45° angle, and a pair of mixers is used instead of one mixer, an increase in mixing effectiveness is seen even when the distance between mixers is short (2 inches). Mixing effectiveness increases with an increase in the distance between the mixers. When louver-baffle mixer is compared with louvers mixer for same flow conditions high pressure drop is seen across louver-baffle mixer with slight improvement in mixing effectiveness.

Third highest mixing effectiveness is seen for the same geometry when the distance between two mixers is 18 inches and the flow ratio for hot and cold air is different. The best mixer also performed well for low flowrate conditions, 6% more mixing effectiveness is seen when compared with Geometry-4 (louver), under the same flow conditions. In this case, inlet for hot and cold airstreams are swapped, hot air enters at the bottom and cold air enters at the top of the duct.

Overall, it can be concluded that both geometric parameter and flow condition play a key role in the performance of a mixer, however we found that the orifice-target mixer yields the best mixing performance for longer ducts and orifice provides better mixing for shorter ducts at expense of high pressure drop.

Table 5.16: Comparison of pressure drop and mixing effectiveness within 69 inches. of the duct length. In this case, first plane is near the inlet of the duct. Where S.D. represents the surface standard deviation and S.A. represents the surface average.

Name		Inlet	Plane 12
	Location of Plane (inch)	0	69
2000-1c1h-LB-45-18	S.D. of Temp. (F)	10.0	4.31
	Mixing Effectiveness (%)		56.9
	S.A. Static Pressure (Pa)	992	-63.6
	Pressure Drop (Pa)		1055
200-1c1h-LB-45-18	S.D. of Temp. (F)	10.0	4.62
	Mixing Effectiveness (%)		53.8
	S.A. Static Pressure (Pa)	10.21	-0.65
	Pressure Drop (Pa)		10.86
2000-1c1h-L-45-18	S.D. of Temp. (F)	10.0	4.72
	Mixing Effectiveness (%)		52.8
	S.A. Static Pressure (Pa)	187.8	-28.8
	Pressure Drop (Pa)		217
200-1c1h-L-45-18	S.D. of Temp. (F)	10.0	4.48
	Mixing Effectiveness (%)		55.2
	S.A. Static Pressure (Pa)	2.04	-0.26
	Pressure Drop (Pa)		2.30
2000-1c1h-O-7.2	S.D. of Temp. (F)	10.0	2.90
	Mixing Effectiveness (%)		71.0
	S.A. Static Pressure (Pa)	1802	-309
	Pressure Drop (Pa)		2111
2000-1c1h-OT-7.2	S.D. of Temp. (F)	10.0	2.42
	Mixing Effectiveness (%)		75.5
	S.A. Static Pressure (Pa)	1875	-223
	Pressure Drop (Pa)		2098

5.7.2 Performance Evaluations of Air-Mixers within 1.5D$_h$

Industry requirement is sometimes different than those of researchers analyzing in labs and industry. For example, in industry manufacturers and the people who perform testing are more interested in short duct length. To fulfill that requirement, we selected the duct of 1.5D$_h$ length. The above discussed cases are analyzed for their

mixing effectiveness and pressure with different flowrate for $1.5D_h$ of duct length which is a realistic space constraint in a HVAC equipment testing company. The results of this analysis are presented below. To make it clear, no additional duct is used, just two planes are selected at a distance of $1.5D_h$ length. First plane is placed just before the mixer to calculate flow properties like temperature, static pressure, and velocity. In all our CFD simulations, first mixer is placed at 42 inches inside the duct. The first plane is taken at 41.95 inches. In all cases, the maximum distance between two mixers is 18 inches, Hence the selected length will cover all simulations performed in this study. To avoid confusions with the names of planes, these planes are named plane-11 and plane-12. This additional analysis is done for a few selected cases. Comparison is made between the two cases for each Geometry-3 and Geometry-4. The variable is total flowrate and those are 2000 CFM and 200 CFM with same flow ratio for both hot and cold air. The similar analysis is done for only one case for Geometry-5 and Geometry-6.

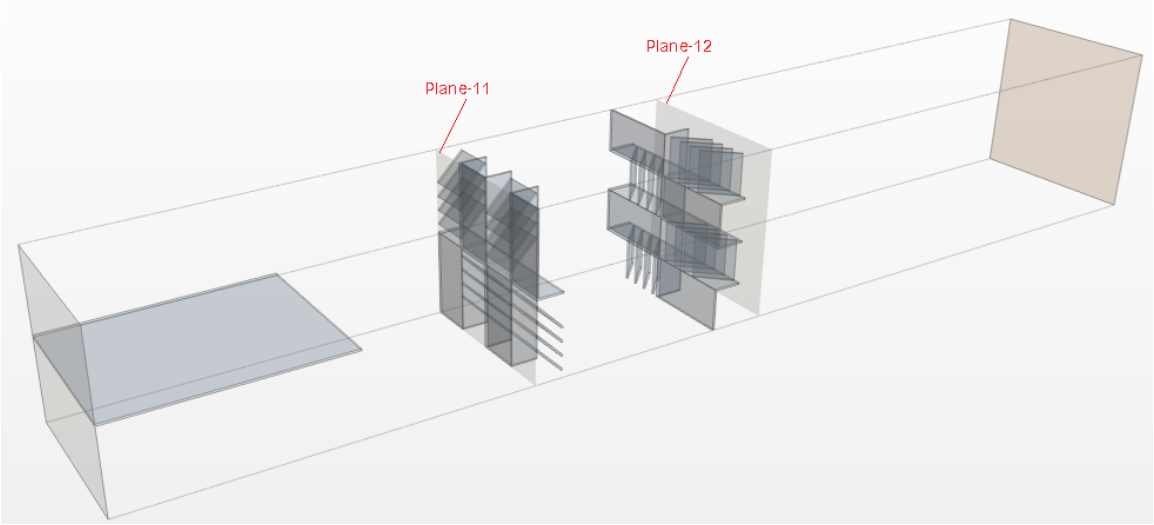

Figure 5.53: Planes location

From table 5.17, it can be seen that Geometry-6 which has only orifice has a maximum mixing effectiveness. But there is also a high pressure drop in this case. When we compare Geometry-6 with Geometry-5 which has additional target plate,

it has almost the same pressure drop. The difference between mixing effectiveness is 15.3%. When louver-baffles mixer is compared with the louver mixer, louver-baffles mixer shows 5.6% improvement in mixing at the expense of almost 5 times more pressure drop. When both mixers are compared with total flowrate of 200 CFM, louver-baffles mixer again performed well. The difference in the mixing effectiveness is very less around 0.3%. However, the pressure drop is 5 times more than the louver mixer.

Plots for pressure drop and mixing effectiveness for these cases are shown in figure 5.54. Trend-lines for pressure drop with an increase in volume flowrate are shown in the same figure. These trend-lines showed that pressure drop using equation 5.1 is almost the same as calculated by CFD simulations for 2000 CFM. In table 5.18, the values of pressure drop and mixing effectiveness for length of approximately 69 inches are given. In this study, plane-12 is kept at the same location but plane-11 is taken at inlet. In this analysis the same trend is seen. The only difference is seen in the mixing effectiveness of orifice-target mixer. The orifice-target mixer shows 20% higher mixing with respect to the $1.5D_h$ length. Same trend can be seen for this case in figure 5.55 for the pressure drop.

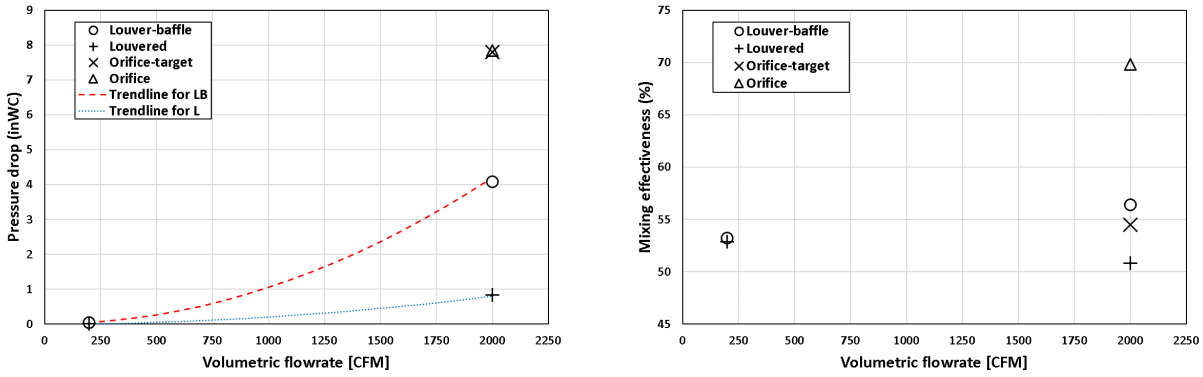

(a) Pressure drop

(b) Mixing effectiveness

Figure 5.54: Comparison of pressure drop and mixing effectiveness within $1.5D_h$ which is equal to 27 inches. In this case, first plane is near the inlet of the mixer

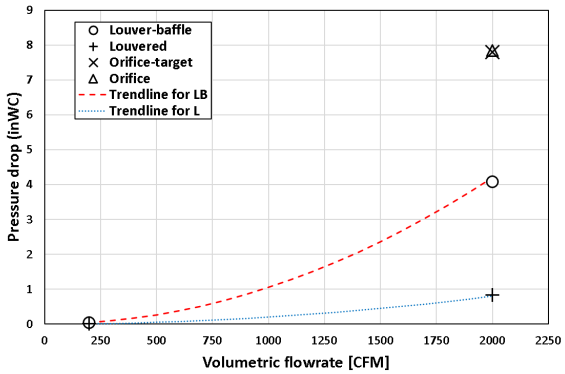

(a) Pressure drop

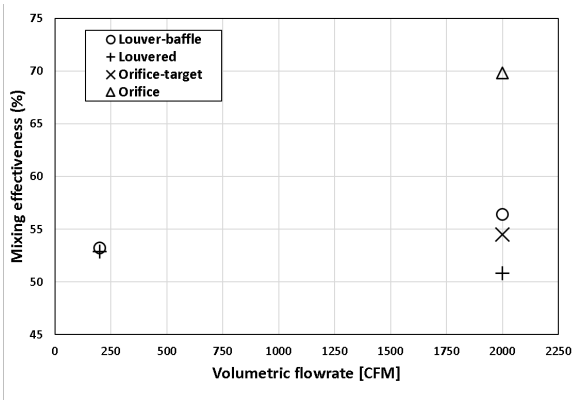

(b) Mixing effectiveness

Figure 5.55: Comparison of pressure drop and mixing effectiveness within 69 inches. of the duct length. In this case, first plane is near the inlet of the duct

$$\Delta P_2 = \Delta P_1 \cdot \left(\frac{V_2}{V_1}\right)^2 \tag{5.1}$$

where "P" is pressure and "V" is the flowrate (CFM)

Table 5.17: Comparison of pressure drop and mixing effectiveness within $1.5D_h$ which is equal to 27 inches. In this case, first plane is near the inlet of the mixer. Where S.D. represents the surface standard deviation and S.A. represents the surface average.

Name		Plane-11	Plane 12
	Location of Plane (inch)	41.95	68.95
2000-1c1h-LB-45-18	S.D. of Temp. (F)	9.88	4.31
	Mixing Effectiveness (%)		56.4
	S.A. Static Pressure (Pa)	952	-64
	Pressure Drop (Pa)		1016
200-1c1h-LB-45-18	S.D. of Temp. (F)	9.87	4.62
	Mixing Effectiveness (%)		53.2
	S.A. Static Pressure (Pa)	9.80	-0.65
	Pressure Drop (Pa)		10.45
2000-1c1h-L-45-18	S.D. of Temp. (F)	9.59	4.72
	Mixing Effectiveness (%)		50.8
	S.A. Static Pressure (Pa)	177.3	-28.9
	Pressure Drop (Pa)		206.12
200-1c1h-L-45-18	S.D. of Temp. (F)	9.50	4.48
	Mixing Effectiveness (%)		52.9
	S.A. Static Pressure (Pa)	1.93	-0.26
	Pressure Drop (Pa)		2.19
2000-1c1h-O-7.2	S.D. of Temp. (F)	9.62	2.90
	Mixing Effectiveness (%)		69.8
	S.A. Static Pressure (Pa)	1643	-309
	Pressure Drop (Pa)		1952
2000-1c1h-OT-7.2	S.D. of Temp. (F)	5.32	2.42
	Mixing Effectiveness (%)		54.5
	S.A. Static Pressure (Pa)	1715	-224
	Pressure Drop (Pa)		1939

Table 5.18: Comparison of pressure drop and mixing effectiveness within 69 inches. of the duct length. In this case, first plane is near the inlet of the duct. Where S.D. represents the surface standard deviation and S.A. represents the surface average.

Name		Inlet	Plane 12
	Location of Plane (inch)	0	69
2000-1c1h-LB-45-18	S.D. of Temp. (F)	10.0	4.31
	Mixing Effectiveness (%)		56.9
	S.A. Static Pressure (Pa)	992	-63.6
	Pressure Drop (Pa)		1055
200-1c1h-LB-45-18	S.D. of Temp. (F)	10.0	4.62
	Mixing Effectiveness (%)		53.8
	S.A. Static Pressure (Pa)	10.21	-0.65
	Pressure Drop (Pa)		10.86
2000-1c1h-L-45-18	S.D. of Temp. (F)	10.0	4.72
	Mixing Effectiveness (%)		52.8
	S.A. Static Pressure (Pa)	187.8	-28.8
	Pressure Drop (Pa)		217
200-1c1h-L-45-18	S.D. of Temp. (F)	10.0	4.48
	Mixing Effectiveness (%)		55.2
	S.A. Static Pressure (Pa)	2.04	-0.26
	Pressure Drop (Pa)		2.30
2000-1c1h-O-7.2	S.D. of Temp. (F)	10.0	2.90
	Mixing Effectiveness (%)		71.0
	S.A. Static Pressure (Pa)	1802	-309
	Pressure Drop (Pa)		2111
2000-1c1h-OT-7.2	S.D. of Temp. (F)	10.0	2.42
	Mixing Effectiveness (%)		75.5
	S.A. Static Pressure (Pa)	1875	-223
	Pressure Drop (Pa)		2098

CHAPTER VI

CONCLUSIONS AND FUTURE WORK

6.1 Conclusions

In this study, different geometries and flowrates were analyzed to see their impact on the mixing performance, considered to be the main performance index for mixers. Another important parameter in the selection of a mixer is the pressure drop. Two main design criteria were considered (i) geometrical parameters in design configuration (ii) flow conditions (i.e, flowrate, and temperature). Both characteristics, mixing effectiveness and pressure drop, were analyzed for almost all the geometries, however, mixing effectiveness was emphasized in the study.

There are five parameters, that are very important in the selection of air mixers. These parameters are (1) flowrate at the inlet of the duct, (2) length of the duct, (3) mixing effectiveness, (4) pressure drop, and (5) non-uniformity of the velocity after the mixer. The length of the duct must be equal to $1.5D_h$, a limit set by the industry. This restriction is imposed by the PMS (Project Management Subcommittee) of ASHRAE RP-1733. The second restriction imposed by the PMS is the acceptable amount of pressure drop, 2 inWC (498 Pa). Above 2 inWC, the PMS anticipated major problems with air leak tightness and mechanical integrity of temporary testing ducts. The third restriction is the non-uniformity of velocity at the face of heat exchanger which is placed after the mixer. According to ASHRAE standard 33-2016, section 7.1.2, the standard deviation of velocity should not exceed 20%. Ideally, all these restriction should be fulfilled for both low and high flowrates within the acceptable pressure drop. The limit trend of all these parameters in relation to each

other is shown in figures 6.1 to 6.3. The vertical lines indicate the aforementioned limits; points to the left part of these limit lines are acceptable. From these plots, it can be easily concluded that only the louver mixer worked well satisfying most of the constrains with an exception of the velocity variation.

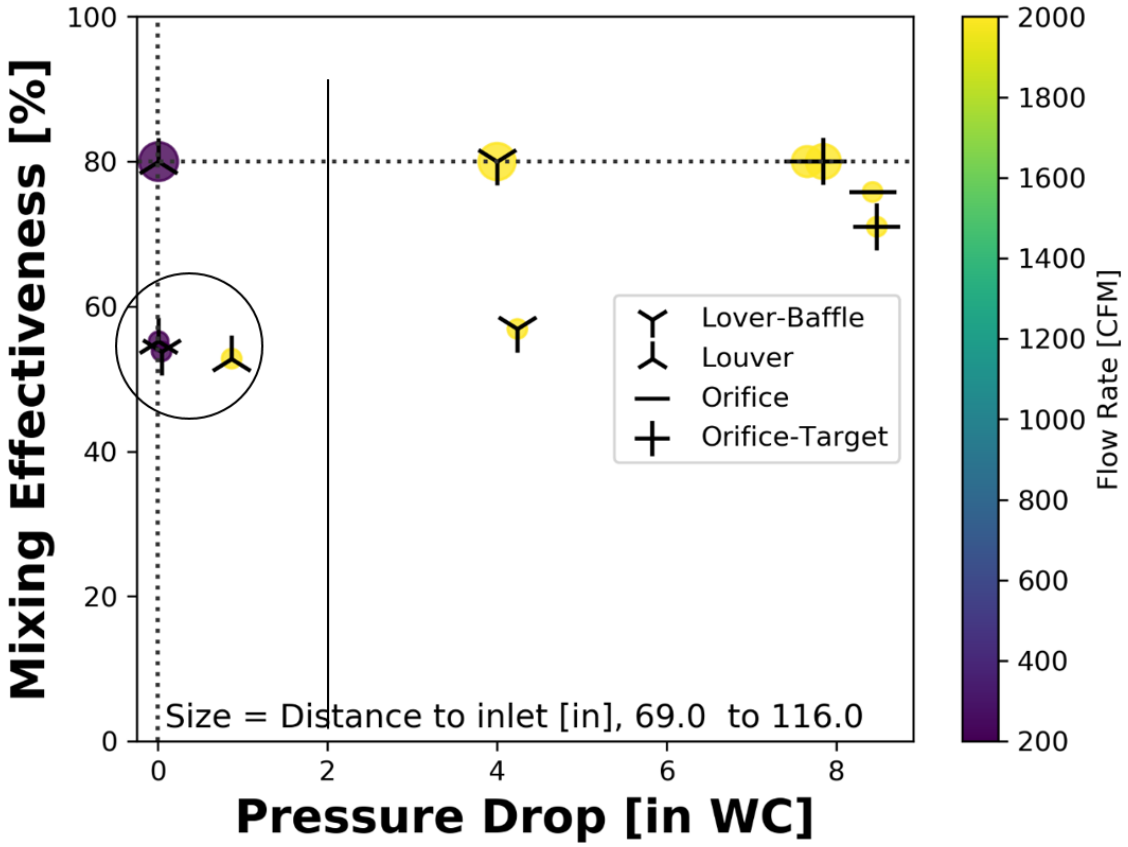

Figure 6.1: Mixing effectiveness as function of pressure drop; color = flowrate; marker size = distance to inlet

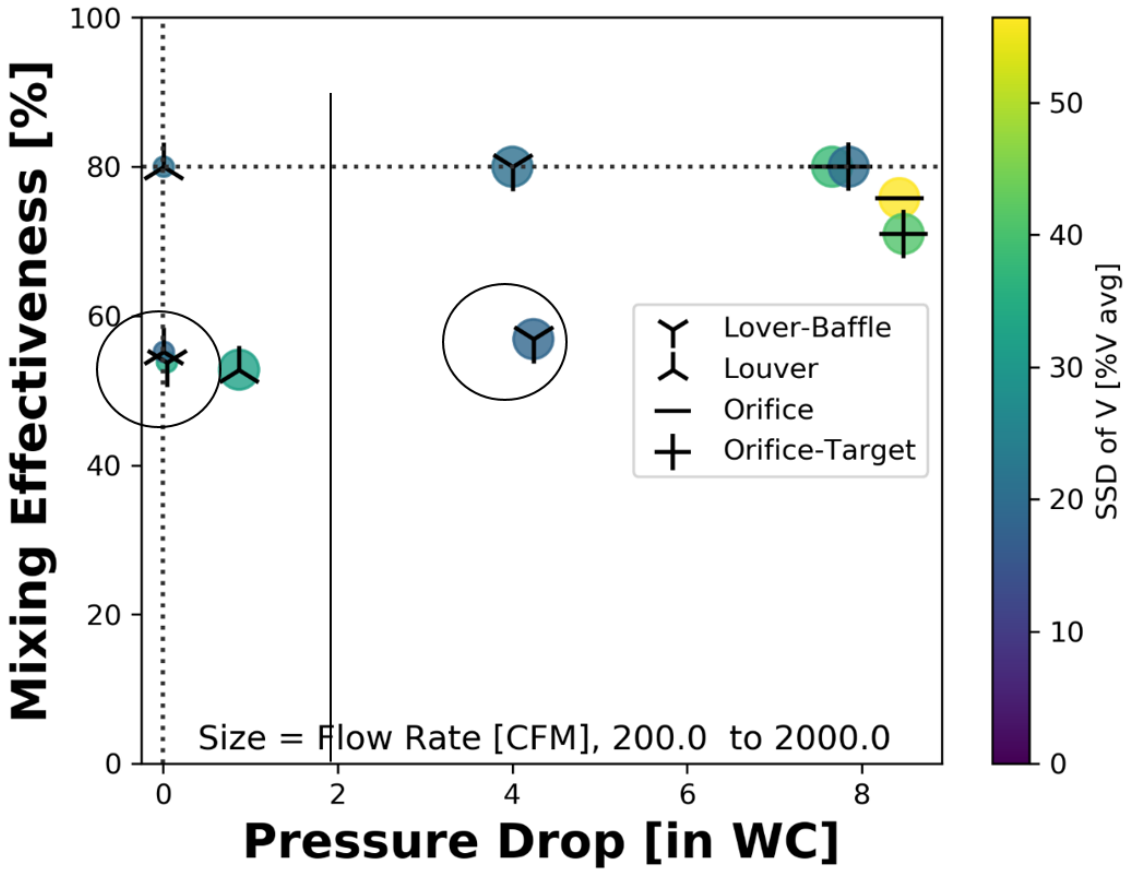

Figure 6.2: Mixing effectiveness as function of pressure drop; color = standard deviation of velocity; marker size = flowrate

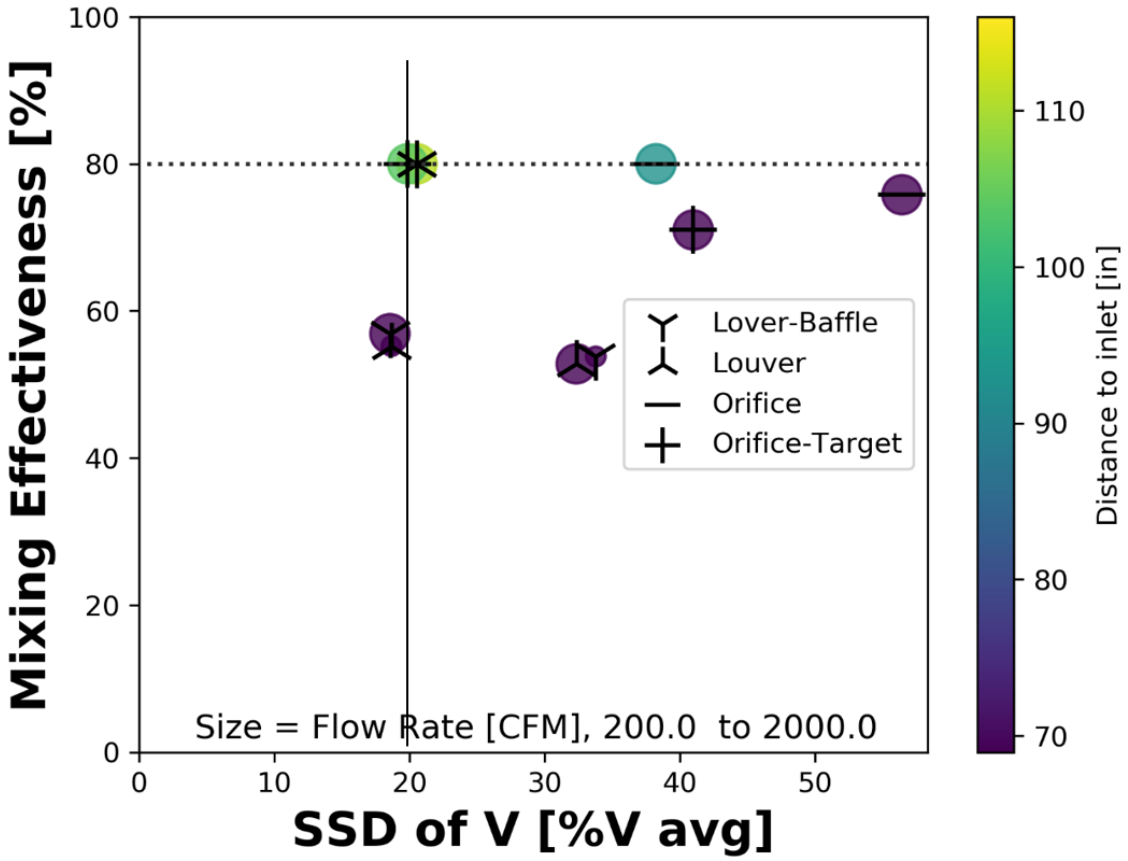

Figure 6.3: Mixing effectiveness as function of standard deviation of velocity; color = distance to inlet ; marker size = flowrate

6.2 Future Work: Geometries

It is observed that mixing effectiveness is enhanced at the expense of high pressure drop and there is a need for developing new air mixers with lower pressure drop. The following items could be considered for future studies:

1. Louvered-target mixer combination.
2. Effect of distance between midwall and inlet of the mixer.
3. Different orientation of the louvers in different sections of the individual mixer.
4. For louvered mixer velocity settling means can be used to reduce non-uniformity of velocity.
5. Utilization of increased duct cross-section to reduce pressure drop.
6. Aerodynamic improvement of air redirection and turbulence generation in mixer.

6.3 Future Work: Computational Modeling Approaches

There is a need for computational strategies that can significantly decrease the computational cost of HVAC mixing apparatus and airflow models without compromising their physical accuracy. Although CFD analyses (equipped with RANS/LES closures) would provide very detailed information, and are invaluable to our understanding of complex airflow patterns and heat transfer characteristics in HVAC systems, whole building energy and comfort analyses typically require models for numerous physical situations. Indeed, it is really interesting to know the best location and the number of sensors to be adequate in the buildings, still in a process of thermal comfort and reduce energy costs (Tallet et al., 2015). The current state-of-the-art is to use static models of the HVAC systems to support design decisions. In order to increase the

efficiency of HVAC system, the real time knowledge of temperature distribution is crucial for simulation and control of indoor thermal environment of buildings. The data-driven model reduction techniques offer a new perspective on these system simulations (Tallet et al., 2015; Li et al., 2013; Sun and Wang, 2010), gathering snapshot data from high-fidelity computations and/or experiments. However, despite the rapid development of high-fidelity computational tools to understand the physics of thermal and transport phenomena, there has been slow progress in generating reliable reduced order models that effectively brings controls, optimization, and uncertainty analysis together to focus attention on low energy design. Further research efforts are needed to build reliable model reduction techniques for achieving energy efficient designs in cost and time effective ways. Based on experimentally validated high-fidelity CFD computations, this new paradigm could provide a significant increase in efficiency of our computational models with deeper understanding of the nonlinear system dynamics.

References

Abdilghanie, A. M., Collins, L. R., and Caughey, D. A. (2009). Comparison of turbulence modeling strategies for indoor flows. *Journal of Fluids Engineering*, 131(5):051402.

Ai, Z. and Mak, C. (2013). Pressure losses across multiple fittings in ventilation ducts. *The Scientific World Journal*, 2013:195763.

Angel, W. L. (2011). *HVAC design sourcebook*. McGraw Hill Professional.

Awbi, H. (1989). Application of computational fluid dynamics in room ventilation. *Building and Environment*, 24(1):73–84.

Axley, J. (2007). Multizone airflow modeling in buildings: History and theory. *HVAC&R Research*, 13(6):907–928.

Baker, A., Kelso, R. M., Gordon, E. B., Roy, S., and Schaub, E. G. (1997). Computational fluid dynamics: A two-edged sword. *ASHRAE Journal*, 39(8):51.

Bird, R. B., Stewart, W., and Lightfoot, E. (1960). *Transport phenomena*. John Willey & Sons Inc, New York.

Brodkey, R. (1975). *Turbulence in mixing operations: theory and application to mixing and reaction*. Academic Press, New York.

Burfoot, D., Hall, K., Brown, K., and Xu, Y. (1999). Fogging for the disinfection of food processing factories and equipment. *Trends in Food Science & Technology*, 10(6-7):205–210.

Chen, H., Moshfegh, B., and Cehlin, M. (2012). Numerical investigation of the flow behavior of an isothermal impinging jet in a room. *Building and Environment*, 49:154–166.

Chen, Q. (1995). Comparison of different k-ε models for indoor air flow computations. *Numerical Heat Transfer, Part B Fundamentals*, 28(3):353–369.

Chen, Q. (2009). Ventilation performance prediction for buildings: A method overview and recent applications. *Building and Environment*, 44(4):848–858.

Chen, Wei Zhang, Q. (2000). Large eddy simulation of natural and mixed convection airflow indoors with two simple filtered dynamic subgrid scale models. *Numerical Heat Transfer: Part A: Applications*, 37(5):447–463.

Chiang, W.-H., Wang, C.-Y., and Huang, J.-S. (2012). Evaluation of cooling ceiling and mechanical ventilation systems on thermal comfort using CFD study in an office for subtropical region. *Building and Environment*, 48:113–127.

Chow, W. and Fung, W. (1996). Numerical studies on the indoor air flow in the occupied zone of ventilated and air-conditioned space. *Building and Environment*, 31(4):319–344.

Emmerich, S. J. and McGrattan, K. B. (1998). Application of a large eddy simulation model to study room airflow. *Transactions-American Society of Heating, Refrigeration and Air Conditioning Engineers*, 104(1128-1140):10.

Faison, T., Davis, J., and Achenbach, P. (1966). A test apparatus for the study of forced air-mixing devices. *Journal of Research NBS C*, 70.

Faison, T., Davis, J. C., and Achenbach, P. R. (1970). *Performance of louvered devices as air mixers*, volume 27. US National Bureau of Standards.

Faison, T. K., Davis, J. C., and Achenbach, P. R. (1967). *Performance of Square-edged Orifices and Orifice-target Combinations as Air Mixers*, volume 12. US Government Printing Office.

Gan, G. (1995). Evaluation of room air distribution systems using computational fluid dynamics. *Energy and Buildings*, 23(2):83–93.

HandbookFundamentals, A. and Edition, S. (2009). chapter 21-22. *American Society of Heating, Refrigerating and Air-Conditioning Engineers, Atlanta, Ga, USA*.

Harral, B. and Burfoot, D. (2005). A comparison of two models for predicting the movements of airborne particles from cleaning operations. *Journal of Food Engineering*, 69(4):443–451.

Hessel, V., Löwe, H., and Schönfeld, F. (2005). Micromixersa review on passive and active mixing principles. *Chemical Engineering Science*, 60(8-9):2479–2501.

Huang, L., Kumar, K., and Mujumdar, A. (2003). A parametric study of the gas flow patterns and drying performance of co-current spray dryer: Results of a computational fluid dynamics study. *Drying Technology*, 21(6):957–978.

Idelchik, I. (1994). Handbook of hydraulic resistance. 3rd.

Inard, C., Bouia, H., and Dalicieux, P. (1996). Prediction of air temperature distribution in buildings with a zonal model. *Energy and Buildings*, 24(2):125–132.

Jiang, Z., Chen, Q., and Moser, A. (1992). Indoor airflow with cooling panel and radiative/convective heat source. *ASHRAE Transactions*, 98(1):33–42.

Jones, P. and Whittle, G. (1992). Computational fluid dynamics for building air flow predictioncurrent status and capabilities. *Building and Environment*, 27(3):321–338.

Kim, G., Schaefer, L., Lim, T. S., and Kim, J. T. (2013). Thermal comfort prediction of an underfloor air distribution system in a large indoor environment. *Energy and Buildings*, 64:323–331.

Lam, J. C. and Chan, A. L. (2001). CFD analysis and energy simulation of a gymnasium. *Building and Environment*, 36(3):351–358.

Launder, B. and Ying, W. (1972). Secondary flows in ducts of square cross-section. *Journal of Fluid Mechanics*, 54(2):289–295.

Li, K., Su, H., Chu, J., and Xu, C. (2013). A fast-POD model for simulation and control of indoor thermal environment of buildings. *Building and Environment*, 60:150–157.

Liu, S. and Novoselac, A. (2014). Lagrangian particle modeling in the indoor environment: A comparison of RANS and LES turbulence methods (RP-1512). *HVAC&R Research*, 20(4):480–495.

Maatouk, K. (2007). A simplified procedure to investigate airflow patterns inside tall buildings using COMIS. *Architectural Science Review*, 50(4):365–369.

Megri, A. C. and Haghighat, F. (2007). Zonal modeling for simulating indoor environment of buildings: Review, recent developments, and applications. *HVAC&R Research*, 13(6):887–905.

Mokhtari, M., Gerdroodbary, M. B., Yeganeh, R., and Fallah, K. (2017). Numerical study of mixed convection heat transfer of various fin arrangements in a horizontal channel. *Engineering Science and Technology, an International Journal*, 20(3):1106–1114.

Mustafaraj, G., Lowry, G., and Chen, J. (2011). Prediction of room temperature and relative humidity by autoregressive linear and nonlinear neural network models for an open office. *Energy and Buildings*, 43(6):1452–1460.

Nguyen, N.-T. and Wu, Z. (2004). Micromixersa review. *Journal of Micromechanics and Microengineering*, 15(2):R1.

Norton, T. and Sun, D.-W. (2006). Computational fluid dynamics (cfd)–an effective and efficient design and analysis tool for the food industry: a review. *Trends in Food Science & Technology*, 17(11):600–620.

Ottino, J. M. (1990). Mixing, chaotic advection, and turbulence. *Annual Review of Fluid Mechanics*, 22(1):207–254.

Ottino, J. M. and Ottino, J. (1989). *The kinematics of mixing: stretching, chaos, and transport*, volume 3. Cambridge University Press, New York.

Peng, X. and Van Paassen, A. (1998). A state space model for predicting and controlling the temperature responses of indoor air zones. *Energy and Buildings*, 28(2):197–203.

Pulat, E. and Ersan, H. A. (2015). Numerical simulation of turbulent airflow in a ventilated room: Inlet turbulence parameters and solution multiplicity. *Energy and Buildings*, 93:227–235.

Quadros, W. R. and Owen, S. J. (2009). Defeaturing CAD models using a geometry-based size field and facet-based reduction operators. In *Proceedings of the 18th international meshing roundtable*, pages 301–318. Springer.

Riederer, P., Marchio, D., and Visier, J. C. (2002). Influence of sensor position in building thermal control: criteria for zone models. *Energy and Buildings*, 34(8):785–798.

Robinson, K. D. (2001). A test apparatus and method to rate the mixing performance of air mixers. *ASHRAE Transactions*, 107:136.

Ruano, A. E., Crispim, E. M., Conceiçao, E. Z., and Lúcio, M. M. J. (2006). Prediction of building's temperature using neural networks models. *Energy and Buildings*, 38(6):682–694.

Shao, L. and Riffat, S. (1995). Accuracy of CFD for predicting pressure losses in HVAC duct fittings. *Applied Energy*, 51(3):233–248.

Siriwattanayotin, S., Yoovidhya, T., Meepadung, T., and Ruenglertpanyakul, W. (2006). Simulation of sterilization of canned liquid food using sucrose degradation as an indicator. *Journal of Food Engineering*, 73(4):307–312.

Song, H.-S. and Han, S. P. (2005). A general correlation for pressure drop in a kenics static mixer. *Chemical Engineering Science*, 60(21):5696–5704.

Srebric, J. and Chen, Q. (2002). An example of verification, validation, and reporting of indoor environment CFD analyses (RP-1133). *Transactions-American Society of Heating, Refrigeration and Air Conditioning Engineers*, 108(2):185–194.

Srebric, J., Chen, Q., and Glicksman, L. R. (1999). Validation of a zero-equation turbulence model for complex indoor airflow simulation. *ASHRAE Transactions*, 105:414.

Stamou, A. and Katsiris, I. (2006). Verification of a CFD model for indoor airflow and heat transfer. *Building and Environment*, 41(9):1171–1181.

Su, M., Chen, Q., and Chiang, C.-M. (2001). Comparison of different subgrid-scale models of large eddy simulation for indoor airflow modeling. *Journal of Fluids Engineering*, 123(3):628–639.

Sun, Z. and Wang, S. (2010). A CFD-based test method for control of indoor environment and space ventilation. *Building and Environment*, 45(6):1441–1447.

Tallet, A., Allery, C., and Allard, F. (2015). POD approach to determine in real-time the temperature distribution in a cavity. *Building and Environment*, 93:34–49.

Teodosiu, C., Kuznik, F., and Teodosiu, R. (2014). CFD modeling of buoyancy driven cavities with internal heat sourceApplication to heated rooms. *Energy and Buildings*, 68:403–411.

Tripathi, B. and Moulic, S. (2007). Investigation of the buoyancy affected airflow patterns in the enclosure subjected at the different wall temperatures. *Energy and Buildings*, 39(8):906–912.

Varma, M. N. and Kannan, A. (2006). Cfd studies on natural convective heating of canned food in conical and cylindrical containers. *Journal of Food Engineering*, 77(4):1024–1036.

Wan, M. and Chao, C. (2005). Abstract. *Indoor Air*, 15(5):342–355.

Whittle, G. (1986). Computation of air movement and convective heat transfer within buildings. *International Journal of Ambient Energy*, 7(3):151–164.

Woodward, M. and Berry, C. (Accessed: 2019-05-22)). *Source: U.S. Energy Information Administration, 2015 Residential Energy Consumption Survey.*

Wurtz, E., Nataf, J.-M., and Winkelmann, F. (1999). Two-and three-dimensional natural and mixed convection simulation using modular zonal models in buildings. *International Journal of Heat and Mass Transfer*, 42(5):923–940.

Xu, W. (1998). *New turbulence models for indoor airflow simulation.* PhD thesis, Massachusetts Institute of Technology.

Yao, Y., Yang, K., Huang, M., and Wang, L. (2013). A state-space model for dynamic response of indoor air temperature and humidity. *Building and Environment*, 64:26–37.

Zhai, Z. (2006). Application of computational fluid dynamics in building design: aspects and trends. *Indoor and Built Environment*, 15(4):305–313.

Zhai, Z. J., Zhang, Z., Zhang, W., and Chen, Q. Y. (2007). Evaluation of various turbulence models in predicting airflow and turbulence in enclosed environments by CFD: Part 1Summary of prevalent turbulence models. *HVAC&R Research*, 13(6):853–870.

Zhao, B., Li, X., and Yan, Q. (2003). A simplified system for indoor airflow simulation. *Building and Environment*, 38(4):543–552.

APPENDIX A

APPENDICES

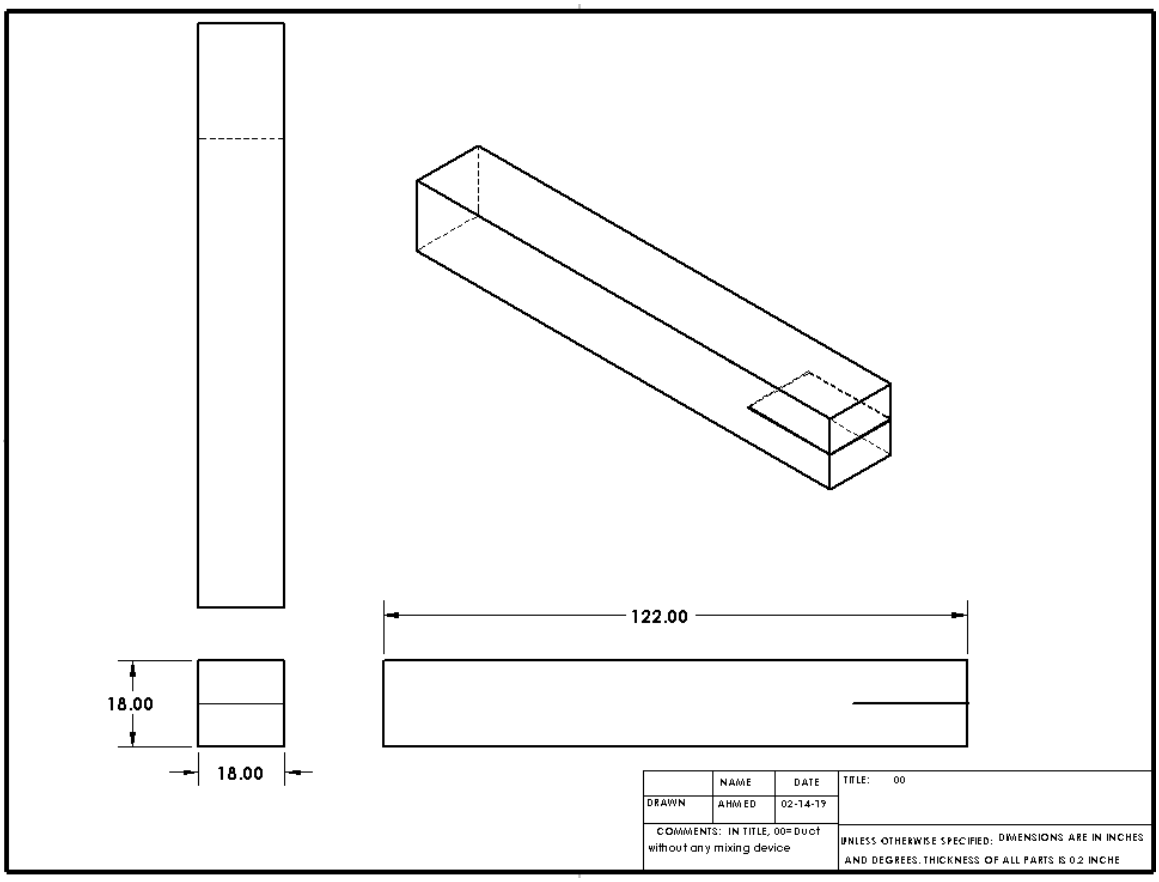

Figure A.1: Duct with midwall

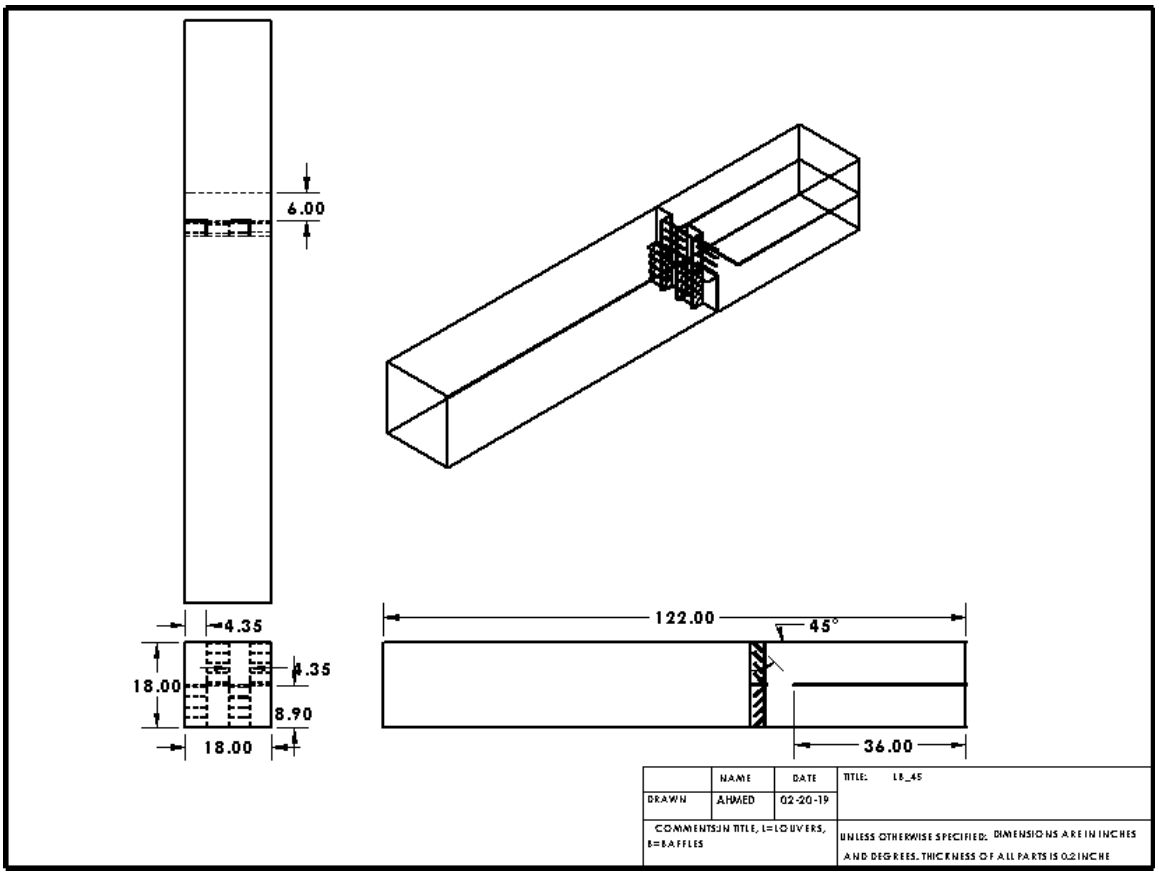

Figure A.2: Duct with Louver baffles mixer with louvers at 45 angle

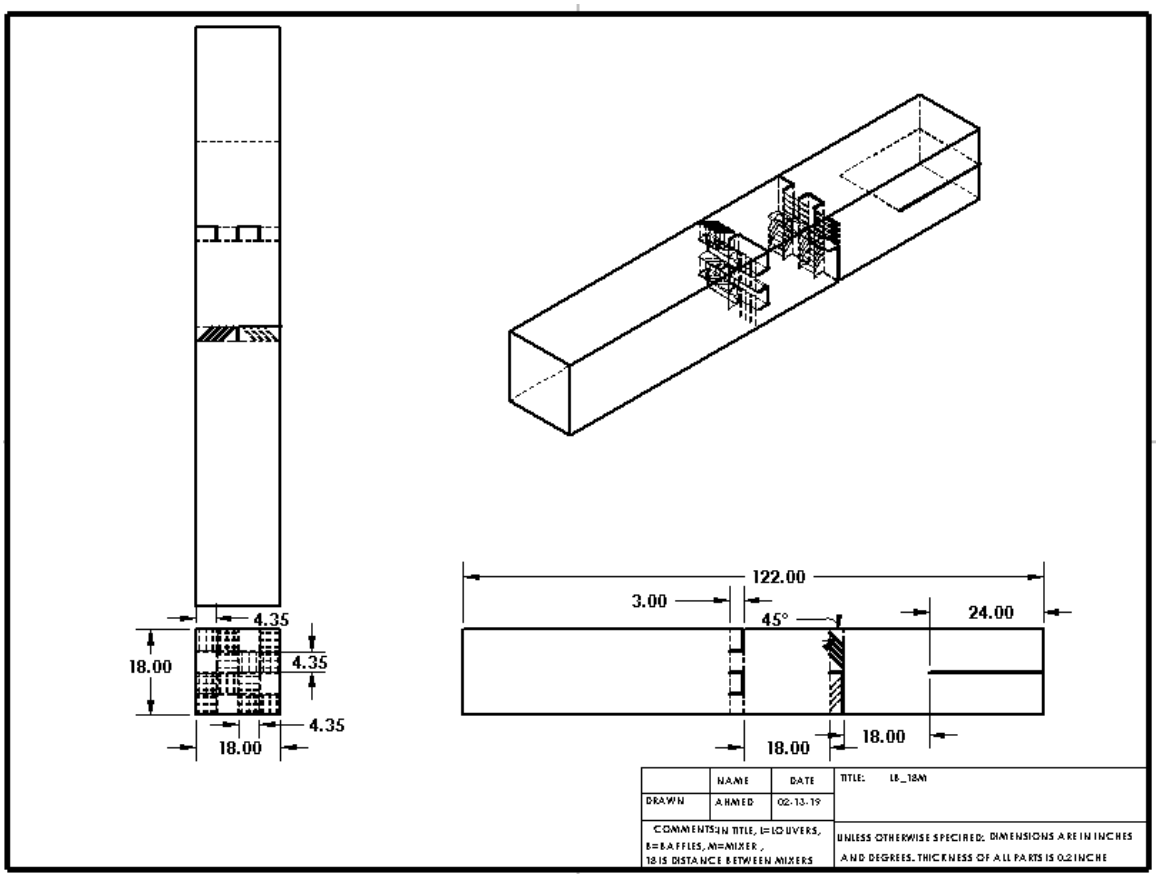

Figure A.3: Duct with Louver baffles mixers louvers at 45 angle

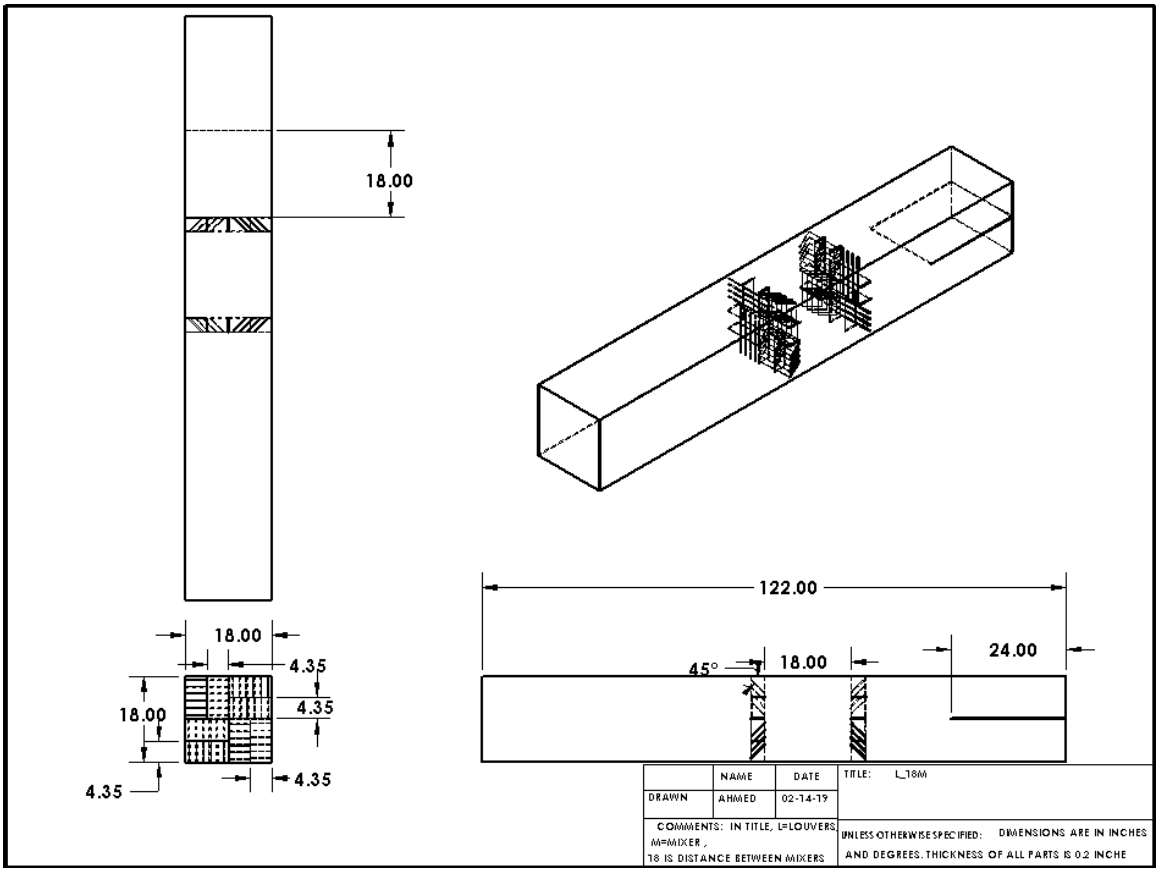

Figure A.4: Duct with Louver mixers louvers at 45 angle

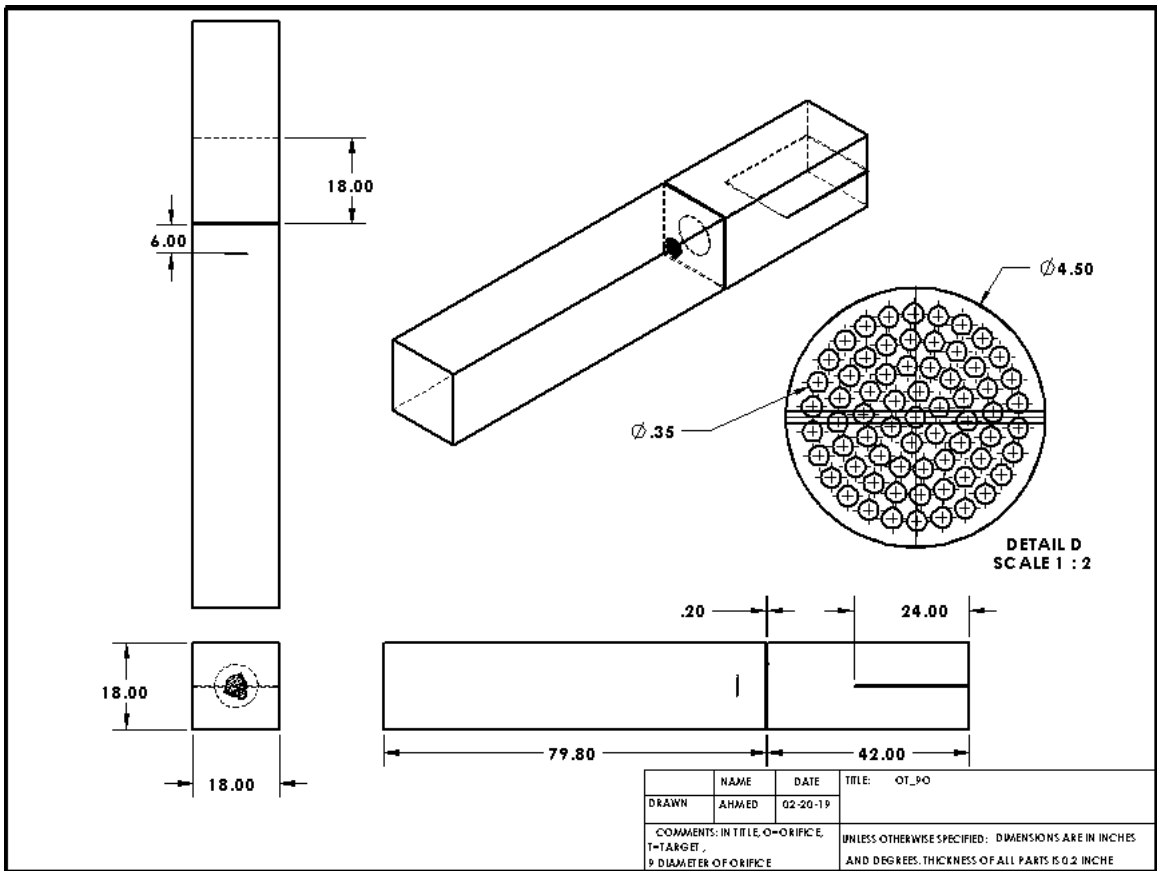

Figure A.5: Duct with Orifice Target mixer arrangement

VITA

MANSOOR AHMED

Candidate for the Degree of

Master of Science

Thesis: NUMERICAL INVESTIGATION OF AIR MIXER PERFORMANCE FOR HVAC TESTING APPLICATIONS

Major Field: Mechanical Engineering

Biographical:

Education:

Completed the requirements for the Master of Science in Mechanical Engieering at Oklahoma State University, Stillwater, Oklahoma in May, 2019.
Completed the requirements for the Master of Science in Engineering Mechanics at KTH-Royal Institute of Technology, Stockholm, Sweden in March 2011.
Completed the requirements for the Bachelor of Science in Mechanical Engineering at University of Engineering and Technology, Lahore, Pakistan, 2007.

Experience:

Worked as a mechanical engineer at Coolpoint (PVT) Ltd, Lahore, Pakistan.
Worked as an associate monitor at TUSDECTechnology Upgradation and Skill Development Company, Lahore, Pakistan.
Worked as a lecturer at University of Management and Technology, Lahore, Pakistan.
Worked as a lecturer at University of Sargodha, Lahore, Pakistan.

Student Affiliations:

ASHRAE